All-Optical Pulse Regeneration in a Faraday Stabilized Ultrafast Nonlinear Interferometer

by

Shelby Jay Savage

Submitted to the Department of Electrical Engineering and Computer Science

in partial fulfillment of the requirements for the degree of

Master of Engineering in Electrical Engineering and Computer Science

at the

MASSACHUSETTS INSTITUTE OF TECHNOLOGY

May 2001

Author .....

Department of Electrical Engineering and Computer Science

May 23, 2001

Certified by .....

Erich P. Ippen

Professor

Thesis Supervisor

Certified by .....

Scott A. Hamilton

MIT Lincoln Laboratory Staff Member

Thesis Supervisor

Accepted by .....

Arthur C. Smith

Chairman, Department Committee on Graduate Students

All-Optical Pulse Regeneration in a Faraday Stabilized Ultrafast Nonlinear Interferometer

by

Shelby Jay Savage

Submitted to the Department of Electrical Engineering and Computer Science
on May 23, 2001, in partial fulfillment of the
requirements for the degree of
Master of Engineering in Electrical Engineering and Computer Science

Abstract

Modern fiber optic communications networks multiplex data onto many different channels, each with its own carrier frequency. In order to meet rising demand for high data rates, researchers have begun to consider methods to use the bandwidth of optical fibers more efficiently. In particular, more efficient use might come from operating fewer channels with each channel at a higher data rate, or perhaps even, ultimately, from operating one ultrafast time division multiplexed channel. High data rate optical channels already surpass the limits of electronic processing, which today cannot handle rates greater than 40 Gbit/s. Researchers must design the individual hardware elements, like address recognizers, demultiplexers, and regenerators, that will be necessary for any practical system. One promising idea is to make these devices all-optical. Already all-optical logical switching has been demonstrated at 100 Gbit/s and all-optical demultiplexing at hundreds of Gbit/s. But, in any long haul system, it is also necessary to develop optical pulse regenerators to regenerate data encoded as optical pulses before those pulses become too distorted to detect. This thesis investigates an all-optical pulse regenerator that reshapes, retimes, and amplifies optical data pulses. A Faraday polarization rotator mirror is used to make it much more polarization stable than other designs. The physical principle on which it is based, the nonlinear index of refraction, is a nearly instantaneous effect and, therefore, does not suffer from the speed limitations of modern electronics. We test the design for its switching window, bit error rates, and sensitivity to timing jitter to show its usefulness as an optical pulse regenerator.

Thesis Supervisor: Erich P. Ippen
Title: Professor

Thesis Supervisor: Scott A. Hamilton
Title: MIT Lincoln Laboratory Staff Member

Acknowledgments

The acknowledgments section is the writer's chance to expand the list of "authors" to its more realistic length. This thesis is the labor of many people, not just of those engineers directly involved in its composition, but of those who gave me their encouragement and friendship during my work on it. This section is the most important single section of this thesis, and it is my honor, among all those "authors," to write it.

My first thanks go to everyone at MIT Lincoln Laboratory. My thesis advisor, Professor Erich Ippen, knows that true understanding comes from comprehension of fundamental concepts, and I thank him for always explaining physics to me with that fact in mind. He has only spoken kindly and patiently to me and has helped me see to the end of some of my most challenging technical problems. My supervisor, Scott A. Hamilton, has always dealt with me gently and patiently. Many days, he spent more time with my work than with his. I thank him for his encouragement, his thorough notes on all my writing, and, most of all, for introducing me to downhill skiing. A student at Lincoln Laboratory, Bryan S. Robinson, taught me, more than anyone else, how to use the equipment in D-409. Without him, I would be, in this moment, answering for hundreds of thousands of dollars of broken hardware rather than submitting this thesis. His knowledge of laboratory methods, his technical imagination, and his doggedness with every idea and every piece of equipment have been the primary reasons that this work has gone as far as it has. Peg Danek has been great help in the laboratory and has given me (or sometimes I might say cursed me with) the knowledge of splicing optical fibers. Thanks as well, to Tom Murphy, who is always ready to answer a question; to Steve Constantine, whose many mortgages have been a source of amusement to me on my worst days, and whose encouragement has always propelled me on; to Sam Wong for suffering along side me; and to Todd Ulmer for expanding my musical horizons.

A large share of credit for the completion of this thesis also belongs to those who reminded me unceasingly that life is more than ultrashort optical pulses and all-optical fiber switches. An aquaintance from California once told me that MIT is a better place to be from than to be at. I owe thanks, however, to my friends at MIT for making MIT just as wonderful a place to be at as it is a wonderful place to be from. My apartment mates, Barb Huppe, Jon Wong, Serena Chan, and Abe McAllister, made me enjoy the little time I had from work and responsibility with games, conversation, and frisbee. It is largely to them that I now owe my subtle understanding of world conquest. My thanks go to Allison Waingold, who has been my friend almost from the beginning of my time at MIT and who endured several terms of Friday night study sessions and a full semester of number theory with me. I also must thank Garrett Cradduck, who caused my first all-nighter at MIT, who shares with me an insatiable passion for numbers and music, who taught me the beautiful gentle strains of "Danny Boy," and who, like me, appreciates undeep edifying poetry. Denise and Paulo Oliveira have filled those parts of my academic interests that lie outside the norm of MIT, and I thank these two friends of mine for bringing some

humanity to a very mechanical campus. Christina Silcox is able to appreciate both the academic and the joyful in life. I thank her for being the most frank of all my friends and for helping me to live life. My thanks also go to Brian Purville, Olu Fashoyin, Danielle Ayodele Hinton and Bapu Jena, my fellows of West Campus. I give special thanks to Michele Micheletti, whom I knew for my first three semesters at MIT, and who was among my first friends. On Halloween night of 1997, she was struck by a car while we crossed Memorial Drive. We bear your memory with us.

The group that made MIT endurable more than any other was the Protestant Student Community. In my personal quest to identify once and for all the nature of Christ's Church on earth, I have only discovered one thing: we are occasionally blessed to find a community in which we unmistakably feel Christ's charity moving gently and tenderly, a part of that Church of Pentecostal Fire. I found it in the Protestant Student Community. Chaplain John Wuestneck has always been my good friend and has brought me new ideas in my growing knowledge of Christianity. John Mckay and Jamie Byrum brought me as fully into their lives as anyone can and shared with me the toils and vicissitudes of life as well as its triumphs. They truly believe, each in his own way, in the life found in Christ and give me hope for our Church. I thank them for being the sort of friends whom a man knows will hang with him in every kind of trial. I also thank Lora Reineck, who joined me in tutoring at the 4th Presbyterian, who brought me into MIT Concert Choir, and who, somehow, challenges me to be better than I could otherwise be. I am proud to be her friend. My thanks go to James Taylor, truly one of the kindest people I know. Jason Andrews and Vicki Schubert have kept me on the straight and narrow in bible study and always give me faith. I offer thanks to my other friends in PSComm: Annika Hill (who has hit me more than any other person on earth), Susanna Mireau, Mark Ethier, Katie Knopp, Lynn Maria Matthew, Onsi Fakhouri, Jack Williard, David Milovich–for their fellowship.

I owe an unpayable debt to my father, my mother, and my brother. My father is an engineer himself, and his help from the beginning has kept me from discouragement and from giving up. I thank him for his unlimited patience, which bore even my sometimes caustic and sarcastic personality. My mother is devoted to her sons. She volunteered at our elementary school, pushed us to succeed, and gave us everything we needed and, sometimes, more than we wanted. My parents were born to lives poorer than almost any American must endure today and are models to which I can only hope to rise. My brother, one year younger than I am, has been my only lifelong friend and peer. I thank him for encouraging me, even while I have been away from home.

Contents

List of Figures

List of Tables

Chapter 1

Introduction

Optical fibers provide most of the bandwidth available in long distance communications systems. Researchers continue to seek new ways to use all the available low loss sections of the optical fiber bandwidth, exceeding 25 THz [1]. It is not enough, however, to demonstrate propagation of optical signals using this bandwidth. At such high data rates, networks must be able to process these signals for tasks like address recognition before any such system can become practical. Many researchers forsee the use of optical time division multiplexing (OTDM) in high data rate systems. In OTDM systems, signals are digitally encoded as short optical pulses, perhaps shorter than a picosecond, and different data channels are interleaved in time [2]. The many tasks required in a high data rate TDM system include time multiplexing and demultiplexing of data [3], wavelength conversion [4], ultrafast data encryption [5], address recognition [6], and clock recovery [7]. Unfortunately, electronics are limited today to about 40 Gbit/s and cannot process the billions or trillions of bits per second in such an OTDM system. Researchers are, however, investigating alternatives that forego the conversion of the optical signal to electronic data. Instead, photonic data are processed using ultrafast all-optical techniques. This thesis studies a design for all-optical pulse regeneration, a problem that has received much attention in the last decade. Pulses that propagate long distances acquire unwanted distortions that make them difficult or impossible to detect. Any long-haul system will require periodic pulse regeneration, and the most efficient and cost-effective solution may be optical rather

than electronic [8].

A number of ideas for all-optical regenerators have been demonstrated (for example, see [9, 10, 11]). Many of these designs use an intensity dependent index of refraction to achieve an optically controlled nonlinear phase shift. An important design choice is the nonlinear waveguide medium. Some designs, like the nonlinear optical loop mirror [12], use optical fiber as the onlinear medium; others, like the ultrafast nonlinear interferometer (UNI) [13] and the semiconductor laser amplifier in a loop mirror (SLALOM) [14], use a semiconductor optical amplifier (SOA). The SOA has a very high nonlinear index of refraction, which makes it possible to use short (~1 mm) devices and low optical pulse powers. This advantage is important in optical logic, where low latency switching is often necessary for a successful design. The UNI has already been shown to switch pulses at 100 Gbit/s in all-optical logic [13]. SOA's have a gain recovery time that is long compared to the nearly instantaneous effects of the nonlinear index of refraction in optical fiber. This recovery time can cause amplitude patterning in the output of the switch. Pulse patterning is an important obstacle to overcome in switch design [15]. One possible solution to the problem of pulse patterning is pulse position modulation (PPM) [16]. Optical fiber, on the other hand, provides an ultrafast nonlinear index and a nearly lossless transmission medium. The nonlinear index in fiber, however, is relatively small and longer lengths (~km) must be used to induce the necessary phase shift. This length can cause unwanted distortions in the pulses as they propagate down the fiber [17]. For long-haul short optical pulse transmission, PPM may be undesirable due to its increased sensitivity to timing jitter compared with on-off key data. For regeneration, however, low latency switching is not required, and optical fiber based switches can be used. The distortions that accompany long propagation in fibers can be reduced by using low dispersion fibers like dispersion shifted fiber. Thus, in the application of regeneration, optical fiber is an important alternative to semiconductor optical amplifiers.

Several regenerator designs use fiber as the nonlinear medium [18]. The UNI itself can be adapted to fiber. This thesis investigates an all-fiber variation we call

the folded UNI. In this thesis we also present the results of switching experiments in the folded UNI and demonstrate this device as an all-optical regenerator. The folded UNI's advantage is its inherent polarization stability. The UNI, as mentioned above, has been shown to perform well as an all-optical switch. But, temperature variations and other slow changes in the fiber can cause the polarization to drift. After a length of time on the order of 30 minutes the polarization of the pulses in the UNI must be adjusted. The design of the folded UNI makes it unnecessary to control the polarization of pulses already in the switch.

Chapter 2 presents the nonlinear Schrödinger equation and the basic theory needed to understand optical pulse propagation in fiber, which includes dispersion and the nonlinear index of refraction. In Chapter 2 we also introduce two examples of all-optical switches, which are useful for optical pulse regeneration.

Chapter 3 reviews previous work in all-optical switching, specifically, the NOLM and the SLALOM. Chapter 3 also lists some important qualities of a good regenerator design and summarizes the disadvantages of the NOLM and the SLALOM in regeneration.

Chapter 4 uses much of the theory developed in Chapter 2 to show how one can measure the dispersion and nonlinear index of refraction of optical fiber. Both of these parameters are important in choosing fiber for the folded UNI regenerator design. This chapter also presents a numerical model to simulate pulse propagation in fiber.

Chapter 5 introduces the design of the folded UNI and gives the experimental setup used to test the folded UNI. The chapter presents data on the switching window, which is important in showing the ability of the folded UNI to correct timing jitter in an incoming network data stream that is to be regenerated. In Section 5.4 we discuss the results of a bit error rate test on the folded UNI. Finally, Chapter 5 presents results on the folded UNI's application to a regenerative XOR all-optical logic gate.

Chapter 6 summarizes this thesis and makes suggestions for future work.

Chapter 2

Physics of All-Optical Switching

The all-optical switches presented in this thesis are various types of fiber interferometers. This chapter intoduces the physical principles that describe the behavior of these fiber interferometer switches. The first section of this chapter introduces the intensity-dependent index of refraction, the physical principle on which most all-optical switches and many all-optical regenerators are based. The intensity-dependent index of refraction can induce a phase shift in an optical pulse. From this simple principle, one can create a fiber interferometer. The second section of this chapter describes a fiber switch, the ultrafast nonlinear interferometer (UNI). The final sections introduce the important physical properties of fiber and of the various nonlinear media that are relevant to the problem of all-optical regeneration.

2.1 The Intensity-Dependent Index of Refraction

The intensity-dependent index of refraction is given by

$$n = n_0 + n_2 I \tag{2.1}$$

where n_0 is the linear index, n_2 is the nonlinear index, and I is the intensity of the electric field envelope. This intensity-dependent index is a consequence of the nonlinear interaction of the optical field with the medium of propagation. More

specifically, in SI units, we have

$$\mathbf{D}(\mathbf{r},t) = \epsilon_0 \mathbf{E}(\mathbf{r},t) + \mathbf{P}(\mathbf{r},t) \tag{2.2}$$

where $\mathbf{D}$ is the electric displacement, $\mathbf{E}$ is the electric field, and ϵ_0 is the permittivity of free space. The nonlinear effects are included in $\mathbf{P}$:

$$\mathbf{P}(\mathbf{r},t) = \epsilon_0 \chi^{(1)} \cdot \mathbf{E}(\mathbf{r},\mathbf{t}) + \mathbf{P_{NL}}(\mathbf{r},\mathbf{t}). \tag{2.3}$$

$\chi^{(1)}$, the linear susceptibility, is a matrix that describes propagation for low optical intensities. $\mathbf{P_{NL}}$ is the nonlinear polarization

$$\begin{aligned} \mathbf{P_{NL}}(\mathbf{r},t) &= \epsilon_0 \{\chi^{(2)} : \mathbf{EE} + \chi^{(3)} \vdots \mathbf{EEE} + \cdots\} \\ &= \mathbf{P}^{(2)}(\mathbf{r},t) + \mathbf{P}^{(3)}(\mathbf{r},t) + \cdots \end{aligned} \tag{2.4}$$

where $\chi^{(2)}$ is the second order susceptibility and $\chi^{(3)}$ is the third order susceptibility. They are second and third order tensors respectively. Notice that Equations 2.3 and 2.4 express each of the cartesian components of $\mathbf{P}(\mathbf{r},t)$ as a multivariable Taylor series expansion in the three cartesian components of $\mathbf{E}(\mathbf{r},t)$, where the constant term of that expansion is zero [19]. That is, $\mathbf{P}(\mathbf{r},t)$ is a nearly arbitrary function of $\mathbf{E}(\mathbf{r},t)$ where $\mathbf{P} = 0$ if $\mathbf{E} = 0$. Assuming the pulses are propagating down a one-dimensional wave guide in the z direction, $\mathbf{r}$ becomes simply z. To do these calculations, we now assume that we can expand $\mathbf{E}(z,t)$ in a Fourier series as

$$\mathbf{E}(z,t) = \sum_n \tilde{\mathbf{E}}(\omega_n) e^{i(\beta_n z - \omega_n t)} \tag{2.5}$$

In Equation 2.5, we have assumed that the waves are propagating in the z direction down a waveguide. We also expand the polarization in a Fourier series to get

$$\mathbf{P}^{(b)}(\mathbf{r},t) = \sum_n \tilde{\mathbf{P}}^{(b)}(\omega_n) e^{-i\omega_n t} \tag{2.6}$$

where the $\mathbf{r}$ dependence of $\tilde{\mathbf{P}}^{(b)}$ has been supressed for notational convenience. Because $\mathbf{E}$ and $\mathbf{P}$ are real, $\tilde{\mathbf{E}}(\omega_n) = \tilde{\mathbf{E}}^*(-\omega_n)$ and $\tilde{\mathbf{P}}^{(b)}(\omega_n) = \tilde{\mathbf{P}}^{(b)*}(-\omega_n)$. The ith component of $\tilde{\mathbf{P}}^{(2)}$ is given by

$$\tilde{P}_i^{(2)}(\omega_n + \omega_m) = \sum_{jk} \sum_{(nm)} \chi_{ijk}^{(2)}(\omega_n + \omega_m; \omega_n, \omega_m) \tilde{E}_j(\omega_n) \tilde{E}_k(\omega_m) e^{i(\beta_n + \beta_m)z} \tag{2.7}$$

where i, j, and k can be any of the cartesian components of the field, x, y, and z. $\tilde{E}_j(\omega_n)$ is the j vector component of $\tilde{\mathbf{E}}(\omega_n)$ of Equation 2.5. The notation (nm) requires that the sum be performed over ω_n and ω_m such that $\omega_m + \omega_n$ remains at a fixed value no matter the values of ω_n and ω_m. More generally, the expression for $\tilde{\mathbf{P}}_i^{(b)}$ is given by

$$\begin{aligned} \tilde{P}_i^{(b)}(\omega_n + \omega_m + \cdots) = \sum_{jk\cdots} \sum_{(nm\cdots)} \chi_{ijk\ldots}^{(b)}(\omega_n + \omega_m + \cdots; \omega_n, \omega_m, \cdots) \cdot \\ [\tilde{E}_j(\omega_n) \tilde{E}_k(\omega_m) \cdots] \cdot e^{i(\beta_n + \beta_m + \cdots)z}. \end{aligned} \tag{2.8}$$

For a more thorough and similar description of the nonlinear polarization, see [20].

Now we show how the nonlinear polarization yields the intensity dependent index of refraction. We assume a medium where the only significant susceptibilities are $\chi^{(1)}$ and $\chi^{(3)}$. This assumption is reasonable in the silica glass of optical fibers, where $\chi^{(2)}$ is zero because of the amorphous nature of SiO_2. To begin, we consider the problem of two interacting plane waves at different optical frequencies. We simplify the problem by first assuming that the fields are copolarized along the x axis:

$$\mathbf{E}_1(z,t) = \tilde{\mathbf{E}}(\omega_1) e^{-i\omega_1 t} + c.c. \text{ with } \tilde{\mathbf{E}}(\omega_1) = \hat{x} \tilde{E}_x(\omega_1) e^{i\beta_1 z} \tag{2.9}$$

$$\mathbf{E}_2(z,t) = \tilde{\mathbf{E}}(\omega_2) e^{-i\omega_2 t} + c.c. \text{ with } \tilde{\mathbf{E}}(\omega_2) = \hat{x} \tilde{E}_x(\omega_2) e^{i\beta_2 z} \tag{2.10}$$

where $c.c.$ denotes the complex conjugate, and ω_1 and ω_2 are parameters for $\tilde{\mathbf{E}}$ rather than variables on which $\tilde{\mathbf{E}}$ is functionally dependent. We assume that $\mathbf{E}_1$ is much more intense than $\mathbf{E}_2$. Let us call $\mathbf{E}_1$ the pump and $\mathbf{E}_2$ the probe.

Equation 2.2 becomes, in the Fourier domain,

$$\tilde{\mathbf{D}}(z,\omega) = \epsilon_0 \tilde{\mathbf{E}}(z,\omega) + \tilde{\mathbf{P}}(z,\omega) \tag{2.11}$$

We would like to calculate the effect of the pump on the probe. Thus, we are interested in calculating $\tilde{\mathbf{P}}^{(3)}(\omega_2)$, which is the nonlinear polarization of the component of $\tilde{\mathbf{D}}$ at frequency ω_2. The ith component of $\tilde{\mathbf{P}}^{(3)}(\omega)$ is given by

$$\begin{aligned}\tilde{P}_i^{(3)}(\omega = \omega_n + \omega_m + \omega_r) = \sum_{jkl} \sum_{(nmr)} \chi_{ijkl}^{(3)}(\omega_n + \omega_m + \omega_r; \omega_n, \omega_m, \omega_r) \\ \tilde{E}_j(\omega_n)\tilde{E}_k(\omega_m)\tilde{E}_l(\omega_r)e^{i(\beta_n+\beta_m+\beta_r)z}.\end{aligned} \tag{2.12}$$

If we substitute in ω_2 for $\omega_n + \omega_m + \omega_r$ we can calculate $\tilde{\mathbf{P}}^{(3)}(\omega_2)$:

$$\begin{aligned}\tilde{P}_i^{(3)}(\omega_2) = \sum_{jkl} \sum_{(nmr)} \chi_{ijkl}^{(3)}(\omega_2 = \omega_n + \omega_m + \omega_r; \omega_n, \omega_m, \omega_r) \\ \tilde{E}_j(\omega_n)\tilde{E}_k(\omega_m)\tilde{E}_l(\omega_r)e^{i(\beta_n+\beta_m+\beta_r)z}.\end{aligned} \tag{2.13}$$

Four facts help us evaluate Equation 2.13.

1. The sum over (nmr) is covered in only six cases, assuming that $\omega_1 \neq \omega_2$. For example, $\omega_n = \omega_2$, $\omega_m = \omega_1$, and $\omega_r = -\omega_2$. The other 5 cases are just the other possible distinct assignments of $\pm\omega_{1,2}$ to $\omega_{n,m,r}$ that still yield $\omega_n + \omega_m + \omega_r = \omega_2$.

2. Because the $\mathbf{E}$ of Equation 2.5 is real, $\tilde{\mathbf{E}}(-\omega_1)$ must equal $\tilde{\mathbf{E}}^*(\omega_1)$. Thus, $\tilde{\mathbf{E}}(\omega_1)\tilde{\mathbf{E}}(-\omega_1)$ equals $|\tilde{\mathbf{E}}(\omega_1)|^2$.

3. Because silica is an isotropic medium, $\chi_{ijkl}^{(3)}$ must be zero if the indices, $ijkl$, take on values that repeat an odd number of times. For example, $\chi_{xyyy}^{(3)} = \chi_{xyyz}^{(3)} = 0$ becuase in the first case x and y are repeated an odd number of times, and in the second x and z are repeated an odd number of times. If, for example, $\chi_{xyyy}^{(3)} \neq 0$, then a field in the $+y$ direction would create a response in the $+x$ direction. But the symmetry of an isotropic medium implies that there is no reason there should be a response in the $+x$ direction rather than the $-x$

direction. Moreover, because both $\mathbf{E}_1$ and $\mathbf{E}_2$ are polarized on the x axis, the sum over jkl in Equation 2.13 is nonzero only when jkl are all x. Therefore, we are concerned only with $\chi^{(3)}_{ixxx}$, which is nonzero only when $i = x$. So, the only relevant nonzero $\chi^{(3)}_{ijkl}$ is $\chi^{(3)}_{xxxx}$, and, for simplicity, we drop the subscripts.

4. The intrinsic permutation property states that $\chi^{(3)}_{ijkl}(\omega_n + \omega_m + \omega_r; \omega_n, \omega_m, \omega_r) = \chi^{(3)}_{ijlk}(\omega_n + \omega_r + \omega_m; \omega_n, \omega_r, \omega_m)$. This equation is true because the names of the subscripts themselves are arbitrary and, therefore, interchangeable, although Equation 2.13 implies that a change in the order of ω's requires a corresponding change in the order of the subscripts of $\chi^{(3)}$.

These four points imply that all $\chi^{(3)}$ tensor values relevant to this problem have the subscripts $xxxx$ and have some ordering of ω_1, $-\omega_1$, and ω_2, and thus are all equal. Therefore, we drop all subscripts and arguments of $\chi^{(3)}$ to obtain

$$\tilde{\mathbf{P}}_{NL}(\omega_2) = \hat{x}\tilde{P}^{(3)}_x(\omega_2) = \hat{x}6\epsilon_0\chi^{(3)}|\tilde{E}_x(\omega_1)|^2\tilde{E}_x(\omega_2)e^{i\beta_2 z} \tag{2.14}$$

where $\tilde{E}_x$ is defined in Equations 2.9 and 2.10. Substituting Equation 2.3 into Equation 2.2 and taking it into the Fourier domain, we have

$$\tilde{\mathbf{D}}(\mathbf{r}, \omega) = \epsilon_0\tilde{\mathbf{E}}(\mathbf{r}, \omega) + \epsilon_0\chi^{(1)} \cdot \tilde{\mathbf{E}}(\mathbf{r}, \omega) + \tilde{\mathbf{P}}_{\mathbf{NL}}(\mathbf{r}, \omega). \tag{2.15}$$

We are interested in the component of the field at the probe frequency ω_2 so we consider Equation 2.15 only at ω_2:

$$\tilde{\mathbf{D}}(\mathbf{r}, \omega_2) = \epsilon_0\tilde{\mathbf{E}}(\mathbf{r}, \omega_2) + \epsilon_0\chi^{(1)} \cdot \tilde{\mathbf{E}}(\mathbf{r}, \omega_2) + \tilde{\mathbf{P}}_{\mathbf{NL}}(\mathbf{r}, \omega_2). \tag{2.16}$$

We substitute Equation 2.14 and the positive frequency component of Equation 2.10 into equation 2.16. All of the vectors are nonzero only for their x components, so we drop the vector notation

$$\tilde{D}(z, \omega_2) = [\epsilon_0\tilde{E}_x(\omega_2) + \epsilon_0\chi^{(1)}\tilde{E}_x(\omega_2) + 6\epsilon_0\chi^{(3)}|\tilde{E}_x(\omega_1)|^2\tilde{E}_x(\omega_2)]e^{i\beta_2 z}. \tag{2.17}$$

In Equation 2.17, $\tilde{D}(\omega_2)$ depends on both the pump field at carrier frequency ω_1 and the probe field at carrier frequency ω_2. We can rewrite Equation 2.17 as

$$\tilde{D}(z,\omega_2) = \epsilon_0(1+\chi^{(1)}+6\chi^{(3)}|\tilde{E}_x(\omega_1)|^2)\tilde{E}_x(\omega_2)e^{i\beta_2 z} = \epsilon_{eff}\tilde{E}_x(\omega_2)_x e^{i\beta_2 z} \tag{2.18}$$

where

$$\epsilon_{eff} \equiv \epsilon_0(1+\chi^{(1)}+6\chi^{(3)}|\tilde{E}_x(\omega_1)|^2). \tag{2.19}$$

By the definition of the index of refraction, we have $n^2 = c^2\mu\epsilon_{eff}$. In a nonmagnetic medium, this equation reduces to

$$n^2 = \frac{\epsilon_{eff}}{\epsilon_0}. \tag{2.20}$$

In Equation 2.18, we see that $|\tilde{E}_x(\omega_1)|^2$ implies an intensity-dependent refractive index. By Equation 2.9, the pump wave is given by $\mathbf{E}_1(z,t) = \hat{x}[\tilde{E}_x(\omega_1)e^{i(\beta_1 z-\omega_1 t)}+c.c.]$ so that the time averaged electric field intensity is given by

$$\langle|\mathbf{E}_1(z,t)|^2\rangle = 2\tilde{E}_x(\omega_1)\tilde{E}_x^*(\omega_1) = 2|\tilde{E}_x(\omega_1)|^2. \tag{2.21}$$

Thus, assuming a linear relationship between the index of refraction and the electric field intensity, we have

$$n = n_0 + 2n_2|\tilde{E}_x(\omega_1)|^2. \tag{2.22}$$

We substitute Equations 2.22 and 2.19 into Equation 2.20 to get

$$[n_0 + 2n_2|\tilde{E}_x(\omega_1)|^2]^2 = 1+\chi^{(1)}+6\chi^{(3)}|\tilde{E}_x(\omega_1)|^2. \tag{2.23}$$

The left side of Equation 2.23 equals

$$n_0^2 + 4n_0n_2|\tilde{E}_x(\omega_1)|^2 + 4n_2^2|\tilde{E}_x(\omega_1)|^4 \approx n_0^2 + 4n_0n_2|\tilde{E}_x(\omega_1)|^2 \tag{2.24}$$

where we assume that $n_2 \ll n_0$. If we substitute the approximation of Equation 2.24 into Equation 2.23, then we have

$$n_0^2 + 4n_0 n_2 |\tilde{E}_x(\omega_1)|^2 = 1 + \chi^{(1)} + 6\chi^{(3)} |\tilde{E}_x(\omega_1)|^2. \tag{2.25}$$

From Equation 2.25, we find that

$$n_0 = \sqrt{1 + \chi^{(1)}(\omega_2)} \tag{2.26}$$

and that

$$n_2 = \frac{3\chi^{(3)}(\omega_1)}{2n_0}. \tag{2.27}$$

Remember, that in this derivation it was assumed that the pump was much more intense than the probe. Therefore, the effect of the pump on the index of refraction seen by the probe was much more significant than the effect of the probe on the same index of refraction. This change in index of refraction changed the optical path length for the probe, in effect adding a phase shift to the probe. The case we studied in this section demonstrated the phase shift induced on a probe by a very intense pump. This effect, where a signal of one carrier frequency induces a phase shift in a signal of a different carrier frequency is called cross-phase modulation (XPM) [21]. Nonetheless, a probe signal, even in the absense of a pump signal, can induce a phase shift in itself. This effect is called self-phase modulation (SPM). In this thesis, we shall limit our discussion to the case of an intense pump with a probe too weak to induce a noticeable phase shift in itself.

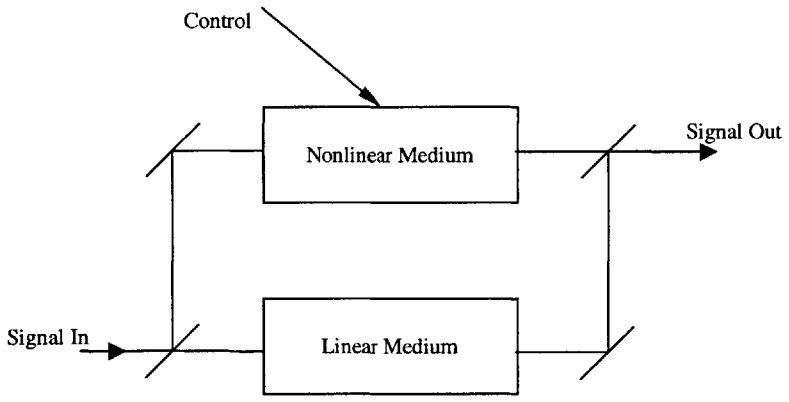

Figure 2-1: Nonlinear Mach-Zehnder interferometer.

2.2 Examples of All-Optical Switches

2.2.1 The Nonlinear Mach-Zehnder Interferometer

The nonlinear index of refraction has been used in a number of optical interferometers, including the nonlinear optical loop mirror (NOLM) and the ultrafast nonlinear interferometer (UNI). Before describing the operation of the UNI in Section 2.2.2, we first consider the simple Mach-Zehnder interferometer (see Figure 2-1). In the nonlinear Mach-Zehnder interferometer the incoming signal pulses are split by a 50/50 splitter into two paths. One path is purely linear and nondispersive (for example, it could simply be free space). The other path contains a nonlinear medium, perhaps an optical fiber, which has an intensity-dependent index of refraction. Suppose that the signal pulses have a carrier wavelength of λ_0. Also, let L_l be the length of the linear medium and let L_{nl} be the length of the nonlinear medium. If the lower path contains only linear material with an index of refraction equal to n_0^l, then the linear medium's optical path length is $n_0^l L_l$. The upper path contains a nonlinear medium, and its index of refraction is given by $n_0^{nl} + n_2 I_c$, where n_0^{nl} is the linear index of refraction, n_2 is the nonlinear index of refraction, and I_c is the intensity of the control pulse that temporally overlaps the signal pulse. The optical path length of the nonlinear medium is $(n_0^{nl} + n_2 I_c) L_{nl}$.

We would like to calculate the relative phase shift induced between the signal

pulses in the two arms of the interferometer. Taking the difference of the two optical path lengths, we have

$$n_0^l L_l - (n_0^{nl} + n_2 I_c) L_{nl}. \tag{2.28}$$

Dividing by $\lambda_0/2\pi$ gives us the relative phase shift:

$$\Phi_{rel} = \frac{2\pi}{\lambda_0}[n_0^l L_l - (n_0^{nl} + n_2 I_c) L_{nl}]. \tag{2.29}$$

At the output, the signal pulses in the two optical paths are recombined. If, at the input, we have a signal with a field given by $\mathbf{E}_s = \hat{x}(E_s e^{-i\omega_0 t} + c.c.)$ then at the output we have the field

$$E_{out} = \frac{1}{2}(E_s e^{-i\omega_0 t} + c.c.) + \frac{1}{2}(E_s e^{-i\omega_0 t - i\Phi_{rel}} + c.c.) \tag{2.30}$$

where each term in Equation 2.30 is the field from one of the two arms. From this equation, we calculate the time averaged intensity:

$$\begin{aligned} I_{out} &\propto \langle |E_{out}|^2 \rangle \\ &= \langle |(E_s e^{-i\omega_0 t} e^{-i\frac{\Phi_{rel}}{2}} \cos\Big(\frac{\Phi_{rel}}{2}\Big) + c.c.|^2 \rangle \\ &= 2|E_s|^2 \cos^2\Big(\frac{\Phi_{rel}}{2}\Big) \\ &\propto I_{in} \cos^2\Big(\frac{\Phi_{rel}}{2}\Big). \end{aligned} \tag{2.31}$$

Because Φ_{rel} is linearly related to I_c, we can control the phase shift between the pulses in the two arms to cause constructive or destructive interference at the output. The output intensity, in normalized units, is plotted against the relative phase difference in Figure 2-2.

We can easily apply this interferometer to all-optical switching. The presence or absence of the control pulse can determine whether or not a signal pulse is transmitted. In the absense of control pulses, both arms are linear. Suppose we adjust L_l and L_{nl} so that, when no control pulses are present, a π relative phase shift is added between

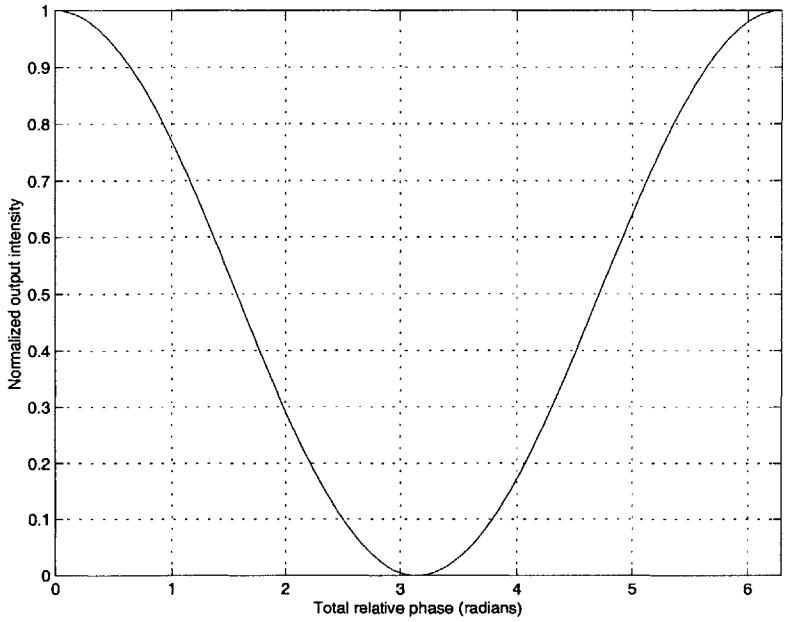

Figure 2-2: Normalized output intensity of the nonlinear Mach-Zehnder interferometer versus Φ_{rel}.

the signal pulses in the two arms. The pulses destructively interfere at the output and no signal pulses are transmitted. On the other hand, when control pulses are present and when they are intense enough to induce another π phase shift between the pulses in the two arms, the signal pulses in the two arms constructively interfere at the output and are transmitted.

Although simple, the nonlinear Mach-Zehnder design has several problems. First, there may be undesirable and uncontrollable asymetries between the two arms. If the carrier wavelength is 1550 nm, then even small variations in temperature between the two arms could affect the difference in their optical path lengths enough to move the bias point of the switch from ON to OFF. Even acoustic vibration from ambient sound could noticeably affect the switch's performance. Active electronic control of the path length could stabilize these asymetric variations, but it adds hardware and complexity. Another problem with the nonlinear Mach-Zehnder interferometer arises when the medium used in the nonlinear arm does not have an instantaneous response. The ultrafast nonlinear interferometer discussed in Section 2.2.2 uses a semiconductor

based nonlinear medium that is described by several effects that range in speed from several femtoseconds to several nanoseconds [22]. The long carrier density relaxation will affect switching if the nonlinear response exceeds one bit length. A control pulse might then induce a phase shift both in the pulse it temporally overlaps and in a subsequent pulse. N. S. Patel wrote simulations showing distortion of a 40 Gbit/s pulse stream due to long-lived index changes in a semiconductor based nonlinear Mach-Zehnder interferometer [23].

2.2.2 The Ultrafast Nonlinear Interferometer (UNI)

Many of the problems with the nonlinear Mach-Zehnder interferometer are mitigated if the switch design is changed to the ultrafast nonlinear interferometer shown in Figure 2-3. The UNI is a single arm interferometer (SAI). Rather than having signal pulses propagate through two separate arms, the signal pulse is temporally separated into two pulses, which propagate down a single arm. Therefore, the thermal and acoustic variations that limite the nonlinear Mach-Zehnder interferometer's performance do not affect the UNI. The UNI has been demonstrated to switch at rates up to 100 Gbit/s without the active control that would be necessary in the Mach-Zehnder [24].

The UNI can modulate the data pattern of the control pulses onto the signal pulses. The signal pulses enter at the left of the UNI. The first polarization controller (PC1) is set so that each signal pulse is linearly polarized and passes maximally through the polarizer (PZR1). A length of birefringent fiber, aligned at 45 degrees to the linearly polarized signal pulses, separates each signal pulse into two equally-intense temporally-separated orthogonal polarizations. The control pulses, of a different wavelength than the signal pulses, are coupled into the UNI in a 50/50 coupler. They temporally overlap one of the two signal pulse polarizations. These control pulses will be used to switch the signal pulses ON or OFF. The semiconductor optical amplifier (SOA) is used as the nonlinear medium in the UNI. In the SOA, a control pulse induces a phase shift in the signal pulse polarization that it temporally overlaps. The two polarization components of the signal pulse are recombined tem-

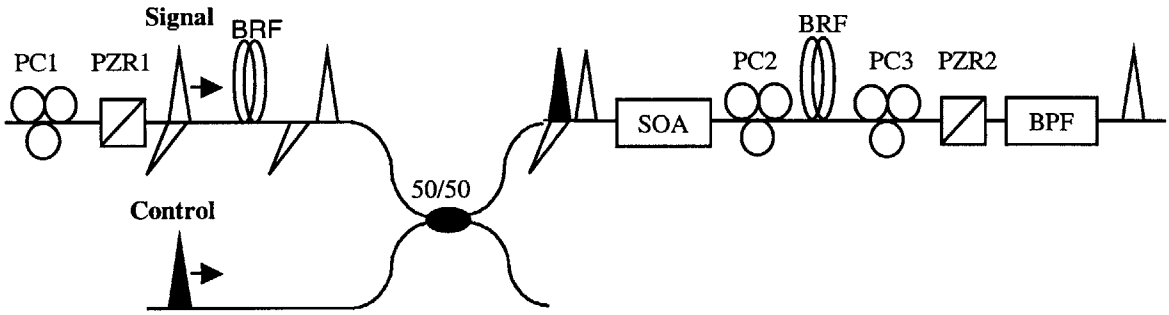

Figure 2-3: The Ultrafast Nonlinear Interferometer (UNI) separates the signal pulse into orthogonal components. The control pulse induces a phase shift in one component; both components are then interfered at PZR2. The components are polarization controllers 1, 2, and 3 (PC1, PC2, and PC3), polarizers 1 and 2 (PZR1 and PZR2), birefringent fiber (BRF), semiconductor optical amplifier (SOA), and band pass filter (BPF).

porally in the second length of cross-spliced birefringent fiber and then interfered in the polarizer (PZR2). The control pulses are then filtered out in the band pass filter (BPF).

SOAs provide a very high nonlinear index of refraction, with n_2 on the order of 10^{-16} m^2/W [22]. In contrast, optical fibers typically have an n_2 on the order of 10^{-20} m^2/W [21]. In optical switching applications, the SOA's high nonlinear index of refraction can be an important advantage. At 100 Gbit/s, pulses are separated in time by only 10 ps. In an SOA, which can be less than 1 mm long, only one or two pulses will be propagating in the nonlinear medium at any point in time. If we use fiber as the nonlinear medium, then its low nonlinear index force would require hundreds of meters of fiber to acheive the desired nonlinear phase shift. A 500 m length of fiber, when used as the nonlinear medium in an all-optical switch, creates a logical latency of 250,000 bits simultaneously propagating in the fiber. Although this latency could cause problems in many applications of all-optical switching, it does not necessarily affect regeneration.

2.3 Relevant Physical Properties

In this section, we will discuss several physical properties of optical fiber that are relevant to all-optical nonlinear switching. First, we will discuss chromatic dispersion and its effects on the propagation of Gaussian pulses in optical fibers. Then, we will derive the nonlinear wave equation used to describe pulse propagation in an optical fiber, the nonlinear Schrödinger equation (NLS). Last, we will discuss loss and birefringence and their role in all-optical switching and regeneration.

2.3.1 Dispersion

A short optical pulse contains many frequencies. In fact, the shorter the pulse is in time, the wider it is in the frequency spectrum. In a dispersive medium, each frequency component propagates down the fiber at a different speed, leading to pulse distortion. These dispersive effects are very important in deciding which nonlinear medium to select for an all-optical switch or regenerator. We can express these dispersive effects mathematically by defining a frequency dependent propagation constant, $\beta(\omega)$. After propagating a distance z, the component of the field at ω, $\tilde{E}(\omega)$, receives a phase shift of $\beta(\omega)z$ to become $\tilde{E}(\omega)e^{i\beta(\omega)z}$.

We consider first the case of the dispersion of a Gaussian pulse, because this problem can be solved analytically. We expand $\beta(\omega)$ in a Taylor series around the carrier frequency ω_0:

$$\beta(\omega) = \beta_0 + \beta_1(\omega - \omega_0) + \frac{1}{2}\beta_2(\omega - \omega_0)^2 + \cdots . \tag{2.32}$$

The constants β_n in 2.32 are equal to $\frac{\partial^n \beta}{\partial \omega^n}|_{\omega=\omega_0}$. β_0 is an initial and constant phase shift on the pulse. β_1 is the group delay and determines the velocity of the center of the Gaussian pulse envelope. β_2 is called the group velocity dispersion (GVD) and, as we will see later, causes the pulse width to increase. We write the electric field for

the pulse at $z = 0$ as

$$E(z=0,t) = E_0 \exp\left[\frac{-2t^2 \ln 2}{T_0^2}\right] e^{-i\omega_0 t} \tag{2.33}$$

where we have dropped the *c.c.* because dispersion is a linear effect, making the *c.c.* term is unnecessary. This optical pulse's full width at half its maximum intensity (FWHM) is

$$T_{FWHM} = T_0. \tag{2.34}$$

The propagation of the Gaussian pulse in a dispersive medium is easily solved in the frequency domain, so we calculate the Fourier transform of this field:

$$\begin{aligned} \tilde{E}(z=0,\omega) &= \frac{1}{2\pi}\int_{-\infty}^{\infty} E(z=0,t)e^{-i\omega t}\,dt \\ &= \frac{1}{2\pi}\int_{-\infty}^{\infty} E_0 \exp\left[\frac{-2t^2 \ln 2}{T_0^2}\right] e^{-i(\omega-\omega_0)t}\,dt. \end{aligned} \tag{2.35}$$

We can easily solve this equation by completing the square in the exponent and consulting standard integral tables [25]:

$$\tilde{E}(z=0,\omega) = \frac{T_0}{2\sqrt{2\pi \ln 2}} \exp\left[\frac{-(\omega-\omega_0)^2 T_0^2}{8 \ln 2}\right]. \tag{2.36}$$

Thus, the spectrum of the Gaussian pulse is another Gaussian pulse in ω with a spectral intensity FWHM of

$$\Delta\omega_{FWHM} = \frac{4 \ln 2}{T_0} \tag{2.37}$$

In a purely dispersive medium, in which nonlinear effects are negligible, the field,

after propagating a distance L, is given by

$$\begin{aligned}\tilde{E}(z=L,\omega) &= \tilde{E}(z=0,\omega)e^{i\beta(\omega)L} \\ &= \tilde{E}(z=0,\omega)e^{i[\beta_0+\beta_1(\omega-\omega_0)+\frac{1}{2}\beta_2(\omega-\omega_0)^2+\cdots]L}\end{aligned} \tag{2.38}$$

where we have substituted Equation 2.32 into $\beta(\omega)$. We neglect terms higher than β_2 because in fiber β_3 only becomes significant for very short pulses. Then we have from Equation 2.38

$$\begin{aligned}\tilde{E}(z=L,\omega) &= \tilde{E}(z=0,\omega)e^{i[\beta_0+\beta_1(\omega-\omega_0)+\frac{1}{2}\beta_2(\omega-\omega_0)^2]L} \\ &= \frac{T_0}{2\sqrt{2\pi\ln 2}}\exp\left[-\left(\frac{T_0^2}{8\ln 2}-\frac{i\beta_2 L}{2}\right)(\omega-\omega_0)^2\right. \\ &\left.+\,i\beta_1 L(\omega-\omega_0)+i\beta_0 L\right].\end{aligned} \tag{2.39}$$

Equation 2.39 is still a Gaussian pulse with the same spectral intensity FWHM given in Equation 2.37. So the spectrum of the pulse has the same envelope, but now has a phase shift equal to $\beta(\omega)L$. We take the inverse Fourier transform of Equation 2.39 to see how the pulse evolves in time at $z = L$:

$$\begin{aligned}E(z=L,t) &= \int_{-\infty}^{\infty} E(z=L,\omega)e^{i\omega t}\,d\omega \\ &= \frac{T_0}{2\sqrt{2\pi\ln 2}}e^{i(\beta_0 L-\omega_0 t)}e^{\phi}\exp\left[\frac{-(t-\beta_1 L)^2T_0^2}{2\ln 2\left(\frac{T_0^4}{4(\ln 2)^2}+4\beta_2^2L^2\right)}\right]\end{aligned} \tag{2.40}$$

where ϕ is a phase factor given by

$$\phi(t,z=L) = \frac{-(\beta_1^2 L-t)^2}{4\left[\frac{T_0^2}{8\ln 2}-i\frac{\beta_2}{2}\right]}. \tag{2.41}$$

As can be seen in Equation 2.40, the pulse is still a Gaussian, although a new phase factor is present, and the pulse's width has changed. We now make several important definitions related to the coefficients, β_n, in the propagation constant that will help us to understand the physical significance of each coefficient. First, the phase velocity

of the pulse, $v_\phi = \omega_0/\beta_0$, is the speed at which the carrier frequency propagates through the medium. Second, the group velocity, $v_g = 1/\beta_1$ is the speed at which the pulse envelope propagates through the medium. Last, we call β_2 the group velocity dispersion, which is related to the rate at which the pulse broadens in a second order dispersive medium.

We can justify the definition for the phase velocity, v_ϕ, by looking at the factor $e^{i(\beta_0 z - \omega_0 t)}$ of Equation 2.40 and noticing that a point of constant phase exists at $\beta_0 z - \omega_0 t = 0$, so $v_\phi = dz/dt = \omega_0/\beta_0$. This exponential factor is the underlying carrier freqency. We can justify the other definitions by looking at the argument of the exp in Equation 2.40:

$$\frac{-(t-\beta_1 z)^2 T_0^2}{2\ln 2\left(\frac{T_0^4}{4(\ln 2)^2} + 4\beta_2^2 z^2\right)}. \tag{2.42}$$

To justify the definition of the group velocity, we note that the center of the pulse exists where $t - \beta_1 z = 0$ and so, $v_g = dz/dt = 1/\beta_1$. To justify the group velocity dispersion, we note that β_2 influences the pulse width. A larger β_2 implies a larger denominator in Equation 2.42 and, therefore, a wider gaussian in Equation 2.40. It is also useful to calculate the intensity FWHM, as we did in Equation 2.34:

$$T_{FWHM} = \frac{2\ln 2}{T_0}\sqrt{\frac{T_0^4}{4(\ln 2)^2} + 4\beta_2^2 z^2} \tag{2.43}$$

In Figure 2-4 we plot a Gaussian pulse propagating in a second order dispersive medium. As can be seen in the plot and in Equation 2.40, the pulse broadens and its peak intensity drops as the pulse propagates farther in fiber. This distortion, caused by the second-order dispersion, has a significant effect on the choice of nonlinear medium for the all-optical switch or regenerator. For example, the decreased peak intensity of the pulse reduces the effect of the nonlinear index of refraction, which is the principle on which all switches in this thesis are based. The lower intensity causes a smaller phase shift, forcing the use of a longer nonlinear medium.

Dispersion causes other problems as well. In the UNI described in Section 2.2.2,

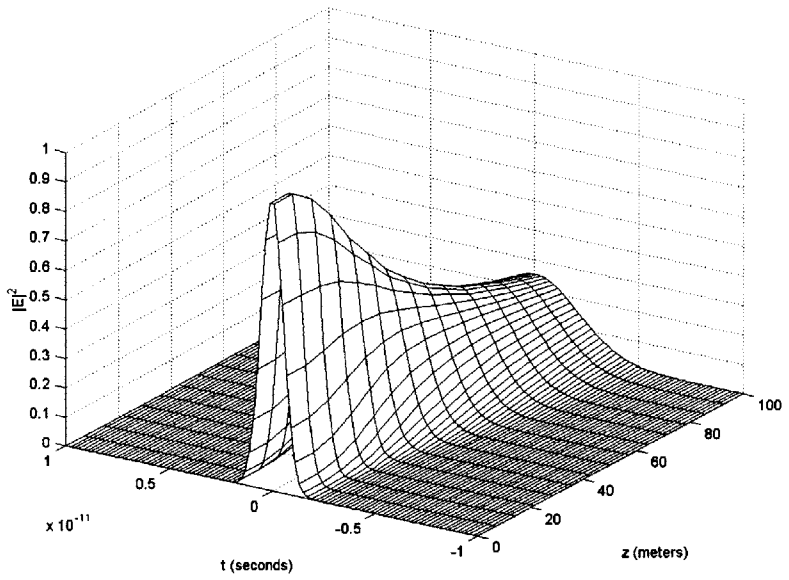

Figure 2-4: Dispersion induced broadening of a Gaussian pulse in an optical fiber.

the signal pulses are separated temporally into two orthogonal polarizations. Ideally, the separation is larger than the pulse width. If it is not, as may happen because of dispersive broadening, the two orthogonally polarized pulses may induce unwanted phase shifts in each other. In the UNI, this problem is solved by using an SOA with high nonlinearity and a short interaction length in order to decrease the dispersive effects. But if we consider using optical fiber as the nonlinear medium, as we will later in this thesis, we must use longer interaction lengths. The design of any fiber based all-optical switch must account for the long interaction lengths and dispersive effects of the fiber.

2.3.2 The Nonlinear Schrödinger Equation

In many cases in fiber optics, the dominant physical effects are second-order dispersion and the nonlinear index of refraction. Both of these effects are included in the nonlinear Schrödinger equation (NLS), a wave equation often used in modelling pulse propagation down an optical fiber. Here we provide an outline of the derivation of the NLS. For a more thorough development see Boyd [20].

First, we assume that the electric field can be represented as a slowly-varying envelope, $A(z,t)$:

$$E(z,t) = A(z,t)e^{i(\beta_0 z - \omega_0 t)} + c.c. \tag{2.44}$$

where we assume the wave propagates in the z direction with propagation constant $\beta_0 = \omega_0\sqrt{\mu_0\epsilon}$. As before, we define the Fourier transform as

$$\tilde{E}(z,\omega) = \frac{1}{2\pi}\int_{-\infty}^{\infty} E(z,t)e^{-i\omega t}\,dt. \tag{2.45}$$

The one-dimensional wave equation is

$$\frac{\partial^2 E}{\partial z^2} - \mu_0\frac{\partial^2 D}{\partial t^2} = 0. \tag{2.46}$$

Now we relate D and E by the constitutive relation

$$\tilde{D}(z,\omega) = \epsilon(\omega)\tilde{E}(z,\omega) \tag{2.47}$$

where the dielectric constant ϵ includes both the linear and nonlinear components. In the Fourier domain, Equations 2.46 and 2.47 yield

$$\frac{\partial^2 \tilde{E}}{\partial z^2} - \mu_0\epsilon(\omega)\omega^2\tilde{E} = 0. \tag{2.48}$$

We take the Fourier transform of Equation 2.44 and assume propagation in the $+z$ direction only to get

$$\begin{aligned}\tilde{E}(z,\omega) &= \tilde{A}(z,\omega-\omega_0)e^{i\beta_0 z} + \tilde{A}^*(z,-\omega-\omega_0)e^{-i\beta_0 z} \\ &\approx \tilde{A}(z,\omega-\omega_0)e^{i\beta_0 z}.\end{aligned} \tag{2.49}$$

Now we substitute Equation 2.49 into Equation 2.48, use the relation $\beta(\omega) = \omega\sqrt{\mu_0\epsilon}$,

and make the slowly varying envelope approximation (that is, $\partial^2 A/\partial z^2 = 0$), to get

$$2i\beta_0 \frac{\partial \tilde{A}}{\partial z} + (\beta^2 - \beta_0^2)\tilde{A} = 0. \tag{2.50}$$

We make another approximation, $\beta^2 - \beta_0^2 \approx 2\beta_0(\beta - \beta_0)$, and substitute it into Equation 2.50:

$$\frac{\partial \tilde{A}(z, \omega - \omega_0)}{\partial z} - i(\beta - \beta_0)A(\omega - \omega_0) = 0. \tag{2.51}$$

Now we approximate the propagation constant $\beta(\omega)$ with a truncated Taylor series that has an extra term, $\Delta\beta_{NL} \propto |A|^2$. This extra term accounts for the nonlinear index of refraction derived in Section 2.1:

$$\begin{aligned} \beta(\omega) &= \beta_0 + (\omega - \omega_0)\beta_1 + (\omega - \omega_0)^2\beta_2 + \Delta\beta_{NL} \\ &= \beta_0 + (\omega - \omega_0)\frac{1}{v_g(\omega_0)} - (\omega - \omega_0)^2 \frac{1}{v_g(\omega_0)} \frac{dv_g}{d\omega}|_{\omega_0} + n_2 I \frac{\omega_0}{c}. \end{aligned} \tag{2.52}$$

By using Equation 2.52, we account for dipsersion up to and including second-order dispersion and the nonlinear index of refraction. We substitute Equation 2.52 into 2.51 and take the inverse Fourier transform to get

$$\frac{\partial A}{\partial z} + \beta_1 \frac{\partial A}{\partial t} + \frac{1}{2} i\beta_2 \frac{\partial^2 A}{\partial t^2} - i\Delta\beta_{NL} A = 0. \tag{2.53}$$

We can make a transformation to a moving reference frame,

$$\tau = t - \beta_1 z \text{ and } U(z, \tau) = A(z, t), \tag{2.54}$$

to get

$$\begin{aligned} \frac{\partial U}{\partial z} &= -\frac{1}{2} i\beta_2 \frac{\partial^2 U}{\partial \tau^2} + i\Delta\beta_{NL} U \\ &= -\frac{1}{2} i\beta_2 \frac{\partial^2 U}{\partial \tau^2} + i\gamma |U|^2 U \end{aligned} \tag{2.55}$$

where we have used the fact that $\Delta\beta_{NL} \propto |U|^2$ and where γ is the nonlinear coefficient.

In Equation 2.55 the dispersion is expressed in the first term on the right side of the equation and the nonlinear phase modulation in the second term. The group delay, β_1, has fallen out of Equation 2.55 because the moving reference frame, given by $\tau = t - \beta_1 z$, moves with the group velocity of the pulse envelope. In this way, a pulse at carrier frequency ω_0 remains centered at $\tau = 0$. Zakharov and Shabat, in a monumental paper, discovered exact solutions to the NLS [26]. Nontheless, adding other terms to this equation to account for effects other than dispersion and the nonlinear index of refraction, render the equation unsolvable. Methods exist that solve these equations numerically, and one such method, the split-step Fourier method [21], generated the plot in Figure 2-4.

We can understand Equation 2.55 better by considering two cases: one in which γ is negligible and the other in which β_2 is negligible. If γ is negligible, we consider pulse propagation in the presence of dispersion alone:

$$\frac{\partial U}{\partial z} = -\frac{1}{2} i \beta_2 \frac{\partial^2 U}{\partial \tau^2}. \tag{2.56}$$

Equation 2.56 is solvable by taking its Fourier transform with respect to τ:

$$\frac{\partial \tilde{U}(z,\omega')}{\partial z} = \frac{1}{2} i \beta_2 \omega'^2 \tilde{U}(z,\omega') \tag{2.57}$$

which has the simple solution

$$\tilde{U}(z,\omega') = \tilde{U}(z=0,\omega') e^{\frac{i}{2}\beta_2 \omega'^2 z}. \tag{2.58}$$

Equation 2.58 describes the effects of second order dispersion, as we discussed in Section 2.3.1. Notice that the magnitude of $\tilde{U}(z,\omega')$ does not change. Nonetheless, the magnitude of the same function in the time domain, $U(z,\tau)$, broadens as the pulse propagates. Now, if β_2 is negligible, we consider pulse propagation in the presence of the nonlinearity alone.

$$\frac{\partial U}{\partial z} = i\gamma |U|^2 U. \tag{2.59}$$

Equation 2.59 is solved by considering U in polar form. We can easily verify the solution

$$U(z,\tau) = U(z=0,\tau)e^{i\gamma|U(z=0,\tau)|^2 z}. \tag{2.60}$$

From Equation 2.60, we see that a phase shift is added to the pulse that is proportional to γ and to the intensity of the pulse. This phase modulation is exactly what we expect from Section 2.1, where we discussed the nonlinear index of refraction. Also notice that, unlike the case above with just the dispersion term, the magnitude of the time domain pulse, $|U(z,\tau)|$, does not change. But, the magnitude of the same pulse in the frequency domain does change.

In single mode fiber (SMF), only the HE_{11} mode is excited. Nonetheless, if z is the direction of propagation, then the electric field can be considered polarized in either the x or y direction to good approximation. Thus, even single mode fiber supports two different modes of polarization [21]. Equation 2.55 does not account for two possible polarizations or loss in the fiber. To include these effects, we must use a coupled set of two partial differential equations:

$$\frac{\partial A_x}{\partial z} + \frac{i}{2}\beta_2\frac{\partial^2 A_x}{\partial \tau^2} + \frac{\alpha}{2}A_x = i\gamma\left(|A_x|^2 + \frac{2}{3}|A_y|^2\right)A_x + \frac{i\gamma}{3}A_x^* A_y^2 e^{-2i\Delta\beta z} \tag{2.61}$$

$$\frac{\partial A_y}{\partial z} + \frac{i}{2}\beta_2\frac{\partial^2 A_y}{\partial \tau^2} + \frac{\alpha}{2}A_y = i\gamma\left(|A_y|^2 + \frac{2}{3}|A_x|^2\right)A_y + \frac{i\gamma}{3}A_y^* A_x^2 e^{-2i\Delta\beta z}. \tag{2.62}$$

In these equations, α is the loss in the fiber, A_x and A_y are the electric field envelopes in the x and y directions, and $\Delta\beta = \beta_{1x} - \beta_{1y}$. So, these equations still account for dispersion and the nonlinear index of refraction, but also account for the fiber loss with α and linear birefringence with $\Delta\beta$. The linear birefringence causes each of the polarization components to propagate at different rates. In fact, microbending in the fiber causes the value of the birefringence to change randomly down the length of the fiber, causing the polarization to change quickly and unpredictably. This effect will be important in the design of all-optical regenerators. One last interesting point in

these equations is the nonlinear terms: $i\gamma\left(|A_x|^2+\frac{2}{3}|A_y|^2\right)A_x$ and $i\gamma\left(|A_y|^2+\frac{2}{3}|A_x|^2\right)A_y$. Notice that the intensity of A_y affects the index of refraction seen by A_x only two-thirds as strongly as the intensity of A_x itself. This weakening of the nonlinear index of refraction between orthogonally polarized fields will also affect regenerator design.

2.3.3 Effects of Loss and Pulse Envelope Shape on Phase Shift

In this thesis, we test all-optical regenerators that use silica optical fibers to provide the nonlinear medium. Optical fibers are inherently low-loss. The single mode fiber common in communications has a loss of about 0.25 dB/km at a wavelength of 1550 nm. As pulses propagate in fiber, their peak intensity falls and, therefore, the intensity-dependent index of refraction decreases. The all-optical switches we presented above all operate by inducing a π phase shift in one pulse with respect to another. These two pulses are then interfered at the output. Therefore, any loss increases the length of fiber or magnitude of optical power needed to induce that phase shift. Because longer fibers can entail more noise and distortion from effects like Rayleigh scattering and dispersion, we must consider carefully how substantial the loss is. We must also remember that each pulse has a nonuniform intensity, so low intensity wings on the pulse receive a smaller nonlinear phase shift than the high intensity peak.

Let $U(z,\tau)$ be the pulse envelope on a carier of frequency ω_0. As we did for dispersion in section 2.3.1, we expand the change in $|U(z,\tau)|^2$ as a Taylor series:

$$\frac{\partial}{\partial z}|U(z,\tau)|^2 = -\alpha|U(z,\tau)|^2 - \alpha_{NL}|U(z,\tau)|^2 + \cdots \tag{2.63}$$

The first term on the right accounts for linear gain or loss (α is positive for loss and negative for gain). In this thesis, we will neglect higher order nonlinear loss terms. α_{NL}, for example, accounts for nonlinear losses such as two-photon absorption, which can become significant with high optical powers [27].

If we neglect higher order losses, then we have

$$|U(z,\tau)|^2 = |U(z=0,\tau)|^2 e^{-\alpha z}. \tag{2.64}$$

First, let us consider how much longer a fiber with loss must be to induce the same self-phase modulation that would be induced in a lossless fiber. To simplify the problem, we assume that the pulse has uniform intensity. In a lossless fiber of length L_0, the self-phase modulation induced from Equation 2.60 is

$$\begin{aligned} \Phi(\tau) &= \int_0^L \gamma |U(z=0,\tau)|^2 \, dz \\ &= \gamma |U(z=0,\tau)|^2 L_0. \end{aligned} \tag{2.65}$$

In a lossy fiber of length L, the self-phase modulation induced is

$$\begin{aligned} \Phi(\tau) &= \int_0^L \gamma |U(z,\tau)|^2 \, dz \\ &= \gamma |U(z=0,\tau)|^2 \left(\frac{1 - e^{-\alpha L}}{\alpha} \right). \end{aligned} \tag{2.66}$$

Equations 2.65 and 2.66 imply that if the phase shift induced in a lossless fiber of length L_0 is to be the same as that induced in a lossy fiber of length L, then we must have $L_0 = [1 - exp(-\alpha L)]/\alpha$. The larger α is, the longer the lossy fiber must be.

Now, let us consider a pulse with a nonuniform Gaussian envelope:

$$U(z=0,\tau) = A e^{-\tau^2/T^2} \tag{2.67}$$

where A is a positive constant. For simplicity, we assume that the pulse is propagating in lossless media. We would like to consider the effects of nonuniform pulse intensity on the output pulses. To test this in an ideal example, consider the nonlinear Mach-Zehnder interferometer of Figure 2-1. Instead of having control pulses, the signal pulse induces a phase shift in itself due to SPM. We assume that both the nonlinear arm and the linear arm have matched lengths of L. The signal pulse is split at a

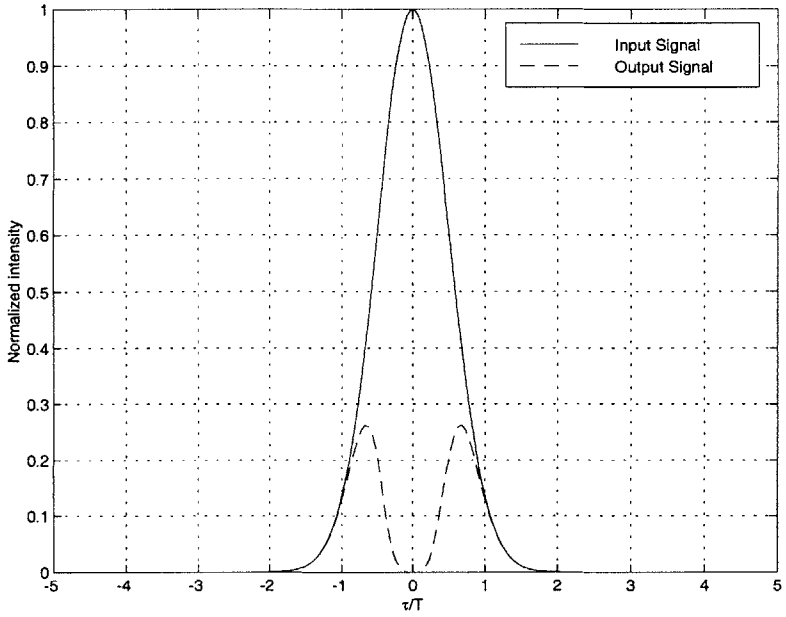

Figure 2-5: Output pulse contrasted with input signal pulse after passing through a nonlinear Mach-Zehnder interferometer with $\gamma A^2 L = \pi$

50/50 splitter. We need to calculate the relative phase shift induced across the pulse in the nonlinear arm with respect to the pulse in the linear arm. We only need to refer to Equation 2.60:

$$\begin{aligned} U(z,\tau) &= U(z=0,\tau)e^{i\gamma|U(z=0,\tau)|^2 z} \\ \Rightarrow \Phi_{NL}(\tau) &= \gamma A^2 e^{-2\tau^2/T^2} L. \end{aligned} \tag{2.68}$$

γ is inherent to the particular nonlinear medium in the nonlinear Mach-Zehnder interferometer. To simplify the analysis, we let $A^2 L = \pi/\gamma$. This choice gives us a maximum phase shift at $\tau = 0$, where $\Phi = \pi$. The phase shift, however, is not uniform over the entire pulse. The maximum phase shift occurs at the pulse center and falls to zero at the pulse edge. When the signal pulse from the linear path is interfered with the signal pulse from the nonlinear path, we get perfect cancellation at the peak. But, the amount of cancellation falls off at the edges. Figure 2-5 shows the input signal pulse and contrasts it with the output pulse. Ideally, the output pulse is identically zero, but Figure 2-5 shows two substantial pulses at the output. This condition is an

important problem, which we consider later in this thesis. One solution is to have a separate control pulse induce the phase shift in the signal pulse that propagates down the nonlinear arm. The control pulse carrier frequency determines its velocity. If chosen care fully, the control pulse "walks through" the signal pulse and thus distributes the nonlinear phase shift more evenly across the signal pulse. The output in Figure 2-5 is ideally zero across the entire pulse width. Because most of the signal pulse power is in the center of the pulse, the walk through does not have to be very large to improve the switching.

Chapter 3

Previous Work in All-Optical Switching

Higher digital data rates require shorter optical pulses, and researchers have already been looking ahead to design the components required in high speed optical networks. Today, electronic processing of signals cannot operate faster than 40 Gbit/s. If we expect to see systems exceeding 100 Gbit/s, then we must consider how to implement them using optical processing [28]. A large body of research in all-optical pulse regeneration already exists. In Chapter 2, we saw an example of an all-optical switch: the ultra fast nonlinear interferometer (UNI). The nonlinear medium in the UNI is the semiconductor optical amplifier. In this thesis, we will use optical fiber as the nonlinear medium. The nonlinear index of refraction in optical fiber occurs on the order of femtoseconds. As mentioned before, all-optical switches and all-optical regenerators are often very similar. An all-optical switch, after all, performs as a regenerator by using network data pulses as control pulses and locally generated clock pulses as signal pulses. In this way, the data (control) pulses coming off the network modulate their own data pattern onto the clock (signal) pulses. In this and later chapters, we will refer to the signal pulses as clock pulses when that is the purpose they serve. We will use the terms "data" and "control" similarly.

Although all-optical switching and all-optical regeneration are functionally similar, the goals and, therefore, the details of design are very different. Regenerators must

use distorted data pulses as control pulses to switch local clock pulses. The data pulses may be attenuated, their amplitude envelopes may be distorted, and they may have moved from the center of their own bit intervals (timing jitter). Regenerators must be designed to deal with these distortions. Different classes of regenerators exist. 3R regenerators reamplify, reshape, and retime network data pulses. 2R regenerators only reamplify and reshape network data pulses. In this chapter, we introduce several common all-optical regenerator designs. In the first section, we describe the nonlinear optical loop mirror (NOLM) [29] and its use in both 2R and 3R regeneration. In the second section, we discuss a variant of the NOLM called the terahertz optical asymetric demultiplexer, sometimes also called the semiconductor laser amplifier in a loop mirror (SLALOM) [14]. In the final section, we discuss some of the problems in these designs and how they may be overcome.

3.1 The Nonlinear Optical Loop Mirror

The nonlinear optical loop mirror (NOLM) has been studied for more than a decade as a demultiplexer [12], switch [30], and pulse regenerator [3]. For all-optical demultiplexing, the NOLM has been demonstrated to operate at 640 Gbit/s [31]. Like the UNI, the NOLM uses the nonlinear index of refraction to induce a phase shift in a pulse. The nonlinear medium of the NOLM is optical fiber [29]. The NOLM is more easily understood if we first consider the linear optical loop mirror, depicted in Figure 3-1. The linear optical loop mirror is simply a loop of fiber joined at the ends by a 50/50 coupler. Pulses that propagate into the input of the loop mirror are simply reflected back out the input with a delay caused by the propagation time through the loop. In an ideal loop mirror, no power exists at the output.

This mirror works because of the phase shift added by the 50/50 coupler. Any power that couples across from port 1 to port 4 in Figure 3-1 receives a $\pi/2$ phase shift with respect to any power that propagates directly from port 1 to port 3. The signal pulses entering at the input of the loop mirror are split into two counterpropagating pulse streams, each identical to the original, but attenuated by 3 dB. The clockwise

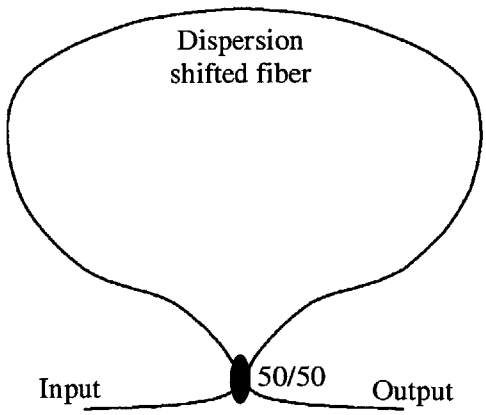

Figure 3-1: The linear optical loop mirror.

propagating stream we refer to as CW and the counterclockwise one as CCW. The power there is the sum of two pulse streams: the CW stream, which propagates from port 1 to 3 to 4 to 2 and receives no relative phase shift; and the CCW stream, which couples across from port 1 to 4 and then couples across from port 3 to 2. Because the CCW stream is coupled between fibers twice, it acquires a π phase shift at the output with respect to the CW stream and destructively interferes. The power at the input is again the sum of two different pulse streams: the CW stream, which propagates from port 1 to 3 and then couples across from port 4 to 1; and the CCW stream, which also couples across from port 1 to 4 and then propagates from port 3 to 1. The CW and CCW fields each couple between fibers once. Thus, the relative phase between the two streams does not change and they constructively interfere. So, any pulse launched into the input of the loop mirror is simply reflected back with a delay equal to the propagation time through the loop.

3.1.1 The NOLM as a 2R regenerator

In a nonlinear optical loop mirror, a phase shift is induced by some nonlinear effect as well as by the coupler. With this imbalance, we can control whether the signal pulses are switched out of the input or the output of the loop mirror. One example is the self-switch shown in Figure 3-2. The self-switch loop contains a short segment

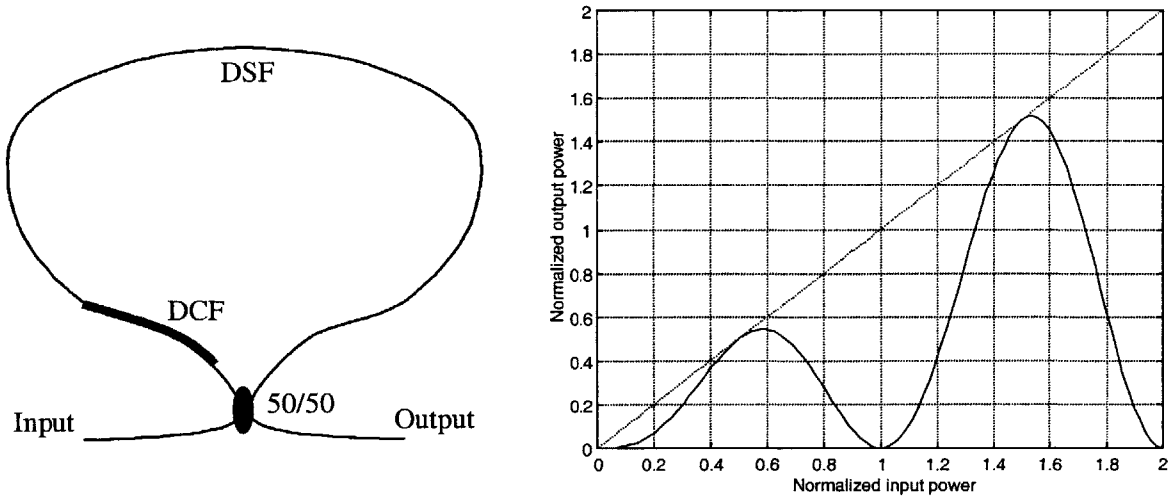

Figure 3-2: The self-switch (left) and the plot of input power verses output power of an ideal self-switch (right).

of dispersion compensating fiber (DCF) and a long segment of dispersion shifted fiber (DSF). DSF has a β_2 that is nearly zero at the carrier frequency of the signal pulses. As discussed in Section 2.3.1, $\beta_2 = 0$ implies that the signal pulses will not broaden substantially due to the GVD in DSF. DCF, on the other hand, has a very large β_2, and pulses propagating through it broaden substantially. Because the DCF is placed far from the center of the loop, an asymetry exists between the path that the CW pulse stream takes and the path that the CCW pulse stream takes. The CW pulse stream propagates first through the DCF, where those pulses are broadened by the group velocity dispersion. Even if no loss is present, the peak power of each pulse is decreased for the remaining portion of their trip around the loop. The CCW pulse stream, on the other hand, propagates through most of the loop before reaching the DCF and its peak power remains nearly constant while it propagates through the DSF. Because the nonlinear phase shift induced by SPM is proportional to the instantaneous intensity of the pulse envelope, the CCW pulses are phase shifted more than the CW pulses. Let us assume Gaussian pulses with initial peak envelope amplitude U_0. Let us also assume that the GVD in the dispersion compensating fiber lowers the peak intensity of the Gaussian pulses by some constant

factor independent of the initial intensity (see Section 2.3.1). Finally, let us assume that the DCF segment is too short to induce a measurable nonlinear phase shift in either pulse stream. Then, the phase shift induced at the center of the pulses in the CCW stream is $\gamma|U_0|^2L$, where L is the length of the DSF fiber in the loop. The phase shift induced in the CW stream is $\gamma\alpha U_0^2 L$, where α gives the drop in peak power due to the effects of group velocity dispersion in the DCF segment. The relative phase difference between the two pulse streams at the output is

$$\gamma(1-\alpha)|U_0|^2L + \pi, \tag{3.1}$$

where the π comes from the phase shift added by the coupler to the CCW pulse stream. Equation 3.1 implies that the power switched to the output of the NOLM self-switch depends on the input power. The normalized output power versus normalized input power for the self-switch is shown on the right in Figure 3-2.

This self-switch, with an optical amplifier like an erbium doped fiber amplifier (EDFA), can operate as a 2R regerator, reamplifying and reshaping, though not retiming, a pulse stream. An EDFA at the input can provide the amplification, and the loop itself reshapes the pulses. If the data pulse stream has some desired peak intensity, we can bias the self-switch by choosing the apropriate length of DSF to completely switch that peak power to the NOLM output. If we bias the self-switch at the first peak in the plot in Figure 3-2, then small additive noise at the peak is attentuated. Moreover, the tails of the pulse are attenuated, and the pulse width narrowed.

3.1.2 The NOLM as a 3R Regenerator

The nonlinear optical loop mirror can also serve as a 3R regenerator. A very basic 3R regenerator design is shown in Figure 3-3. As in the UNI, control pulses and signal pulses are separated by their carrier wavelength. The band pass filter at the output of the NOLM filters out the control pulses. In the case of regeneration, the control pulses are the network data pulses, amplified to provide the necessary nonlinear phase

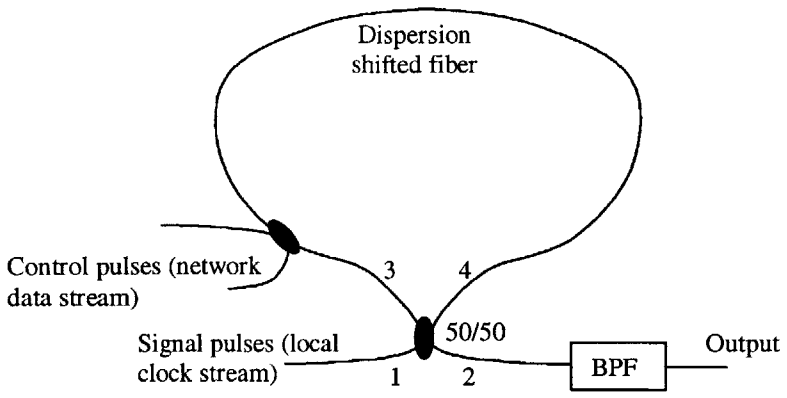

Figure 3-3: The nonlinear optical loop mirror with control pulses adding an imbalance between CW and CCW pulse streams for 3R all-optical regeneration.

shift via XPM. The signal pulses are locally generated clock pulses. In the absence of data pulses, the NOLM becomes simply an optical loop mirror and the clock pulses are switched back out the input. If data pulses are present, then they are coupled onto the loop mirror to temporally overlap the clockwise propagating clock pulses. These amplified data pulses copropagate with the CW clock pulses, inducing a nonlinear phase shift in the CW clock pulses. By adjusting the power of the data pulses, we can control how much of the clock pulses' energy is switched out the output. For the regenerator application, we would bias the NOLM so that the presence of data pulses completely switches out any clock pulse it temporally overlaps to the output port. In this way, the output clock pattern matches the original data pattern.

Of course, the simple description above neglects many important details. First, the regenerated pulse stream that we see at the output is at a different carrier wavelength than the original data pulse stream. We can overcome this problem by alternating carrier wavelengths in the network, switching the carrier wavelengths of the data and clock pulses from one regenerator to the next. This solution, however, complicates the network design. Second, although the data pulses do not copropagate with the counterclockwise propagating clock pulses, they do, nonetheless, pass through them. The data pulses propagate quickly through the CCW clock pulses, but they still induce a small phase shift in those clock pulses. Third, the control pulses are not

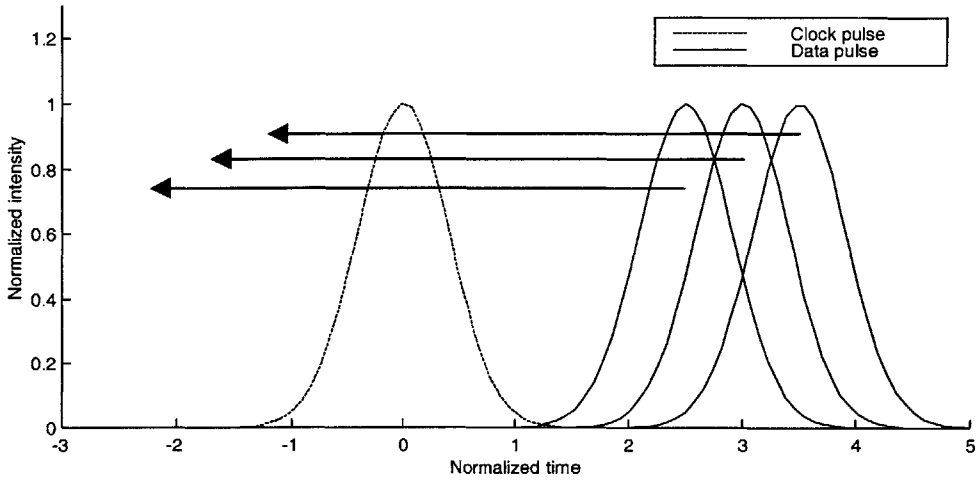

Figure 3-4: Walk-off of a data pulse through a clock pulse. Timing jitter in the data pulse makes the time at which it is coupled onto the NOLM, relative to the clock pulse, unpredictable.

square, so the phase shift they induce in the CW clock pulses depends, in part, on the clock pulse intensity profile. This problem was discussed in Section 2.3.3 and in Figure 2-5.

Let us discuss these last two points in more detail, since they will be useful in understanding the folded UNI described in Section 5.1 later. The group velocity dispersion of fiber causes pulses of different carrier frequencies to propagate at different rates. We can, therefore, have a data pulse walk through the clock pulse it temporally overlaps. This walk-off eases two problems: the dependence of the phase shift on the intensity profile and the timing jitter in the incoming data pulses. In Figure 3-4, the data pulse is shown as three pulses, each one representing a possible arrival time due to timing noise caused by the network. The walk-off designed into the regenerator between the data and clock pulses ensures that in spite of the timing jitter, the data pulse will, for some time, temporally overlap the clock pulse. During that time, the data pulse will induce a nonlinear phase shift in the clock pulse.

Researchers have carefully studied the effects of this walk-off on the NOLM's switching performance [32]. Let us begin by assuming a stream of Gaussian control

pulses in a NOLM of length L:

$$P_{data}(z,t) = \sum_{n=-\infty}^{\infty} x_n P_0 exp\left[-\left(\frac{t - nT - \frac{t_w}{L}z}{T_0}\right)^2\right] \tag{3.2}$$

where P_{data} is the intensity profile of the data pulses, T is the bit period, t_w is the total walk-off time of the control pulses with respect to the signal pulses, x_n is 1 for a "mark" (that is, for the presence of a control pulse) and 0 for a "space" (absence of a control pulse), and T_0 is related to the intensity full width at half maximum by $T_{FWHM} = 2T_0\sqrt{\ln 2}$. The signal pulses are taken as a moving reference frame. Hence, the argument of the exponential in the control pulses is $t - nT - \frac{t_w}{L}z$, so that after propagating from $z = -L/2$ to $z = L/2$, the center of the control pulses have moved t_w seconds with respect to the signal pulses. Let us assume that disperive effects are negligible. We also assume that the control pulses are much more intense than the signal pulses, so that the phase shift is caused by the control pulses only. At each length element, dz, along the fiber, Equation 2.60 predicts that the phase shift induced in the signal pulse is equal to $\gamma P_{data} dz$. Thus, the total phase shift induced in the signal pulses by the control pulses is given by the integral

$$\phi_c = \int_{-\frac{L}{2}}^{\frac{L}{2}} \gamma P_{data}(z,t)\, dz. \tag{3.3}$$

We can solve this integral by separating it into two integrals:

$$\begin{aligned}\phi_c =& \gamma \int_{-\frac{L}{2}}^{0} \sum_{n=-\infty}^{\infty} x_n P_0 exp\left[-\left(\frac{t - nT - \frac{t_w}{L}z}{T_0}\right)^2\right] dz + \\ & \gamma \int_{0}^{\frac{L}{2}} \sum_{n=-\infty}^{\infty} x_n P_0 exp\left[-\left(\frac{t - nT - \frac{t_w}{L}z}{T_0}\right)^2\right] dz.\end{aligned} \tag{3.4}$$

We solve Equation 3.4 in terms of the error function defined by

$$erf(t) = \frac{2}{\sqrt{\pi}} \int_0^t exp(-u^2)\, du. \tag{3.5}$$

If we make the substitution $u = (t - nT - \frac{t_w}{L}z)/T_0$ and notice that this changes the

limits of integration (that is, we must change the limits from the values of z to the corresponding values of u), then we get the solution

$$\phi_c = 2\sqrt{\pi}\gamma L P_0 \frac{T_0}{t_w}\left[\sum_{n=-\infty}^{\infty}\frac{x_n}{2}\left\{erf\left(\frac{t+t_w/2-nT}{T_0}\right) - erf\left(\frac{t-t_w/2-nT}{T_0}\right)\right\}\right]. \tag{3.6}$$

We can use Equation 3.6 to calculate the switching window of this NOLM 3R regenerator. The switching window is a plot of the switched out power versus the relative temporal separation of the control and signal pulses. For example, let us assume that we have no walk-off between the two pulses. Let us also assume that the signal pulses are too weak to induce any phase shift in the control pulses, and that the control pulse peak power is biased to induce a π phase shift in the part of the signal pulse that that peak temporally overlaps. If we assume that both pulses are Gaussian, we can calculate the phase shift induced in the signal pulse given a certain separation of the two pulses. Also, using Equation 2.31, which shows that the power reflected out the input of the NOLM is proportional to $\cos^2(\phi_c/2)$, we can calculate the power switched out. Figure 3-5 shows the switching window for 2.5 ps Gaussian signal and control pulses with no relative walk-off between the two. The switching window's full width at half maximum is about 3.3 ps.

Now, we consider the switching window of signal and control pulses that have a relative walk-off of 8 ps. We can calculate it just as we did for the case of no walk-off, but with $t_w = 8$ ps substituted into Equation 3.6. The resulting ϕ_c is substituted into $\cos^2(\phi_c/2)$, giving the induced phase of the clock pulses. If we again assume 2.5 ps Gaussian signal and control pulses, then we obtain the switching window shown in Figure 3-6. The switching window's full width at half maximum is 8.0 ps. Notice that the switching window with walk-off is not only wider, but has a long center section in which the switching is complete. If the control pulse falls in this section, it is switched

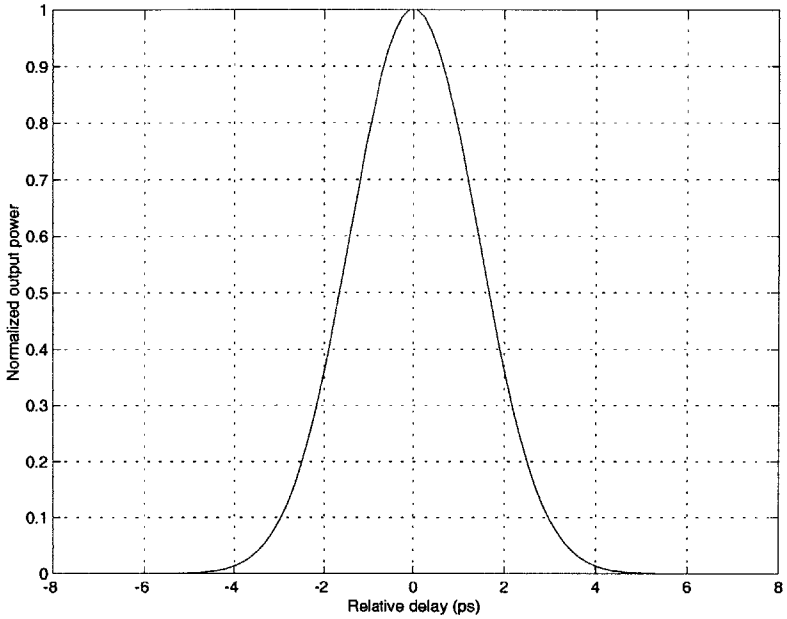

Figure 3-5: NOLM switching window for 2.5 ps FWHM clock and data pulses with no temporal walk-off.

out unaltered. The height of this plateau is calculated using Equation 3.6:

$$\phi_c^{plateau} = 2\gamma P_0 L\sqrt{\pi}\left(\frac{T_0}{t_w}\right) \tag{3.7}$$

Moreover, the wider switching window increases the tolerance for timing jitter in the control pulses. Walk-off between clock and data pulses does have disadvangtages for optical regenerators. For a long walk-off, like 8.0 ps, the control pulse temporally overlaps the signal pulse for only a fraction of the length of the fiber in the NOLM. So, the smaller interaction length between the signal and control pulses reduces the phase shift. We must, therefore, either use a longer NOLM or higher powers in the control pulse. Each of these two solutions can make more significant other effects that we neglected, like dispersion, Rayleigh scattering, and Raman scattering.

We must also remember that the control pulses cause a nonlinear phase shift in the counterclockwise propagating signal pulses, even though they do not propagate in the same direction. This interaction reduces the relative phase difference between the counterpropagating signal pulses. Let us assume that the temporal length of

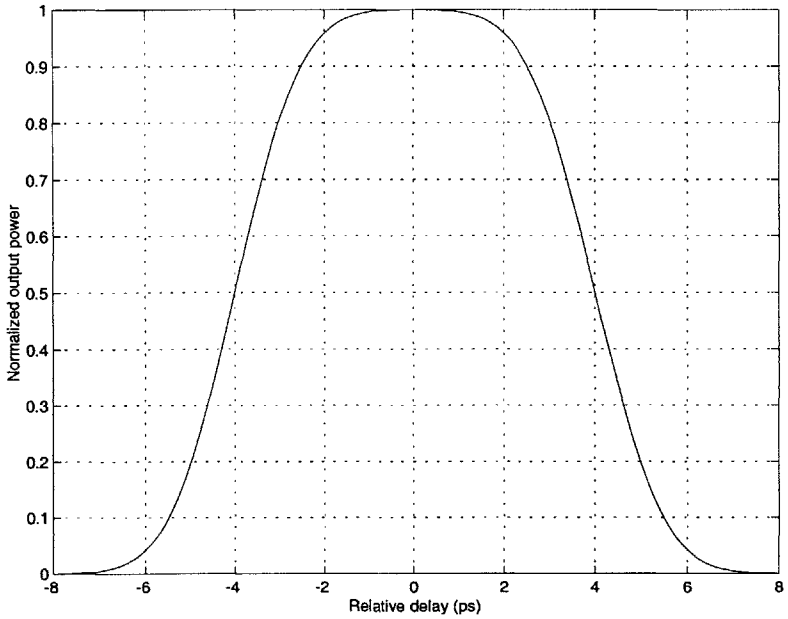

Figure 3-6: NOLM switching window for 2.5 ps FWHM clock and data pulses with 8 ps of relative walk-off.

the bit slot width, T, is much less than twice the length of the NOLM. That is, $cT \ll 2nL$ where n is the index of refraction of the fiber. Thus, each counterclockwise propagating signal pulse passes through many clockwise propagating control pulses. If we assume that half of the control pulses are marks and half are spaces, then the phase shift induced in the counterclockwise propagating signal pulses is

$$\phi_{ccw} = 2\gamma P_0 L\sqrt{\pi}\left(\frac{T_0}{2T}\right) \tag{3.8}$$

and the power switched to the output is

$$P_{out}(t) \propto 1 - \cos^2\left(\frac{\phi_c - \phi_{ccw}}{2}\right). \tag{3.9}$$

In fact, in the folded UNI design we will be considering later, the assumption $cT \ll 2nL$ is reasonable because the bit period's temporal length at 10 Gbit/s is 10 ps, which corresponds to a spatial length of 20 mm. The fiber length used in the folded UNI is typically hundreds of meters long.

3.2 Semiconductor Laser Amplifier in a Loop Mirror (SLALOM)

Both types of nonlinear optical loop mirror described in Section 3.1 required some kind of imbalance to supply the nonlinear phase shift between the clockwise (CW) and counterclockwise (CCW) rotating clock pulses. In Section 3.1.1 a segment of dispersion compensating fiber created the imbalance. In Section 3.1.2 data pulses coupled onto the NOLM to temporally overlap the clockwise propagating clock pulses provided the imbalance. In both cases, the nonlinear phase shift was induced by fiber nonlinearities caused by the third order nonlinear effects described in Section 2.1. The nonlinear phase shift, however, could be induced using a semiconductor optical amplifier (SOA). The UNI described in Section 2.2.2, for example, used an SOA to provide the nonlinear phase shift. A NOLM that uses an SOA to provide the nonlinear phase shift is called a semiconductor laser amplifier in a loop mirror (SLALOM) and is also often called a terahertz optical asymetric demultiplexer (TOAD) [14]. A SLALOM is shown in Figure 3-7. Because the SOA provides a high nonlinearity, the device can be made much smaller than the NOLM and the switching power is lower [14].

In the absence of the SOA, the SLALOM behaves just like the linear loop mirror described in Section 3.1.1. The presence of the SOA provides gain. Pulses launched into the input are split into clockwise and counterclockwise propagating pulse trains. The SOA's offset from the center of the loop causes an imbalance between CW and CCW pulses. As in Sections 3.1.1 and 3.1.2, we would like to characterize the transfer relationship between the input power and the output power. We assume that the fiber loop itself is lossless and dispersionless. Let t_d be the round trip time of the fiber loop and let $T/2$ be the pulse propagation time from the center of the loop to the SOA. The input field is given by $E_{in}(t) = A_{in}(t)e^{-i\omega t} + A^*_{in}(t)e^{i\omega t}$. The complex gain seen by CW pulses will be

$$g_{cw}(t) = G_{cw}(t) \cdot exp(i\phi_{cw}(t)) \tag{3.10}$$

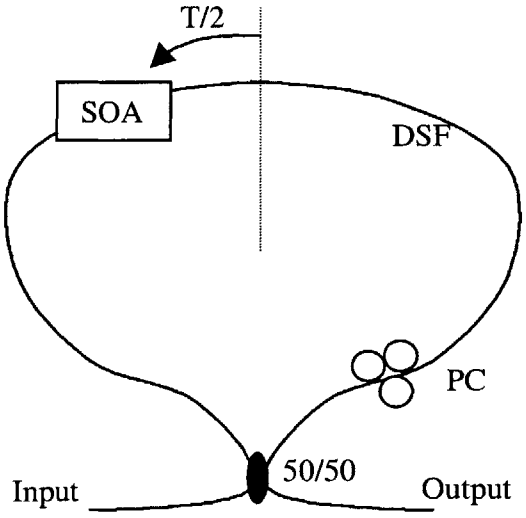

Figure 3-7: In the SLALOM, the imbalance between clockwise and counter clockwise propagating clock pulses is provided by an SOA set off-center in the loop. The DSF is dispersion shifted fiber and the PC is a polarization controller.

where $G_{cw}(t)$ is the magnitude of $g_{cw}(t)$ and $\phi_{cw}(t)$ is the phase of $g_{cw}(t)$. $G_{cw}(t)$ and $\phi_{cw}(t)$ are given by

$$G_{cw}(t) = g\left(t + \frac{t_d}{2} - \frac{T}{2}\right) \text{ and } \phi_{cw}(t) = \phi\left(t + \frac{t_d}{2} - \frac{T}{2}\right). \tag{3.11}$$

The counterclockwise propagating pulses do not arrive at the SOA until T seconds later than the corresponding CW pulses. So, the gain applied to the CCW pulses is

$$g_{ccw}(t) = G_{ccw}(t) \cdot \exp(i\phi_{ccw}(t)). \tag{3.12}$$

For these pulses, $G_{ccw}(t)$ and $\phi_{ccw}(t)$ are given by

$$G_{ccw}(t) = g\left(t + \frac{t_d}{2} + \frac{T}{2}\right) \text{ and } \phi_{ccw}(t) = \phi\left(t + \frac{t_d}{2} + \frac{T}{2}\right). \tag{3.13}$$

In the fiber NOLM described in Section 3.1, switching occurred because of a nonlinear phase shift, which was fast enough for us to consider to be instantaneous. The SLALOM, on the other hand, depends on the gain of an SOA to generate the nonlinear

index of refraction, which we cannot condsider instantaneous. In fact, operation of the SLALOM relies on the gain saturation of the SOA. So, the complex gain on any particular pulse depends on the effects of preceeding pulses.

As we did in Section 3.1, we calculate the field at the output,

$$E_{out} = A_{out}(t) \cdot e^{-i\omega t} + A^*_{out}(t) \cdot e^{i\omega t}. \tag{3.14}$$

The field is the sum of the two counterpropagating pulse trains. The CW pulse train never crosses through the coupler in order to reach the output arm of the SLALOM. The CCW pulse train must cross the coupler twice to reach the output arm and thus receives a $-\pi$ phase shift. Adding these two fields at the output arm gives

$$\begin{aligned} A_{out} &= \frac{1}{2}A_{in}(t-t_d) \cdot e^{i\omega t_d} g_{cw}(t-t_d) - \frac{1}{2}A_{in}(t-t_d) \cdot e^{i\omega t_d} g_{ccw}(t-t_d) \\ &= \frac{1}{2}A_{in}(t-t_d) \cdot e^{i\omega t_d} \cdot [g_{cw}(t-t_d) - g_{ccw}(t-t_d)]. \end{aligned} \tag{3.15}$$

The factor of $1/2$ comes from our assumption that we have a perfect 50/50 coupler. Half of the power in each pulse train is coupled to the input of the SLALOM and half to the output. Each term in Equation 3.15 receives a phase shift of ωt_d because of the optical path length of the loop. The second term in Equation 3.15 is negative because of the $-\pi$ phase shift induced by the coupler.

Now we can calculate the output power. By Equation 2.21, we know that the power of the pulses is given by $2A_{out}(t) \cdot A^*_{out}(t)$ assuming that $A_{out}(t)$ is a slowly varying envelope over the carrier. With this assumption, we can calculate P_{out}:

$$\begin{aligned} P_{out} &= 2A_{out}(t) \cdot A^*_{out}(t) \\ &= \frac{1}{4}G^2_{cw}(t-t_d)P_{in}\Big[1 + \frac{G^2_{ccw}}{G^2_{cw}} - 2\frac{G_{ccw}}{G_{cw}}\cos(\phi_{cw} - \phi_{ccw})\Big]. \end{aligned} \tag{3.16}$$

From Equation 3.16 we notice two important facts: the output power depends on the ratio of the CCW and CW gains, $\Delta g = (G_{ccw}/G_{cw})$; and the output power depends on the phase difference $\Delta\phi = \phi_{cw} - \phi_{ccw}$. We can alter the values of Δg and $\Delta\phi$ by saturating the semiconductor optical amplifier. There is no need to develop a

precise theory of gain dynamics in the SOA here because this simple model sufficiently describes the operation of the SLALOM.

There are several ways to get the gain and phase differences, Δg and $\Delta\phi$, many of which depend on saturation of the SOA. If a short intense pulse propagates through the SOA, then gain in the SOA can become saturated. The gain does recover, however, and the recovery time constant is on the order of 100 ps. Figure 3-8 shows gain saturation in an SOA after the arrival of a short pulse at $t = 10$ ps. Any pulse that arrives while the gain is saturated will see a smaller gain than it would if the amplifier were unsaturated. It is on this fact that the three principle methods for obtaining phase and xsgain differences are based.

1. A single pulse enters the input of the SLALOM. The CW pulse saturates the gain of the SOA. If we make T smaller than the gain recovery time, τ_e, then the CCW pulse propagates through a saturated SOA.

2. Two pulses enter the SLALOM input temporally spaced by approximately T seconds. The CCW portion of the first pulse saturates the SOA so that the CW portion of the second pulse propagates through a saturated SOA.

3. This case will interest us the most. As in the first two cases, a signal pulse enters at the output. Moreover, a control pulse is coupled on at another point in the loop, as shown in Figure 3-9. If timed properly, the control pulse can saturate the SOA after the arrival at the SOA of the CW signal pulse but before the arrival of the CCW signal pulse. Thus, the CCW pulse sees a saturated SOA. The control pulse could be at a different carrier wavelength. CP2 in Figure 3-9 would then be a wavelength dependent coupler. If such a coupler is used, switch efficiency is maximized becuase no CW signal pulse power couples out of the loop and all the control pulse power couples into the loop.

The third point in the list above is the one relevant to 3R pulse regeneration. In this case, the control pulses are replaced with network data pulses and the signal pulses with local clock pulses.

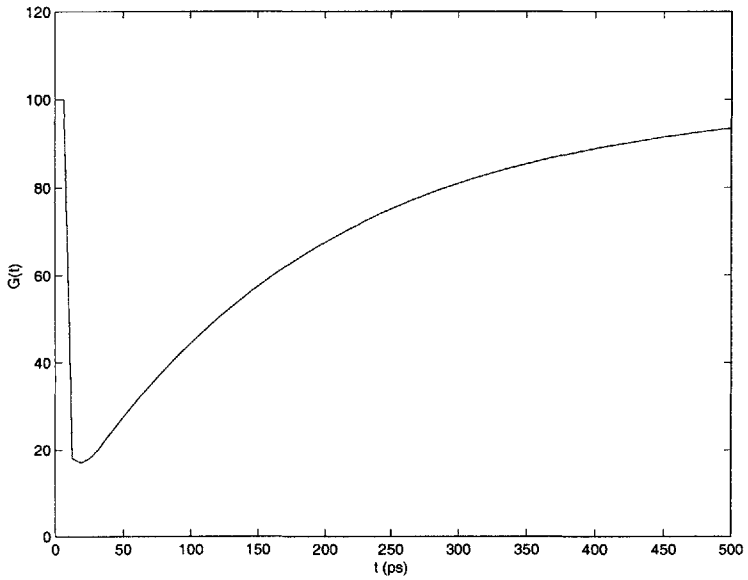

Figure 3-8: SOA gain saturation due to the arrival of a short intense pulse at 10 ps. The recovery constant τ_e is on the order of 100 ps and the small signal gain is 100.

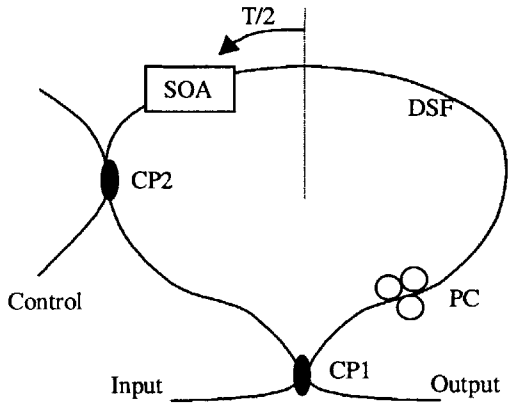

Figure 3-9: SLALOM with control pulses that saturate the SOA. This design can be applied as a regenerator by replacing the control pulses with data pulses. In order to maximize switch efficiency, CP1 is a 50/50 coupler and CP2 is a wavelength dependent coupler.

3.3 Considerations Specific to Regeneration and Problems with Loop Mirror Switches

All-optical logical switches and all-optical regenerators very often have similar designs. After all, an all-optical switch, like the UNI described in Section 2.2.2, can be adapted to a regenerator design. When used as a regenerator, the control pulses are replaced with network data pulses in the UNI. The signal pulses, which are switched on or off by the presence or absence of control pulses, are replaced by locally generated clock pulses. Some of the considerations of regenerator design, however, are different from those of general switch designs. The regenerator design challenges we will focus on in this thesis include:

1. We must expect timing jitter on the incoming data stream. As we will see in Section 4.1, one possible solution is to have the data and clock pulses "walk through" each other.

2. The time it takes to switch a pulse is not so important in regeneration. That is, logical latency does not matter.

3. The polarization drifts slowly in fiber because of changes in the fiber due to temperature changes and twisting. In the UNI, this problem requires the active monitoring of 3 polarization controllers. In Section 5.1, we will present a regenerator that provides inherent polarization stabilization within the regenerator.

4. Acoustic effects can cause changes in the polarization too fast to actively monitor. In fiber NOLMs, the pulses propagate in the same length of fiber, but they counterpropagate. Thus, polarization changes in the fiber may affect CW clock pulses but not the CCW clock pulses, causing asymetry and higher error rates. In Section 5.1, we will present a regenerator that is insensitive to acoustif effects.

As mentioned in the list above, the fiber NOLMs of Sections 3.1.1 and 3.1.2 are very sensitive to acoustic vibrations. Sound waves cause time varying pressure in the

fiber of the NOLM, which, in turn, cause birefringence in the silica, thus altering the polarization of the pulses as they propagate [33]. Because the pulses counter-propagate, a particular CW pulse may see different fiber characteristics than the corresponding CCW pulse. At the output the different polarizations of the two clock pulses recombine but no longer have the same polarization and only imperfectly interfere with each other. This acoustic sensitivity can be reduced by symmetric wrapping of the fiber loop around a drum [34]. The folded UNI, introduced in Section 5.1, will offer another solution to acoustic sensitivity without the need for special wrapping of the fiber.

The SLALOM does not have the same problems with acoustic senstitivity because the nonlinear medium is an SOA rather than a long length of fiber. The loop is very short and thus less sensitive to vibration. The SLALOM, however, does suffer from problems related to gain saturation of the SOA. As described in point 3 of the list in Section 3.2, the SLALOM can operate as a switch or a pulse regenerator. The SLALOM works most effectively in data demultiplexing, where every n-th data bit is switched out. The signal pulses in this case are the data pulses. Every n-th contol bit period contains a control pulse, which saturates the SOA after the arrival at the SOA of the CW signal pulse but before the arrival of the CCW signal pulse. The resulting phase difference between the CW and CCW signal pulses causes that signal pulse to switch out the output. Subsequent CW and CCW signal pulse pairs propagate through a slowly recovering saturated SOA (see Figure 3-8). Because of the relatively slow recovery and the fact that a CW signal pulse and its corresponding CCW signal pulse arrive at the SOA at almost the same time, they see nearly identical gains. Thus, they are reflected back out the SLALOM input. Ideally, the SOA will have completely recovered by the time the next control pulse arrives to saturate it.

For regeneration, however, the control pulses are the network data pulses, and we cannot predict which control bit intervals will contain pulses and which will not. Thus, there may be two consecutive pulses in the control stream. The first one saturates the SOA, causing an imbalance in the complex gain seen by the corresponding CW and CCW signal pulses. When the second control pulse arrives at the SOA, it

has not yet had time to fully recover. It does saturate the SOA, but because the SOA was already partially saturated, the difference in the complex gains seen by the CW and CCW signal pulses will not be as large. Therefore, the switched out power of this pulse is less than that of the preceeding pulse This effect causes patterning of the output pulse power in a way that depends on the control pattern. The UNI also shows similar patterning problems, which can be solved by using pulse position modulation of the data [16]. The folded UNI, presented in Section 5.1, uses optical fiber, which provides a nonlinear medium with an instantaneous response. This response eliminates patterning effects in the output pulse streams.

Chapter 4

Characterization of Fiber as a Nonlinear Medium

The folded UNI, presented in Section 5.1, uses fiber as a nonlinear medium. Many of the parameters of fiber vary from spool to spool. This chapter will cover how we choose the values for various design parameters, like the length of the nonlinear fiber, the value of its dispersion, the carrier frequencies of the control and signal pulses, and the nonlinear index of refraction. First, we discuss measurement of the dispersion of the fiber and how that dispersion influences our choice of carrier frequencies. We also will discuss measurement of the nonlinear index of refraction, and its influence on fiber length.

4.1 Dispersion and Walk-off

As discussed in Section 3.1.2 and shown in Figure 3-4, we can correct timing jitter in network data pulses by having the data pulses, which serve as control pulses, walk through the locally generated clock pulses. We can create this walk-off between two pulses by using the fact that two pulses of different carrier frequencies can have different group velocities. In this section we describe how we measure group velocity dispersion and how we use this information to select specific fiber types and fiber lengths. We will measure group velocity dispersion by directly measuring relative

group delays of a sine wave modulation as a function of carrier wavelength.

Optical fiber comes in many types. Most have a step change in the index of refraction. That is, the index of refraction of the inner cylindrical core is uniform and higher than that of the cladding that surrounds it. The core and cladding are made from SiO_2 molecules. Dopants such as GeO_2 and P_2O_5 can raise the index of refraction of the core, while dopants like boron and flourine can lower the index of refraction of the cladding. Manufacturers of fiber can also control the radius of the core. Typical multi-mode fibers have a core radius of 25-30 μm. Single-mode fiber, the standard in modern communications, has a core radius of 2-4 μm. The width of the cladding is around 50-60 μm for both single and multi-mode fiber. More thorough information can be found in Agrawal's text [21].

The dopant levels and core diameter all affect the dispersion of the fiber. As in Section 2.3.1, we expand the propagation constant β as a Taylor series:

$$\beta(\omega) = \beta_0 + \beta_1(\omega - \omega_0) + \frac{1}{2}\beta_2(\omega - \omega_0)^2 + \cdots . \tag{4.1}$$

where the β_n in Equation 4.1 are equal to $\frac{\partial^n \beta}{\partial \omega^n}|_{\omega=\omega_0}$. In Section 2.3.1 we discussed the effects of dispersion on a Gaussian pulse. In particular, we solved for the case in which β_0, β_1, and β_2 were the only nonzero coefficients in Equation 4.1. $1/\beta_1$ is called the group velocity v_g because it is the propagation speed of the peak of the Gaussian pulse. The value of β_2 determines the rate at which the Gaussian pulse width increases. Because we would like the pulses to maintain their shape as they propagate down the nonlinear medium, β_2 ought to be as nearly 0 as possible. The typical carrier wavelength in optical fiber communications is 1550 nm. If we expand β around the frequency corresponding to 1550 nm, then dispersion-shifted fiber (DSF) has a value of β_2 that is very nearly zero. In this thesis, we test only dispersion-shifted fiber as the nonlinear medium. As we shall see in Section 5.1, the pulse broadening induced by dispersion in fiber is undesireable.

We would like to know the relative group delay of pulses of different carrier frequencies, from which we can calculate β_1. We start by modulating a sine wave onto

an optical carrier and launching the sine modulation into the fiber to test. Then, by varying the carrier frequency, we measure the relative arrival delay as a function of carrier frequency on a high speed digital sampling scope. Figure 4-1 shows the experimental setup. A tunable CW source provides the optical carrier. The Mach-Zehnder modulator modulates a 10 GHz sine wave onto the optical carrier. A 10 GHz RF synthesizer provides the electrical input and triggers the digital sampling scope. After the modulated carrier propagates down the test fiber, an erbium-doped fiber amplifier amplifies the signal. The traces taken on the scope contain several cycles of the sine modulation and are avergered over hundreds of traces to eliminate noise in the signal. Traces are recorded for every 2.5 nm change in carrier wavelength and stored on computer. The fast Fourier transform (FFT) provides the spectrum of those traces. The FFT has a DC peak, showing the DC offset, and peaks at plus and minus the frequency of the modulation. The relative group delay is calculated by measuring the phase at these modulation peaks as a function of carrier wavelength. This group delay, however, is not the group delay of just the test fiber, but of the test fiber, the fiber in the setup, and the fiber in the erbium doped fiber amplifier. To separate the group delays of the test fiber from the rest of the fiber, we repeat the experiment without the test fiber and then subtract those group delays from the group delays calculated in the experiment with the test fiber. Figures 4-2, 4-3, and 4-4 show the measured group delays as a function of optical carrier wavelength for DSF fibers of lengths 500 m, 2000 m, and 4000 m, respectively.

The second order dispersion is given by

$$\beta_2 = \frac{d^2\beta(\omega)}{d\omega^2} = \frac{d\beta_1(\omega)}{d\omega}. \tag{4.2}$$

The data shown for $\beta_1(\omega)$ are plotted against λ. So, if we let $\tilde{\beta}_1(\lambda) = \beta_1(\omega = \frac{2\pi c}{\lambda})$, then, applying the chain rule to Equation 4.2, we get

$$\beta_2 = \frac{d\tilde{\beta}_1(\lambda)}{d\lambda}\frac{d\lambda}{d\omega}. \tag{4.3}$$

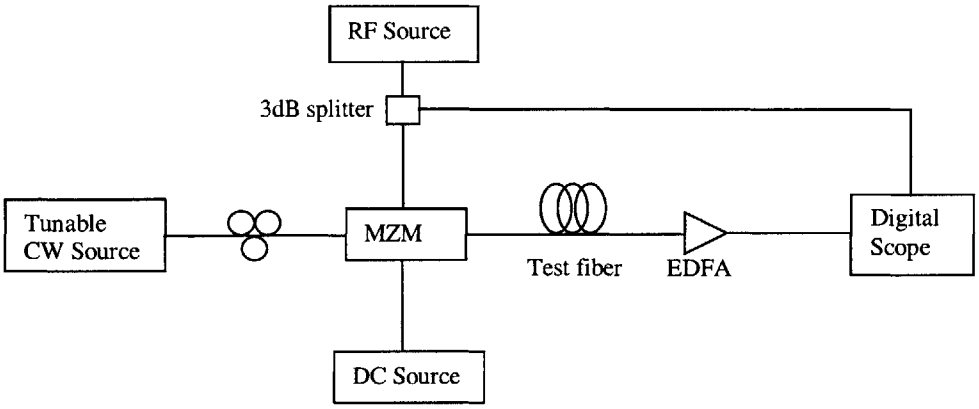

Figure 4-1: Experimental setup to measure group delay as a function of carrier frequency. MZM is a Mach-Zehnder modulator and EDFA is an erbium doped fiber amplifier.

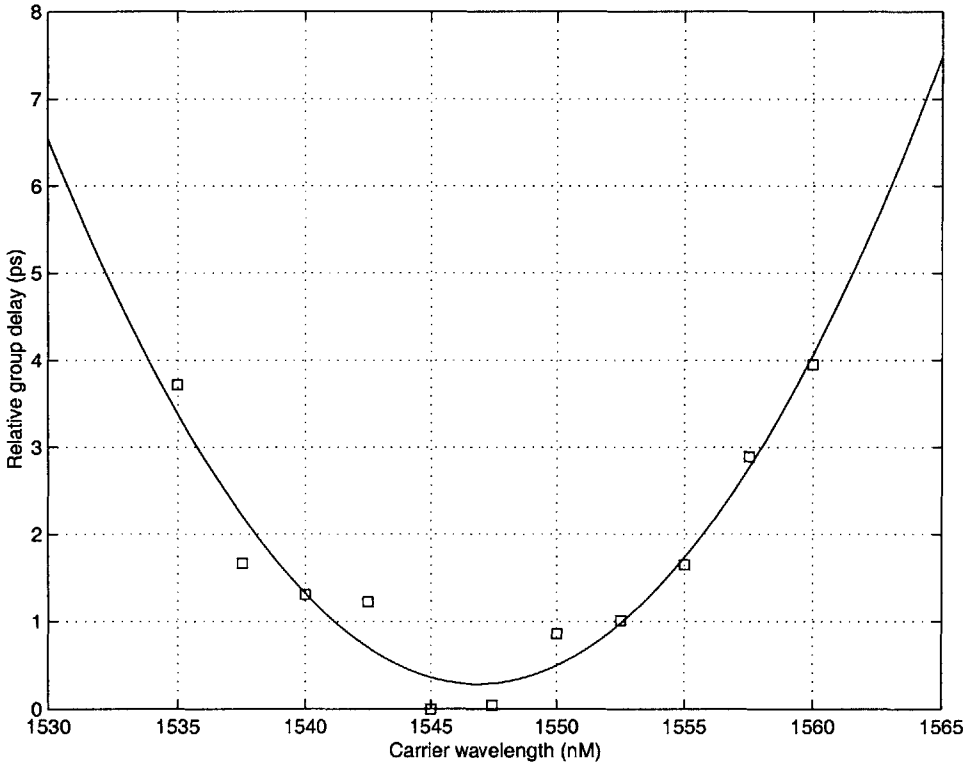

Figure 4-2: Plot of relative group delay of sine wave modulation versus the wavelength of the carrier for the 500 m spool of DSF used in this thesis. The curve is a least squared error parabolic fit.

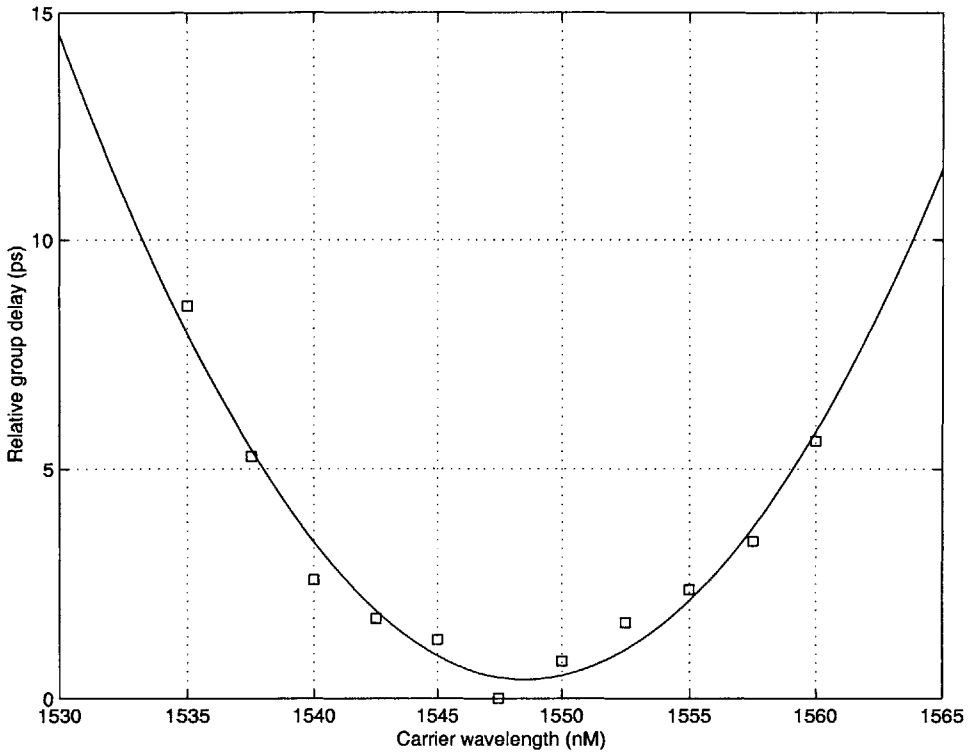

Figure 4-3: Plot of relative group delay of sine wave modulation versus the wavelength of the carrier for the 2,000 m spool of DSF used in this thesis. The curve is a least squared error parabolic fit.

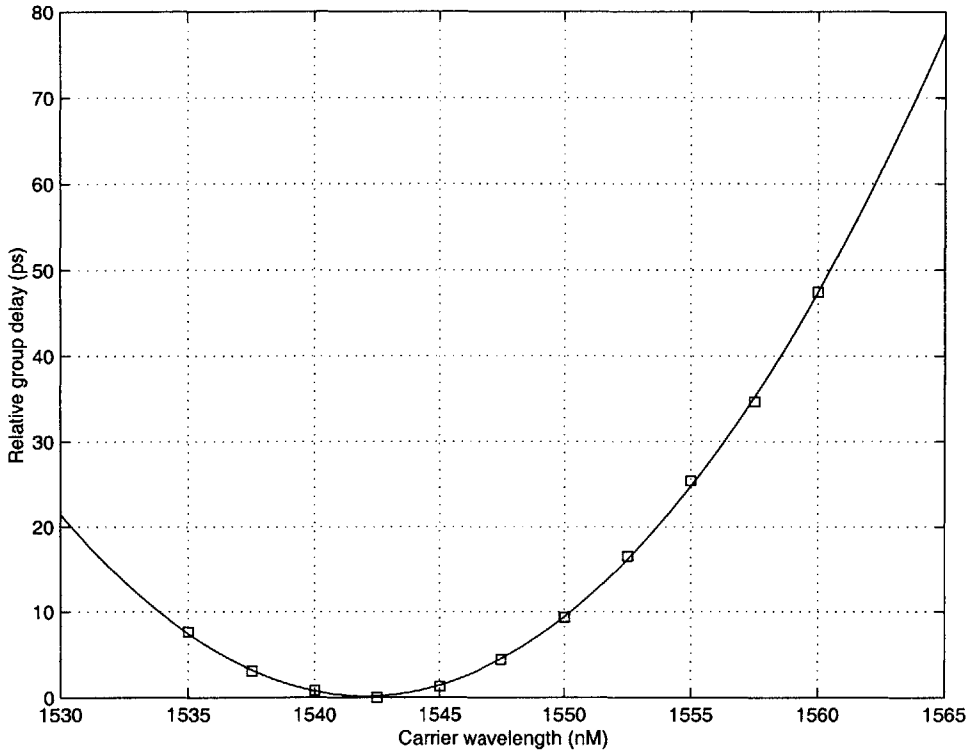

Figure 4-4: Plot of relative group delay of sine wave modulation versus the wavelength of the carrier for the 4,000 m spool of DSF used in this thesis. The curve is a least squared error parabolic fit.

Because $\lambda = 2\pi c/\omega$, we have from Equation 4.3

$$\beta_2(\omega) = -\frac{2\pi c}{\omega^2}\frac{d\tilde{\beta}_1}{d\lambda} = -\frac{\lambda^2}{2\pi c}\frac{d\tilde{\beta}_1}{d\lambda}. \tag{4.4}$$

In Figures 4-2, 4-3, and 4-4, a parabola is fit to the data points by least squared error minimization. In each case, the parabola shown is $L\beta_1$, where L is the length of the relevant fiber. For the three spools of fiber that we will study, the parabolas are given by

$$\begin{aligned} &500 \text{ m: } \beta_1 = 4.15 \times 10^1 \lambda^2 - 1.28 \times 10^{-4}\lambda \\ &2000 \text{ m: } \beta_1 = 2.06 \times 10^1 \lambda^2 - 6.27 \times 10^{-5}\lambda \\ &4000 \text{ m: } \beta_1 = 3.67 \times 10^1 \lambda^2 - 1.13 \times 10^{-4}\lambda \end{aligned} \tag{4.5}$$

where we have neglected the constant term because we are only interested in relative delays. β_1 has units of s/m and λ has units of meters. Substituting these into equation 4.4, we get

$$\begin{aligned} &500 \text{ m: } \beta_2 = -4.41 \times 10^{-8}\lambda^3 + 6.82 \times 10^{-14}\lambda^2 \\ &2000 \text{ m: } \beta_2 = -2.18 \times 10^{-8}\lambda^3 + 3.33 \times 10^{-14}\lambda^2 \\ &4000 \text{ m: } \beta_2 = -3.89 \times 10^{-8}\lambda^3 + 6.00 \times 10^{-14}\lambda^2 \end{aligned} \tag{4.6}$$

where β_2 has units of s^2/m and λ has units of meters. These three equations will be useful to us in Section 4.2.3, where we measure the nonlinear index of refraction. We also use them to determine the carrier wavelengths we will operate at in the folded UNI design presented in Section 5.1. Although we test at 10 Gbit/s, which corresponds to a bit period of 100 ps, the pulse widths we use only have a 2.5 ps intensity FWHM. For this reason, we design our switch to have a switching window of 2 to 3 ps in width. Figures 4-2, 4-3, and 4-4 give the group delays between pulses of two different carrier wavelengths. Because of the double pass through the DSF in the folded UNI design, the group delays read off the chart must be doubled. The desired delay is achieved with the 500 m spool at a signal carrier wavelength of 1555 nm and a control carrier wavelength of 1545 nm. It is under these conditions that we will primarily test.

4.2 Measurement of the Nonlinear Index of Refraction

The nonlinear index of refraction was discussed in Section 2.1. Self-phase modulation (SPM), a consequence of the nonlinear index, was discussed in Section 2.3.2. In that section, we derived the nonlinear Schrödinger equation (NLS):

$$\frac{\partial U}{\partial z} = -\frac{1}{2}i\beta_2\frac{\partial^2 U}{\partial \tau^2} + i\gamma|U|^2U \tag{4.7}$$

where U is the pulse envelope, β_2 is the second order dispersion, γ is the nonlinear coefficient, and τ is a time frame that moves at the group velocity β_1. The second term of the right side of Equation 4.7 accounts for self-phase modulation. This section explains and justifies a method to measure γ, which depends on the nonlinear index of refraction.

4.2.1 Effects of Self-phase Modulation

The method we use to measure γ assumes that dispersion is negligible. That is, β_2 in Equation 4.7 is zero, leaving us with

$$\frac{\partial U(z,\tau)}{\partial z} = i\gamma|U|^2U. \tag{4.8}$$

As we showed in Section 2.3.2, the solution to Equation 4.8 is easily verified as

$$U(z,\tau) = U(z=0,\tau)e^{i\gamma|U(z=0,\tau)|^2 z}. \tag{4.9}$$

In this section, we consider the effects of SPM on pulse propagation and see how we might use these effects to directly measure the value of γ.

In particular, we will look at the effects of SPM on a pulse's spectrum. As can be seen in Equation 4.9, SPM simply adds a phase shift at each point of the pulse's envelope. The phase shift at a point in the envelope is proportional to the intensity of the envelope at that point. So, the magnitude of the pulse envelope is not affected, but the magnitude of the pulse's spectrum is affected. It is useful to introduce the concept of instantaneous frequency. Given the complex sinusoid

$$y(t) = Ae^{-i\phi(t)}, \tag{4.10}$$

the instantaneous frequency is defined by

$$\omega_i(t) = -\frac{d\phi(t)}{dt}. \tag{4.11}$$

Of course, one cannot truly identify a frequency component for each point in time, as the Heisenberg uncertainty principle shows. Nonetheless, the value of a pure frequency is given by the change in phase divided by the corresponding change in time. This idea, taken to its instantaneous limit, gives Equation 4.11. The case we are studying is a Gaussian envelope modulated onto a carrier at frequency ω_0. So, we are most interested in the deviation of the instantaneous frequency from ω_0. The phase change caused by self-phase modulation ϕ_{NL} is given by the argument of the exponential in Equation 4.9. The deviation in frequency is given by

$$\delta\omega(\tau) = -\frac{d\phi_{NL}(\tau)}{d\tau}, \tag{4.12}$$

where $\phi_{NL}(\tau)$ is the phase induced by SPM. The top plot of Figure 4-5 shows the phase induced by SPM on a Gaussian pulse (solid line) and on a third order super-Gaussian (dashed line). The second plot shows the resulting deviation of instantaneous frequency from ω_0, also know as frequency chirp. As we can see from Figure 4-5, the leading tail of the Gaussian shifts to lower frequencies and the lagging tail shifts to higher frequencies. Because frequencies are added to the pulse, the spectrum broadens.

Now, let us consider what happens as a pulse propagates down a fiber in which dispersion can be neglected. The pulse's evolution is described by Equation 4.9. We start with a Gaussian envelope of a pulse with carrier frequency ω_0:

$$U(z=0,\tau) = \sqrt{P_0}exp\Big(\frac{\tau^2}{2T^2}\Big) \tag{4.13}$$

Figure 4-6 shows the spectrum of the pulse at several points in its propagation. Each subplot in the figure is labeled by the amount of nonlinear phase shift induced at the peak of the Gaussian, which is proportional to the distance of propagation. Although the spectrum is changing, the magnitude of the pulse in time is not changing. When the nonlinear phase shift at the peak of the pulse has reached 1.5π, there appears a trough in the middle of the spectrum that dips to zero. It is this interesting fact that we shall use to measure the value of γ in Section 4.2.3.

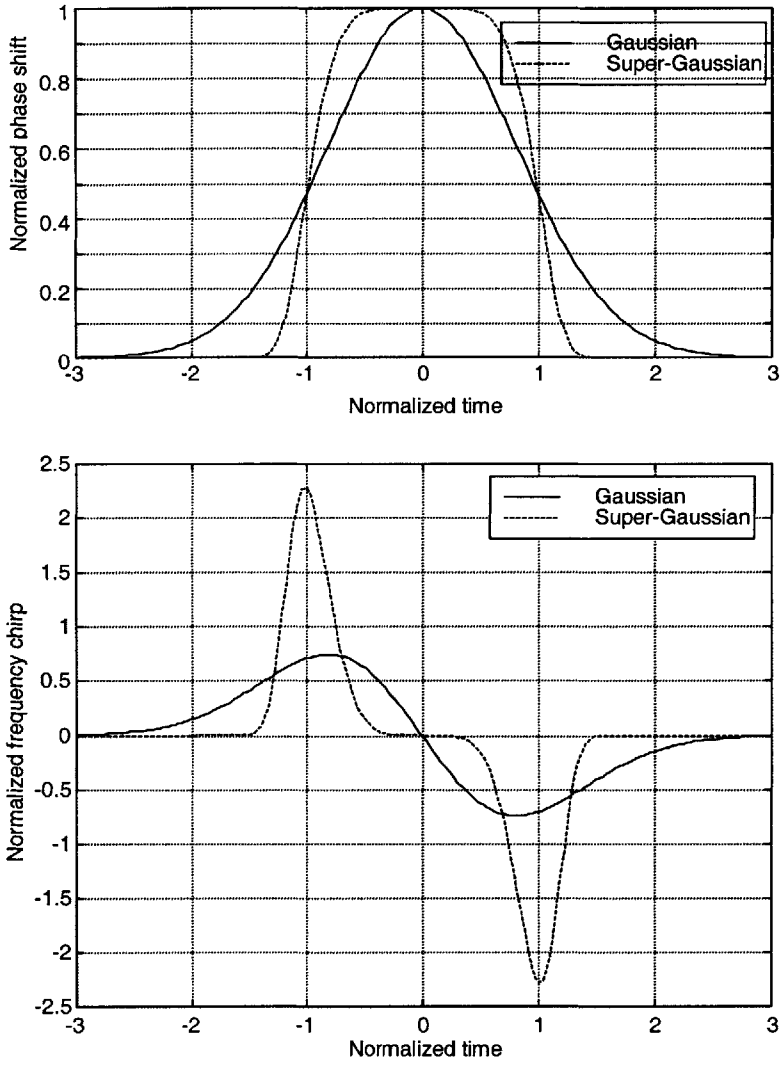

Figure 4-5: The top plot shows the phase shift induced by SPM on a Gaussian pulse and on a super-Gaussian pulse of order 3. The bottom plot shows the frequency chirp of the same pulses. Both plots are in normalized units.

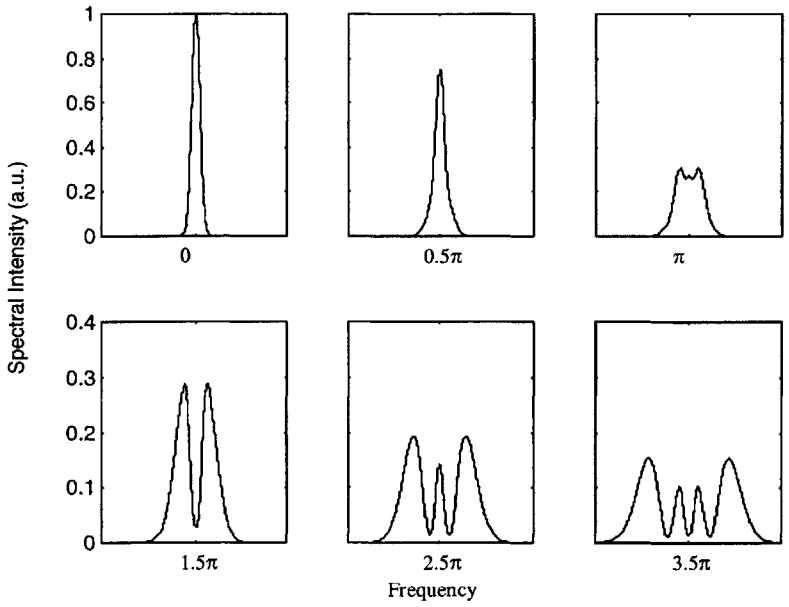

Figure 4-6: Calculated spectra of an SPM-broadened pure Gaussian pulse. The spectra are labeled by the phase shift induced at the peak of the pulse. Notice the difference in scale of the top three and bottom three plots.

4.2.2 Numerical Solution to the NLS

In Section 4.2.1 we neglected dispersive effects and loss in the fiber. We must, therefore consider the effects of dispersion and loss before we can make any measurement of γ. The nonlinear Schrödinger equation with the loss term is:

$$\frac{\partial U(z,\tau)}{\partial z} = -\frac{1}{2}i\beta_2\frac{\partial^2 U(z,\tau)}{\partial \tau^2} - \frac{\alpha}{2}U(z,\tau) + i\gamma|U(z,\tau)|^2 U(z,\tau). \tag{4.14}$$

The standard numerical method used to solve this equation is the split step Fourier method. In this method, Equation 4.14 can be rewritten in operator notation as

$$\frac{\partial U(z,\tau)}{\partial z} = (\hat{L}+\hat{N})U(z,\tau) \tag{4.15}$$

where the operators are given by

$$\hat{L}f = -\frac{\alpha}{2}f - \frac{1}{2}i\beta_2\frac{\partial^2 f}{\partial \tau^2}, \tag{4.16}$$

$$\hat{N}f = i\gamma|f|^2 f. \tag{4.17}$$

The formal solution to Equation 4.15 is

$$U(z = z_2, \tau) = e^{\Psi+\Omega} U(z = z_1, \tau) \tag{4.18}$$

where

$$\Psi = (z_2 - z_1)\hat{L} \text{ and } \Omega = \int_{z_1}^{z_2} \hat{N}(z, \tau)\, dz. \tag{4.19}$$

In general these two operators cannot be dealt with separately because $\exp(\Psi + \Omega) \neq \exp(\Psi)\exp(\Omega)$. But, if $z_2 - z_1$ is very small, then the equality

$$\exp(\Psi + \Omega) = \exp(\Psi)\exp(\Omega) \tag{4.20}$$

is very nearly true.

In the slit-step Fourier method, we consider the nonlinear and linear operators separately. First, we assume periodic boundary conditions with period T. The solution to the nonlinear part, as shown in Section 2.3.2, is simply

$$U(z, \tau) = U(z = 0, \tau) e^{i\gamma|U(z=0,\tau)|^2 z}. \tag{4.21}$$

The solution to the linear part can be found by assuming $U(z, \tau)$ has a Fourier series solution:

$$U(z, \tau) = \sum_{n=-\infty}^{\infty} \tilde{U}_n(z) e^{i\omega_n \tau} \tag{4.22}$$

where $\omega_n = 2\pi n/T$. The linear part of Equation 4.15 is

$$\frac{\partial U(z, \tau)}{\partial z} = -\frac{1}{2} i\beta_2 \frac{\partial^2 U(z, \tau)}{\partial \tau^2} - \frac{\alpha}{2} U(z, \tau). \tag{4.23}$$

If we substitute in Equation 4.22, we obtain

$$\sum_{n=-\infty}^{\infty} \frac{\partial \tilde{U}_n(z)}{\partial z} e^{i\omega_n \tau} = \sum_{n=-\infty}^{\infty} \Big(\frac{1}{2} i\beta_2 \omega_n^2 - \frac{\alpha}{2}\Big) \tilde{U}_n(z) e^{i\omega_n z}, \tag{4.24}$$

yielding the system of equations

$$\frac{\partial \tilde{U}_n(z)}{\partial z} = \Big(\frac{1}{2} i\beta_2 \omega_n^2 - \frac{\alpha}{2}\Big) \tilde{U}_n(z). \tag{4.25}$$

The solutions to Equations 4.25 are

$$\tilde{U}_n(z) = \tilde{U}_n(z=0) e^{(\frac{1}{2} i\beta_2 \omega_n^2 - \frac{\alpha}{2})z}. \tag{4.26}$$

Thus, we have solved the linear part of the NLS in the frequency domain and the nonlinear part of the NLS in the time domain.

Now we consider putting these two solutions together. The spatial coordinate z is discretized into steps of length Δz. We begin with initial conditions of $U(z=0,\tau)$, where U has period T along the temporal axis τ. To demonstrate the split step method, let us consider a slightly simpler version of it. First, we neglect dispersion and use Equation 4.21 to solve for U at $z = \Delta z$. Let us call the results of that calculation $U^{\mathbf{NL}}(z = \Delta z, \tau)$. Now we have to calculate the effects of dispersion by taking $U^{\mathbf{NL}}(z = \Delta z, \tau)$ into the frequency domain to get $\tilde{U}_n^{\mathbf{NL}}(z = \Delta z, \omega_n)$. We use $\tilde{U}_n^{\mathbf{NL}}(z = \Delta z, \omega_n)$ as the initial conditions for one spatial step of dispersion, from $z = 0$ to $z = \Delta z$. Then we return to the time domain to obtain $U(z = \Delta z, \tau)$. We repeat these steps for all subsequent spatial steps. The solution will converge more quickly to the correct solution if we interleave the steps, as shown in Figure 4-7. Instead of solving an entire spatial step of dispersion and then using those intial conditions to solve another full spatial step of SPM, we begin with a half step of dipsersion, then a full step of SPM, and finally a half step of dispersion. We then repeat for subsequent spatial steps.

To run this simulation on a computer, we cannot let the n of Equation 4.22 vary from $-\infty$ to ∞. Instead we truncate the series to vary from $-N$ to N, where we

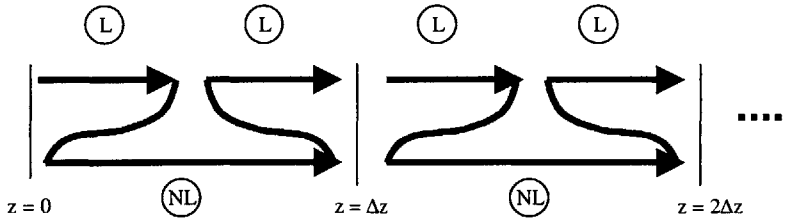

Figure 4-7: The split-step Fourier method of solutions involves alternate applications of the linear and nonlinear operators. Linear steps are labeled with an "L" and nonlinear steps are labeled with "NL." The axis shown is the discretized spatial axis.

choose N based on the accuracy of simulation desired. Once we choose this truncation constant, we can use the fast Fourier transform and inverse fast Fourier transform to move between the frequency and time domains. The fast Fourier transform grows in computational difficulty by the order of $N \log N$, which is why this method is often preferred to much slower algorithms based on the finite difference method. Nonetheless, we must keep in mind the the approximations we have made that can lead to error: space is discretized into small intervals so that we can make the assumption of Equation 4.20; the initial conditions, and, therefore, the solution is assumed to be periodic; in the frequency domain, higher frequencies are truncated from the Fourier series expansion of U; the FFT actually calculates the discrete time Fourier series rather than the desired continuous time Fourier series. We must also keep in mind that at the periodic boundaries, if the function is not continuous and does not have a continuous derivative, then the numerical solution may behave undesirably. After all, most physical pulse trains are continuous at bit boundaries and have countinuous derivatives.

Let us use this algorithm to demonstrate the effects of dispersion and SPM together on the spectrum. As mentioned in Section 4.2.1, when the phase shift induced by SPM at the peak of a Gaussian pulse reaches 1.5π, there appears a trough in the middle of the spectrum of the Gaussian. But, we cannot necessarily neglect the second order dispersion in an optical fiber. Using the MatLab code that is given in Appendix A, we simulate the propagation of a 2.5 ps optical pulse with a Gaus-

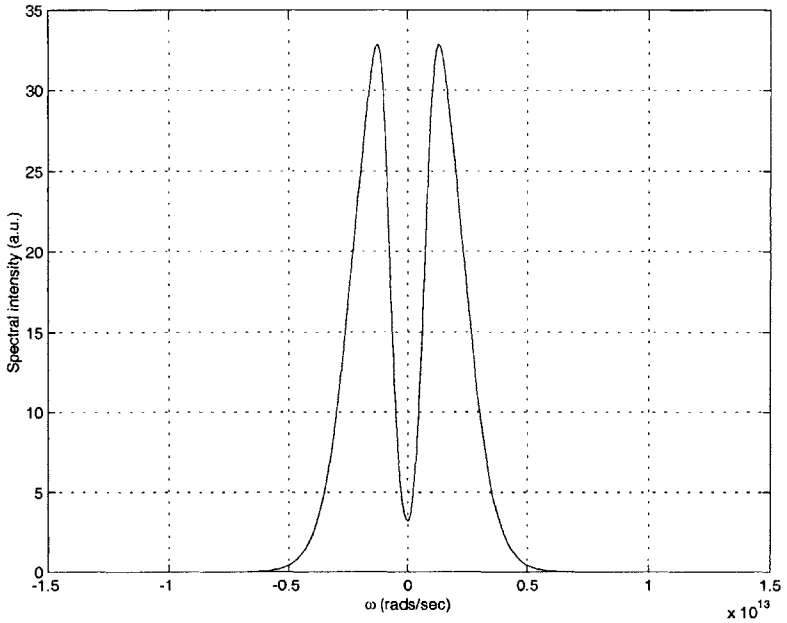

Figure 4-8: Spectrum of a 2.5 ps intensity FWHM Gaussian pulse with .565 W peak intensity after propagating 3135 m in dispersionless optical fiber. γ is set at 0.002 $m^{-1}W^{-1}$. With those parameters, the phase shift acquired at the peak of the pulse is 1.5π. Therefore, the trough is at its minimum.

sian envelope and .565 W peak optical power. The fiber is 3135 m long and has $\gamma = .002\ m^{-1}W^{-1}$. If the fiber is dispersionless (i.e., $\beta_2 = 0$), then the spectrum at the end of the fiber is given by Figure 4-8. The spectrum shown is that of the envelope. The true spectrum is identical, except that it is centered around the frequency of the carrier, $\pm\omega_0$, rather than 0. The trough's minimum value at this point tells us that the phase shift at the peak is 1.5π, and from this fact and the fact that $\beta_2 = 0$ we can deduce the value of γ. Unfortunately, for nonzero β_2 this trough may not appear. In Figure 4-9, we show the propagation of the same pulse down the same fiber, except that the fiber has $\beta_2 = -20\ ps^2/km$. This value is typical for standard single mode fiber. As Figure 4-9 shows, we would not be able to deduce the value of γ solely from the spectrum. This fact will be very important in our analysis of the method of measuring γ suggested in Section 4.2.3.

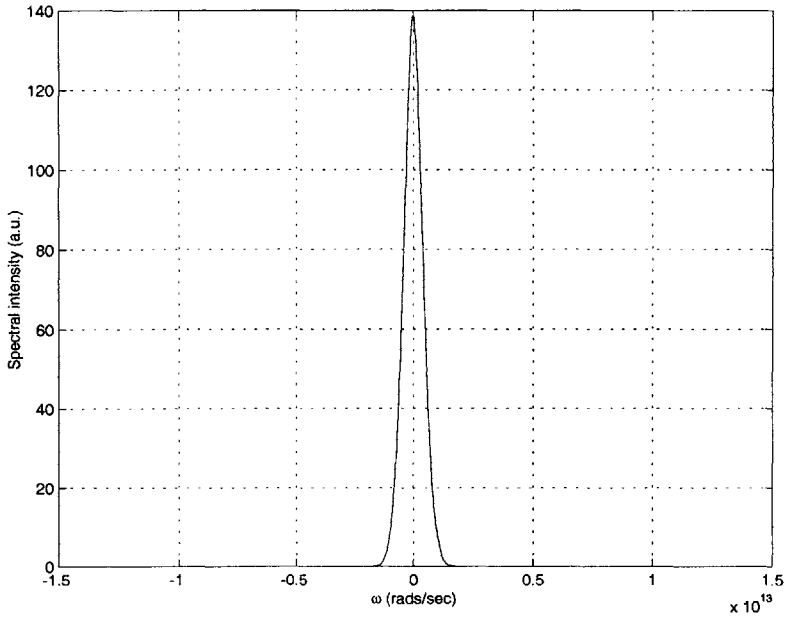

Figure 4-9: Spectrum of a pulse with the same parameters as described in Figure 4-8, except $\beta_2 = -20$ ps^2/km. Notice the difference caused by the nonzero dispersion.

4.2.3 Experimental Measurement of γ

Many of the most significant nonlinear effects are included in the self-phase modulation term of the nonlinear Schrödinger equation. The accurate measurement of the nonlinear index of refraction n_2 and, therefore of γ, is very important. Measured values of n_2 vary from 2.2×10^{-20} to 3.4×10^{-20} m^2/W and depend on core composition, dopant types and levels, and whether or not the fiber is polarization maintaining [21]. The value of γ also depends on the effective area of the fiber core. For a given power level, a smaller core area implies a larger power per unit area, which yields a larger value of γ. This last point is especially significant to us. The dispersion shifted fiber used in the folded UNI of Section 5.1 has a smaller core area than conventional communications fiber. It is this smaller core area, in fact, that shifts the dispersion zero to 1550 nm. The smaller core area also increases the effects of the self-phase modulation. Both the lower value of β_2 and the larger value of γ will help us in the measurement of γ.

Several methods have been proposed to measure the nonlinear index of refrac-

tion [35], and some focus on dispersion shited fiber [36], the fiber we use in this thesis. As mentioned in Sections 4.2.1 and 4.2.2, if an optical pulse propagates down a dispersionless medium with SPM only, then the trough in the center of the spectrum reaches its minimum when the nonlinear phase shift at the peak of the pulse ϕ_{max} reaches 1.5π. This effect is shown in Figure 4-6. Knowing the peak power required for a pulse to obtain this value of ϕ_{max} after propagating down a given fiber can be used to deduce the value of γ. Let us assume that we can neglect dispersion in the fiber. Let us also assume that the pulse has the initial form

$$U(z=0,\tau) = \sqrt{P_0}e^{-2\tau^2/T^2}, \tag{4.27}$$

where P_0 is the peak intensity of the pulse and T is related to the intensity full width at half maximum T_{FWHM} by

$$T = \frac{T_{FWHM}}{\sqrt{\ln 2}}. \tag{4.28}$$

We need an equation that relates the peak power P_0 with γ. We know from Equation 4.9 that the nonlinear phase shift induced at the peak is given by

$$\phi_{max} = \gamma P_0 L \tag{4.29}$$

where L is the length of the fiber. In the experiment, we increase the peak power until we observe the minimum in the trough in the spectrum. We then know that ϕ_{max} in Equation 4.29 equals 1.5π, giving us

$$\gamma = \frac{1.5\pi}{P_{0,1.5\pi}L} \tag{4.30}$$

where $P_{0,1.5\pi}$ is the peak power required to induce a 1.5π phase shift in the center of the pulse. Because the pulses are so short, we cannot directly measure their peak power. If we know the pulse width, the time averaged power, and the pulse repetition

rate, then we can deduce P_0. The energy per pulse is

$$\frac{\text{Energy}}{\text{Pulse}} = \int_{-\infty}^{\infty} |U(z,\tau)|^2 \, d\tau = TP_0\frac{\sqrt{\pi}}{2}. \tag{4.31}$$

The time averaged power is given by

$$P = \frac{\text{Energy}}{\text{Pulse}} \times R = TP_0R\frac{\sqrt{\pi}}{2} \tag{4.32}$$

where R is the pulse repetition rate. In Equation 4.32, we can directly measure P and R. To calculate P_0, we still need to measure T. Equation 4.28 relates T to T_{FWHM}. Although the pulses are too short to make any direct pulse width measurement, we can measure the autocorrelation pulse width. If we assume the Gaussian pulse shape of Equation 4.27, then the autocorrelation is given by

$$A(t) = \int_{-\infty}^{\infty} |U(z=0,\tau)|^2 |U(z=0,\tau+t)|^2 \, d\tau = \frac{P_0^2 T\sqrt{2\pi}}{4} e^{-2t^2/T^2}. \tag{4.33}$$

If we call the full width at half maximum of the autocorrelation $T_{AC,FWHM}$, then we have, by Equation 4.33,

$$T_{AC,FWHM} = T\sqrt{2\ln 2}. \tag{4.34}$$

This equation gives us the necessary relationship between T and the measurable quantity $T_{AC,FWHM}$. Combining Equations 4.30, 4.32, and 4.34 and letting $P \to P_{1.5\pi}$, we obtain

$$\gamma = \frac{1.5\pi^{3/2} T_{AC,FWHM} R}{4LP_{1.5\pi}\sqrt{\ln 2}} \tag{4.35}$$

where $P_{1.5\pi}$ is the time averaged power necessary to induce a 1.5π phase shift at the Gaussian pulse's peak. Now we can obtain γ from the measurable quantities in Equation 4.35.

Equation 4.35 suggests that we can measure γ by varying the power of the pulses. The experimental setup is shown in Figure 4-10. The 1550 nm source is an actively

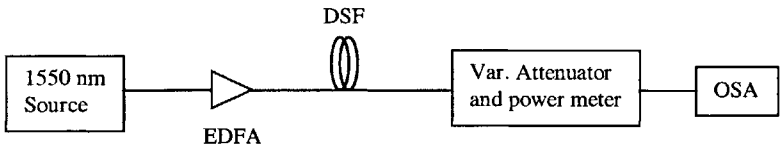

Figure 4-10: Experimental setup for measuring γ. EDFA stands for erbium doped fiber amplifier, and the source generates 2 ps Gaussian pulses at 10 GHz.

Table 4.1: β_2 for various carrier wavelengths in the three spools of fiber tested

	500 m	2000 m	4000 m
β_2 (ps^2/nm) at 1545nm	-0.37	-1.2	-0.71
β_2 (ps^2/nm) at 1550nm	0.16	-0.91	-0.24
β_2 (ps^2/nm) at 1555nm	-0.91	-1.4	-1.2

mode-locked fiber laser generating ~2 ps intensity FWHM Gaussian pulses. The pulse repitition rate is 10 GHz. We can observe spectral intensity on the optical spectrum analyzer and we simply adjust the variable optical attenuator until the characteristic trough reaches its minimum, as shown in Figure 4-6. At that point, ϕ_{max} equals 1.5π, and thus we can measure the time averaged optical power in the fiber and apply Equation 4.35.

Nonetheless, the development above assumed that dispersion is negligible in the test fiber. To test this hypothesis, we run simulations with the dispersion measurements of Section 4.1. Equation 4.6 gives us measurements of β_2 as a function of carrier wavelength. Table 4.1 shows values of β_2 for several carrier wavelengths in the three spools of fiber tested in this thesis. We should note that these data were obtained from the derivative of an interpolation of discrete data, and should only be taken as an estimation of the true value of β_2. Nonetheless, in all cases shown, the second order dispersion measured for DSF is much less than the 20 ps^2/nm that is typical for $|\beta_2|$ in standard single mode fiber, as expected.

We would like to use these data in a simulation to determine whether or not the dispersion of these spools of dispersion shifted fiber are significant enough to affect the spectrum. Let us assume the autocorrelation full width at half maximum of the initial

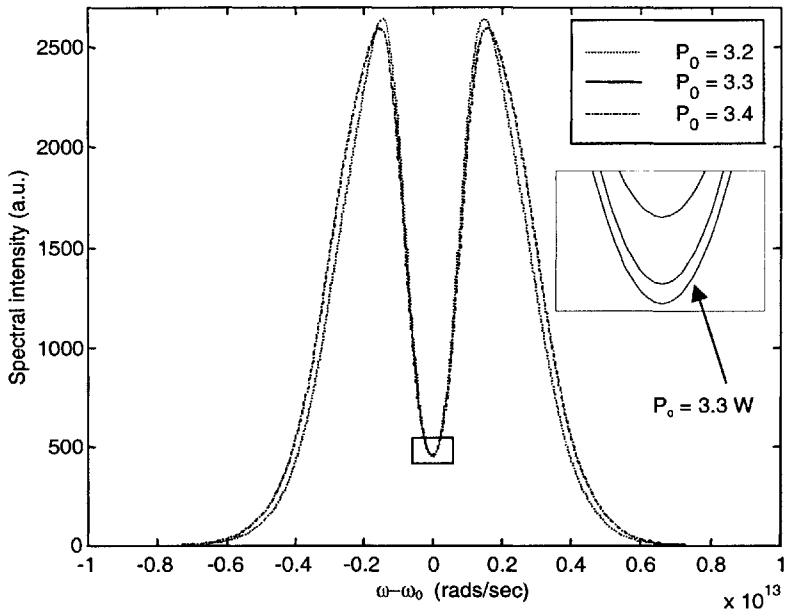

Figure 4-11: Spectra of pulse propagation at the end of a 500 m DSF spool for various peak powers. The inset shows a boxed area of the plot for detail.

pulse is Gaussian with $T_{AC,FWHM} = 3.0$ ps. Let us also assume the input into the test fiber is a 10 GHz pulse stream. Finally, we assume that $\gamma \approx .003$ m^{-1}W^{-1}. We test, in simulation, the 500 m spool of fiber at a carrier wavelength of 1550 nm, where $\beta_2 \approx 0.2$ ps^2/nm. If we assume no dispersion, then $\phi_{max} = 1.5\pi$ occurs at a peak power of $P_0 = 3.14$ W by Equation 4.30. We must check, however, that dispersion plays a negligible role in propagation in 500 m of DSF so that this minimum still occurs at $P_0 = 3.14$ W. The results are shown in Figure 4-11, where the spectra are shown for three test cases. The three plots are the spectra at peak powers of 3.2, 3.3, and 3.4 W. The minumum trough in the spectrum occurs at a power of $P_0 = 3.3$ W. The peak power of $P_0 = 3.14$ W, given the assumptions of this test, corresponds to an time averaged power of $P \approx 71$ mW, as can be seen by Equation 4.32. The peak power of $P_0 = 3.3$ W corresponds to a time averaged power of $P \approx 7.5$ mW. In this case, the error is less than 5%. In Section 4.1, we decided that the desired walk-off between the control and signal pulses was best acheived in the 500 m spool of DSF. Thus, this length of DSF was placed in the experimental setup of Figure 4-10.

Our experimental measurement of γ in the 500 m spool of DSF, using the method developed in this section, was .0022 $W^{-1}m^{-1}$.

Chapter 5

Design and Testing of the Folded UNI

The measurements of nonlinearties and dispersion in Chapter 4 provide us with information necessary to design and predict the behavior of the folded UNI. In this chapter, we introduce the folded ultrafast nonlinear interferometer (FUNI) [37]. Like the UNI, the FUNI is a single arm interferometer that uses a nonlinear medium to induce a phase shift in an optical pulse. The nonlinear medium of the folded UNI is optical fiber rather than a semiconductor optical amplifier. Moreover, the folded UNI uses reflection of the pulses from a Faraday mirror to stabilize polarization within the switch. This inherent polarization control solves many of the difficulties raised in Section 3.3. In the first section, we present the basic design of the folded UNI. The second section describes the experimental setup, including optical pulse sources. The third section presents measurements of the switching window. The fourth section gives the results of bit error rate tests on the FUNI. The fifth section discusses the results of the tolerance of the folded UNI to timing jitter. In the final section we test the sensitivity of the FUNI to timing jitter.

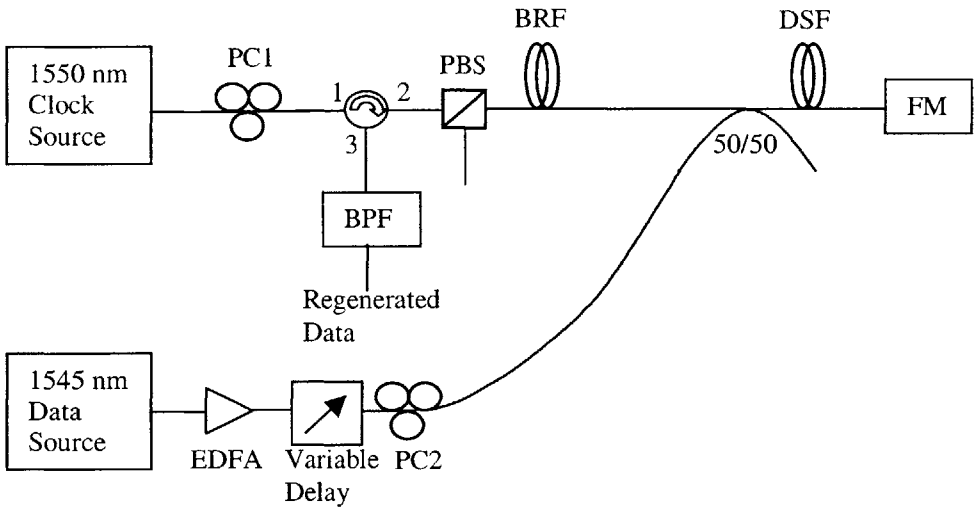

Figure 5-1: In the folded UNI, a Faraday mirror provides polarization stabilization. PC1 and PC2 are polarization controllers, PBS is a polarizing beam splitter, DSF is dispersion shifted fiber, BPF is a band pass filter, BRF is birefringent fiber, FM is a Faraday mirror, and EDFA is an erbium doped fiber amplifier.

5.1 The Folded UNI

Although the UNI has been demonstrated to switch at 100 Gbit/s [13], this device has only recently been considered for all-optical 3R regeneration [38]. Acoustic effects on the polarization are negligible in the UNI because the two orthogonal polarizations of the signal pulse, after being split in the birefringent fiber of Figure 2-3, co-propogate closely through the optical fiber. The UNI does, however, suffer from slow polarization drifts, and the three polarization controllers in Figure 2-3 must be actively monitored. In the folded UNI, shown in Figure 5-1, a Faraday mirror added to one end of the optical path creates inherent polarization stabilization within the switch.

The folded UNI works in a way similar to the UNI of Section 2.2.2 and can be applied in a very direct manner to all-optical 3R regeneration [37]. Incoming network data pulses serve as control pulses and locally generated clock pulse serve as signal pulses in the FUNI. That is, the presence or absence of a data pulse determines whether or not the corresponding clock pulse is switched out the "Regenerated Data" port of Figure 5-1, thus modulating the data pulse stream's bit pattern on the clock

pulse stream. The circulator, shown with a curved arrow in Figure 5-1, passes optical power from port 1 to port 2 and from port 2 to port 3. PC1 controls the polarization of the local clock pulses to be linear and to pass maximally through the polarizing beam spliter. A 3 m length of birefringent fiber (BRF), cross-spliced at 45° to the PBS splits each clock pulse into two orthogonal components separated temporally by 5 ps. The network data stream is coupled onto the regenerator at the 50/50 coupler. The coupling is timed so that the data pulses are each coincident with one of the two temporally separated orthogonal clock components. After the clock and data pulses pass through the dispersion shifted fiber, the Faraday mirror rotates all the pulses by 90° and reflects them back through the FUNI. Due to microbending and slight fabrication irregularities, each point in the optical fiber has an instantaneous orientation and strength of birefringence. The 90° Faraday rotation, therefore, ensures that all birefringent effects accumulated during propagation from left to right are undone during the reverse trip through the folded UNI.

To see how regeneration occurs, we note two cases: for each clock pulse, a data pulse is either present or absent. If there is no data pulse, then the Faraday rotation and reflection ensures that the clock pulse is recombined temporally in the birefringent fiber. Moreover, because of the 90° Faraday rotation, the left propagating clock pulse arrives with a polarization orthogonal to clock pulses propagating right at the PBS. Therefore, the left propagating clock pulse is reflected, rather than transmited, at the PBS. If, on the other hand, a data pulse is present, then it couples onto the FUNI at the 50/50 coupler in Figure 5-1 so that it temporally overlaps one of the two orthogonal polarizations of the clock pulse. Remember that two orthogonal polarizations of the clock pulse were separated temporally in the birefringent fiber. Whichever of these two polarizations temporally overlaps the data pulse receives a nonlinear phase shift. The nonlinear medium in the folded UNI is dispersion shifted fiber, used to minimize the undesired effects of group velocity dispersion [39]. The erbium doped fiber amplifier in Figure 5-1 is adjusted to amplify the data pulse power until a π phase shift is induced in one of the two clock polarizations. This nonlinear phase shift makes the FUNI appear to be a half wave plate oriented at 45° to the

clock pulse. Because it behaves like a half wave plate, the FUNI rotates the linearly polarized clock pulse by 90°. Taken with the 90° rotation of the Faraday mirror, the left propagating clock pulse arrives at the PBS with the same polarization it had when it first propagated to the right through the PBS. It is, therefore, transmitted through the PBS and then directed out port 3 of the circulator. The band pass filter removes the data pulses, leaving behind the regenerated data pattern modulated into the clock pulse train.

Because the Faraday mirror reflects pulses back down the same path, pulses propagating to the right interact with pulses propagating to the left. This interaction is similar to the one between the CW and CCW pulses of the fiber NOLM discussed in Section 3.1.2. But, in the case of the folded UNI, the clock pulses are separated temporally rather than into counterpropagating CW and CCW pulse streams. So, as each temporally separated orthogonal polarization of a clock pulse propagates to the right, both interact with the pulses that are propagating to the left. In this way, the effects of this interaction are smaller in the FUNI than in the fiber NOLM. Nonetheless, the interaction can be different between the two temporally separated orthogonal polarizations of a clock pulse. Recall from Equations 2.61 and 2.62 that polarization affects the magnitude of the nonlinear phase modulation. For example, consider a left propagating data pulse that is polarized in the x direction and a right propagating clock pulse that is separated temporally into two polarizations, one in the x direction and one in the y direction. In the folded UNI then, the phase shift induced in the y directed component of the clock pulse will be two thirds that of the phase shift induced in the x directed component of the clock pulse.

5.2 Experimental Setup

The experimental setup for testing the folded UNI is shown in Figure 5-2. The transmitter block in Figure 5-2 consists of an RF synthesizer driving a mode-locked fiber laser, which produces 2 ps pulses at a 10 GHz repetition rate, a data pattern generator, and an electro-optic modulator (EOM). It is important to note that although

many of the tests reported in this thesis operate at 10 GHz, the pulse widths are on the order of 2 to 3 ps and may, therefore, support data rates of up to 200 GHz. The data is generated in the transmitter by an Anritsu MP1761B Pulse Pattern Generator. The RF drive from the pattern generator is an NRZ data pattern that controls an electro-optic intensity modulator, labeled EOM in Figure 5-2. The EO modulator impresses an on-off keyed data pattern on the 10 GHz optical pulse train generated in the mode-locked fiber laser data source. The data pattern is a pseudorandom bit stream that can be nonrepeating for up to $2^{31} - 1$ bits at a rate of 10 Gbit/s. The regenerator block in Figure 5-2 also contains an RF synthesizer driving a mode-locked fiber laser that produces 2 ps pulses at a 10 GHz repetition rate, a folded UNI regenerator, and a dithering phase-locked loop (DPLL) clock recovery circuit. The network data input to the folded UNI is provided by the transmitter block and the regenerator clock pulse train is generated in the regenerator pblock. In the folded UNI, band pass filter 1 (BPF1) filters out the data pulses after the clock pulses have been switched, as described in Section 5.1. The other band pass filters, BPF1 and BPF2, filter out-of-band spontaneous emission noise introduced by the erbium doped fiber amplifiers (EDFA's).

Both pulse sources are actively mode-locked erbium doped fiber lasers in a sigma configuration and produce a single polarization [40]. The lasers can be tuned in the range of about 1545 nm to 1560 nm. In the experimental setup, each mode-locked fiber laser is tuned to a different carrier frequency. Figure 5-3 shows the autocorrelation trace of a pulse from the fiber laser. The trace itself has a full width at half maximum of 2.7 ps. If we assume a Gaussian pulse shape, then the intensity FWHM of the pulse is 1.9 ps.

5.3 FUNI Switching Window

When data pulses are coupled into the FUNI, they may not perfectly temporally overlap one of the orthogonal clock pulse polarizations. That is, the peak of the data pulse may not overlap the peak of the clock pulse. In order to characterize the switch

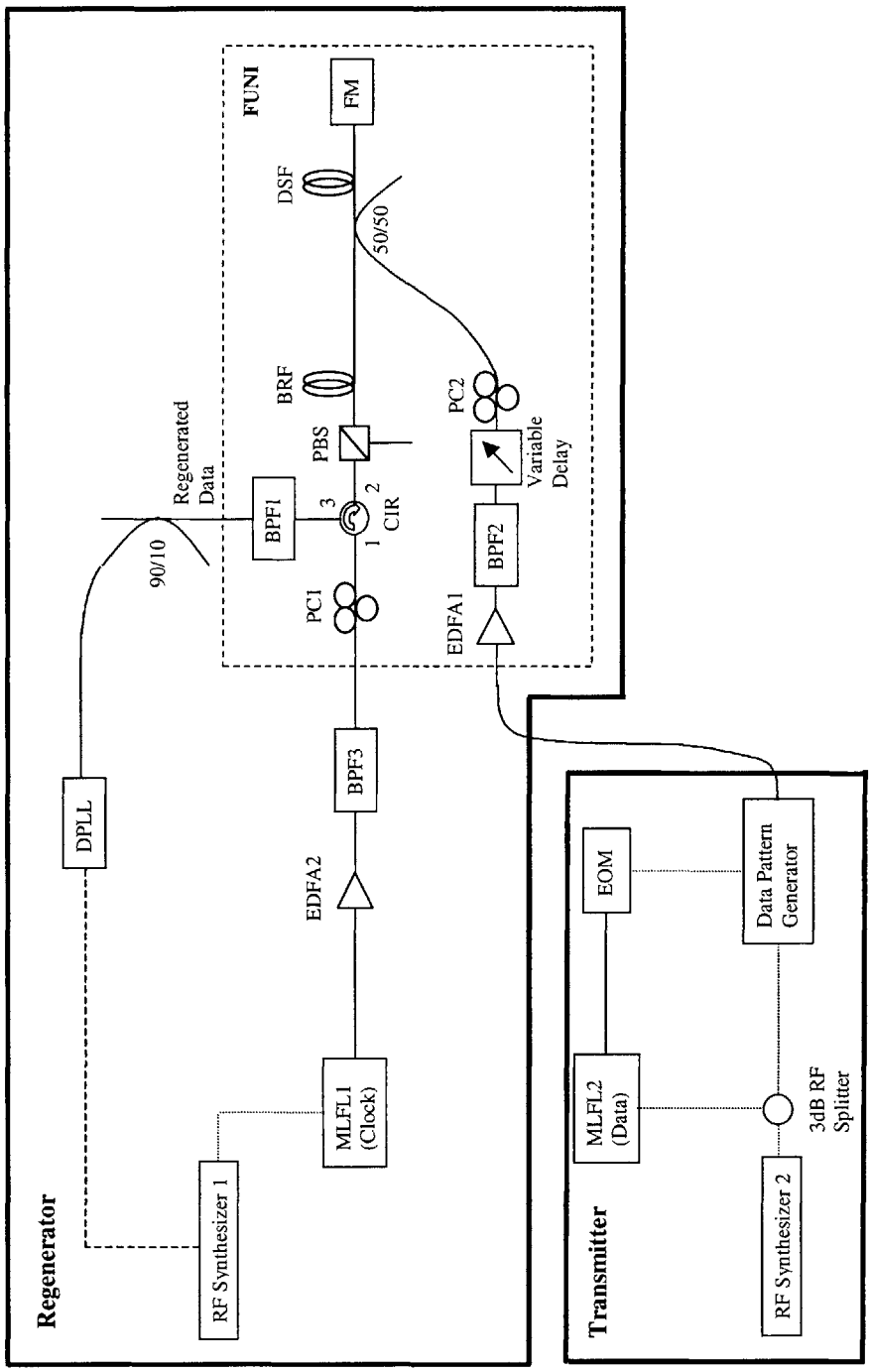

Figure 5-2: Experimental setup to test the Folded UNI as an all-optical regenerator. Solid lines represent optical paths and dotted lines represent electrical paths. EDFA stans for erbium doped fiber amplifier, BPF for band pass filter, EOM for electro-optic modulator, FM for Faraday mirror, PBS for polarizing beam splitter, BRF for birefringent fiber, DSF for dispersion shifted fiber, MLFL for mode-locked fiber laser, and DPLL for dithering phase-locked loop.

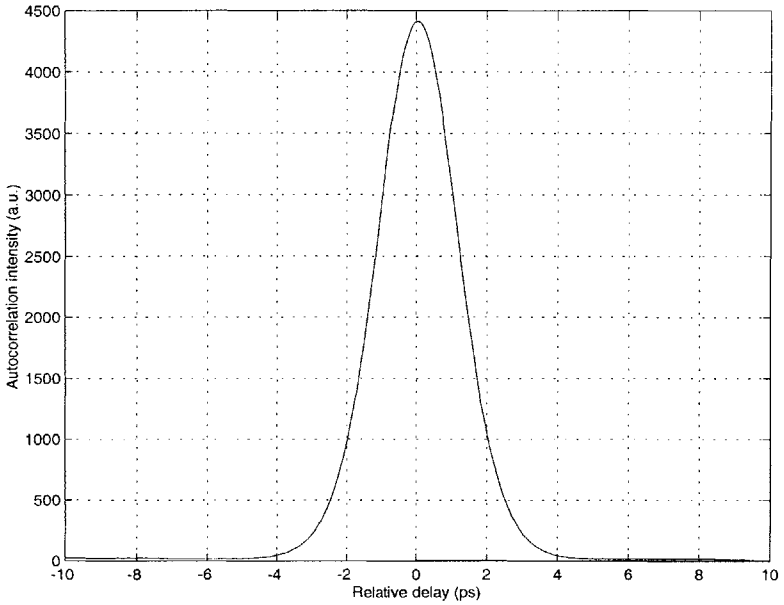

Figure 5-3: Autocorrelation trace of a 1.9 ps pulse from a PriTel laser source operating at 10 GHz.

transfer characteristic as a function of the relative delay between the clock and data pulses, we measure the folded UNI switching window. The switching window plots the power switched out the "regenerated data" port of the folded UNI as a function of the relative delay between the signal pulse and the data pulse. The experimental setup used to measure the switching window is shown in Figure 5-4. A plot of the folded UNI's switching window with the 500 m spool of DSF, with the signal pulses at 1550 nm, and with the control pulses at 1545 nm is shown in Figure 5-5.

Measuring the switching window requires both RF sources in the experimental setup. To measure the switching window, we need to vary the delay between the signal and data pulses. We also set the data pattern generator to produce only "marks" (i.e., all bit periods contain an optical pulse). One direct way to make this measurement is to manually adjust the variable delay in the data pulse arm of the folded UNI. Then we could simply measure the power at the regeneration port for each delay setting. A much quicker method, shown in figure 5-4, is to set one RF synthesizer at 10 GHz and the other at 10 GHz plus 10 kHz. These RF synthesizers drive two mode-locked fiber lasers. The control pulse train has a carrier wavelength

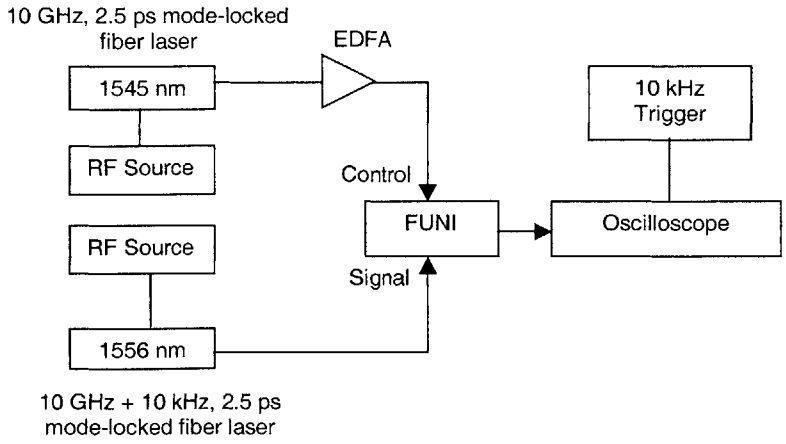

Figure 5-4: Block diagram of experimental setup for taking a switching window. The control and signal pulse trains are at slightly different pulse rates to cause a walk-off that varies with time. The switching window appears on the sampling oscilloscope.

of 1545 nm and the signal pulse train has a carrier wavelength of 1556 nm. Every 1×10^{-4} seconds, i.e., at every millionth pulse, the peak intensities of the two optical pulse streams temporally overlap again. At the output of the folded UNI, we place a photodiode that is slow enough to average over several hundreds of pulses. The output of the photodiode is sent to a oscilloscope, which scans over a period of 100 μs to give us the switching window.

The switching window can give us some idea of the folded UNI all-optical regenerator's tolerance to timing jitter in the bits of the optical data stream. A wider switching window implies a larger allowable relative delay between a data pulse and the clock pulse it temporally overlaps. Figure 5-5 shows a switching window with the signal pulses at a carrier wavelength of 1550 nm and the control pulses at a carrier wavelength of 1545 nm. The two peaks are a consequence of the splitting of the signal pulses into temporally separated orthogonal polarizations. The control pulse can overlap either of these temporally separated polarizations, and each peak corresponds to one of these two cases. Each peak in the switching window has a full width at half maximum of ~5 ps, implying a tolerance to timing jitter on that order. We could widen the switching window by using a longer length of fiber or by adjusting the carrier wavelengths of the clock and data pulses, increasing the walk-off between the

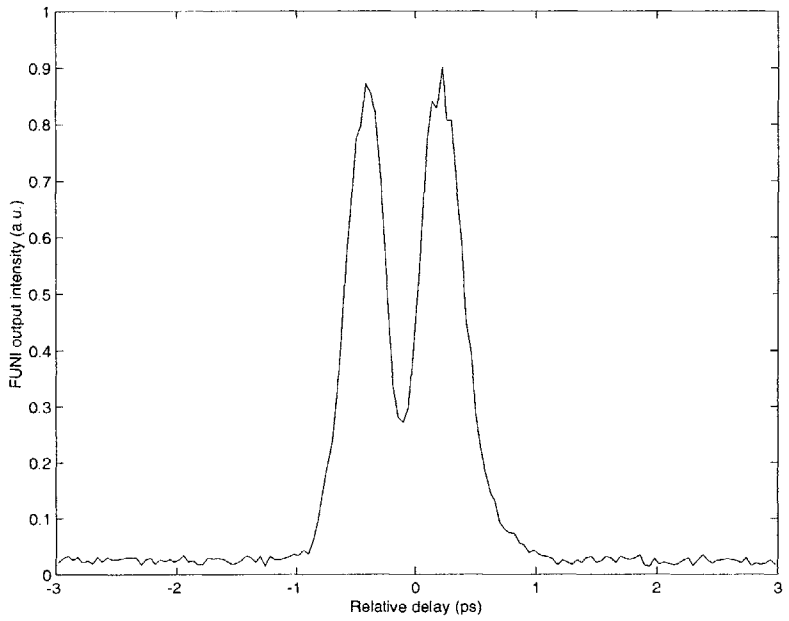

Figure 5-5: Switching window of the folded UNI with the 500 m spool of fiber, with the signal pulses at 1550 nm, and with the control pulses at 1545 nm.

clock pulses and the data pulses.

5.4 FUNI Regenerator Error Performance

In the bit error rate test, we place a receiver at the regenerated data port of the regenerator block of Figure 5-2. This receiver operates at our 10 GHz data test rate, and includes a variable optical attenuator, a low noise gain flattened MPB erbium doped fiber amplifier to amplify the optical signal, and a high speed photodiode to convert the optical pulses into electrical signals. These received electrical signals are detected and the folded UNI performance as an all-optical regenerator is quantified using an Anritsu 12.5 GHz bit error rate tester (BERT). Figure 5-6 shows the experimental layout for the receiver. In the bit error rate test, the bit error rate of the regenerated data from the folded UNI is measured as a function of the power supplied to the receiver. We control this power with the variable optical attenuator.

The first choice of fiber was the 500 m spool. The clock pulse carrier wavelength

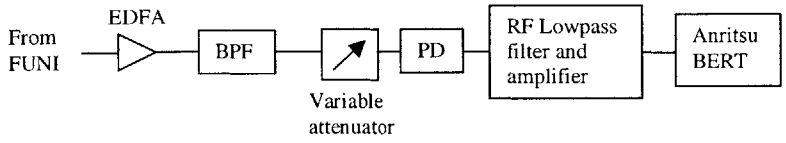

Figure 5-6: The receiver used to test the bit error rate of the folded UNI as a function of receiver input power. The EDFA is an erbium doped fiber amplifier and the PD is a photodiode.

was set at 1556 nm and the data pulse carrier wavelength was set at 1545 nm. By Figure 4-2 these wavelengths yield a walk-off of ~3 ps between the data and clock pulse streams during the dual pass through the 500 m DSF spool (remember that one must double the value read off the figure because both pulse streams propagate twice through the fiber). As shown in Section 4.2.3, γ is large enough for the network data pulses to induce the required π phase shift in the clock pulses in the 500 m DSF spool.

The results of a bit error rate test with these parameters are shown in Figure 5-7. The solid circles show the results of a baseline test, where the data pulse stream at 1556 nm was input directly into the receiver without first propagating through the folded UNI. The hollow circles show the bit error rate of the regenerated data stream coming out of the folded UNI. Both sets of points have linear regressions plotted through them. As shown in Figure 5-7, the folded UNI incurs a 1 dB power penalty at a bit error rate of 10^{-9}. There is also no observable error floor. The control energy was 4.7 pJ per pulse and the signal energy was 170 fJ per pulse. The folded UNI, if it is truly behaving as a pulse regenerator, ought to improve the error rate rather than incur a penalty. In this test, however, it is important to note two points. First, the data stream we are testing did not come off a network. It is a locally generated optical pulse stream with a data pattern modulated onto it. Therefore, the data pulses are not distorted, and we should not expect improvement in the pulses from the folded UNI. Second, although the amplifier in the receiver is gain flattened, there is nonetheless a ripple in the gain as a function of optical wavelength. The ripple is as wide as 1 dB over the gain spectrum of erbium. The data pulses in the baseline

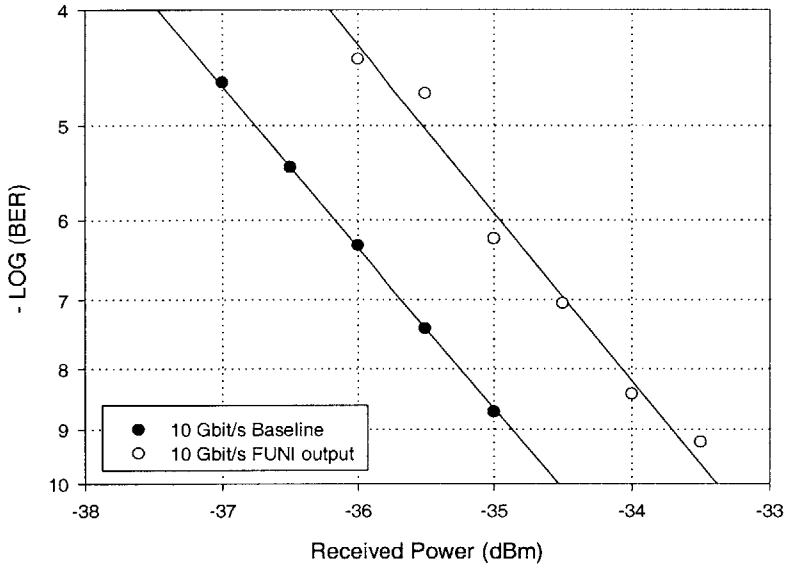

Figure 5-7: Bit error rate test of folded UNI with the 500 m spool compared to a baseline test. The signal carrier wavelength is 1556 nm and the control carrier wavelength is 1545 nm.

test are at a different carrier frequency than the regenerated data pulses of the folded UNI bit error rate test. Thus, wavelength dependence in the erbium doped fiber amplifier could cause the 1 dB power penalty in the bit error rate test of the folded UNI. The folded UNI, therefore, has been successfully demonstrated as an all-optical pulse regenerator.

5.5 Sensitivity to Timing Jitter

Regenerators must be able to correct timing jitter introduced in the data pulses during long propagation. The carrier wavelengths were chosen to introduce walk-off between the data and clock pulses, as described in Section 3.1.2. Larger walk-off times allow for more timing jitter tolerance. The walk-off time, however, cannot be so large that data pulses in one bit period pass through the signal pulse in a neighboring bit period. Moreover, larger walk-off times reduce the effective interaction length between the data pulse and the clock pulse because the peak intensity of the data pulse merely passes through the peak of the clock pulse rather than remaining temporally

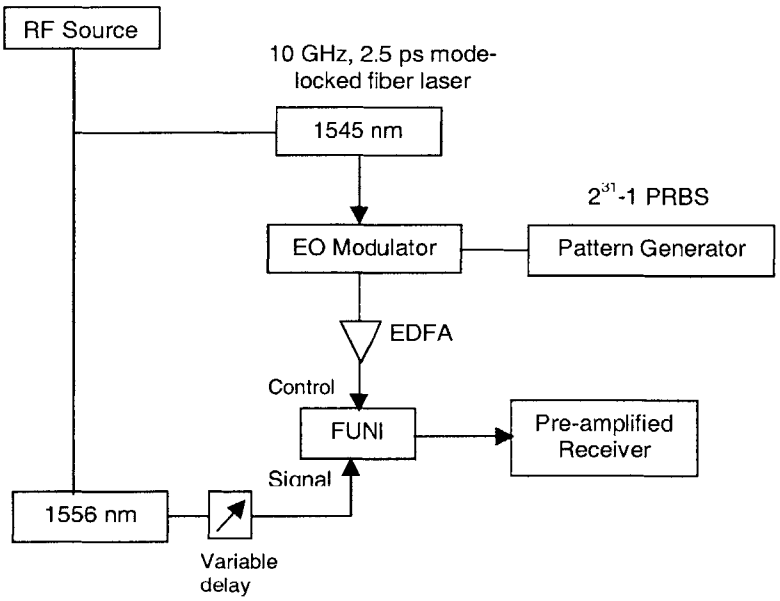

Figure 5-8: Setup for testing the tolerance of the folded UNI to timing jitter. The data pulses are amplified by an erbium doped fiber amplifier (EDFA), and a single RF synthesizer drives both mode-locked fiber lasers.

overlapped with it.

In Section 5.4, the bit error rate was plotted against the received power. In this section, the received power is held constant, and the bit error rate is plotted as a function of the relative delay between the data pulses and the clock pulses. The experimental setup is shown in Figure 5-8. As in Section 5.4, a pattern generator and EO modulator impress a data pattern on the control pulses. The control pulses have a carrier wavelength of 1545 nm and the signal pulses have a carrier wavelength of 1555 nm. In this setup, however, a single RF synthesizer drives both mode-locked fiber lasers. Using a single synthesizer minimizes all unwanted timing jitter between the data pulses and the clock pulses. Instead, timing is adjusted with the variable delay and is held fixed until a bit error rate is taken. The results are shown in Figure 5-8. These data show that the folded UNI performs at a bit error rate of better than 10^{-9} for a relative delay between data and clock of up to 4 ps.

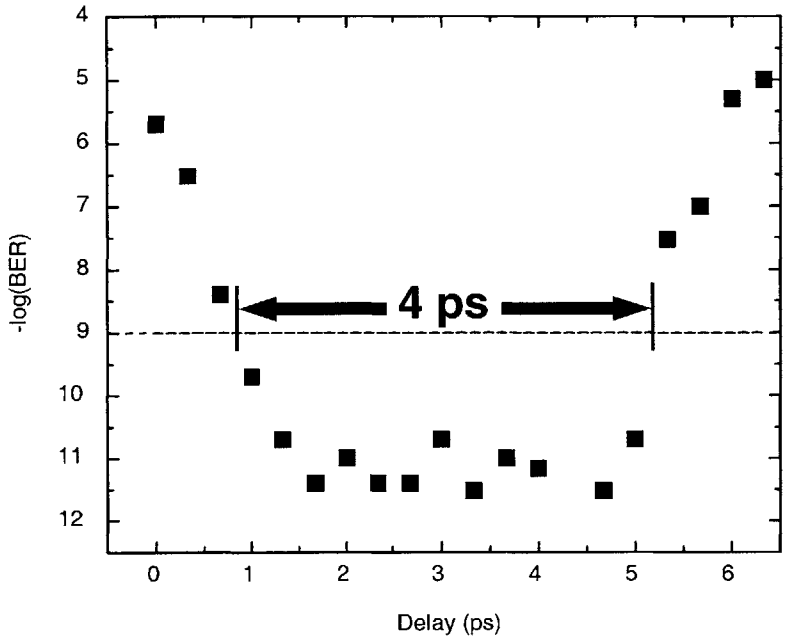

Figure 5-9: The bit error rate of the folded UNI as a function of the relative delay between data pulses and clock pulses.

5.6 Regenerative XOR

One application of all-optical switches is the logical XOR, important for tasks such as address recognition. All-optical XOR has been shown already [41]. The folded UNI can also operate as an XOR switch. In particular, the nearly instantaneous nonlinear index of refraction makes it well-suited to a regenerative XOR operation. Figure 5-10 shows the the folded UNI operating as a regenerative XOR. The control pulses are the optical channels labeled "A" and "B" in the figure. Instead of a single control pulse overlapping one of the two orthogonal signal pulse polarizations, channel "A" pulses overlap with one signal pulse polarization while channel "B" pulses overlap with the other, as shown in Figure 5-10. If neither "A" nor "B" are present, then there is no relative phase shift between the polarizations of the signal pulse and so it is not switched out. If only one is present, then one of the signal pulse polarizations is shifted by π and the other is not, so the signal pulse is switched out the regeneration port. If both "A" and "B" are present, there is no relative phase shift again, and the

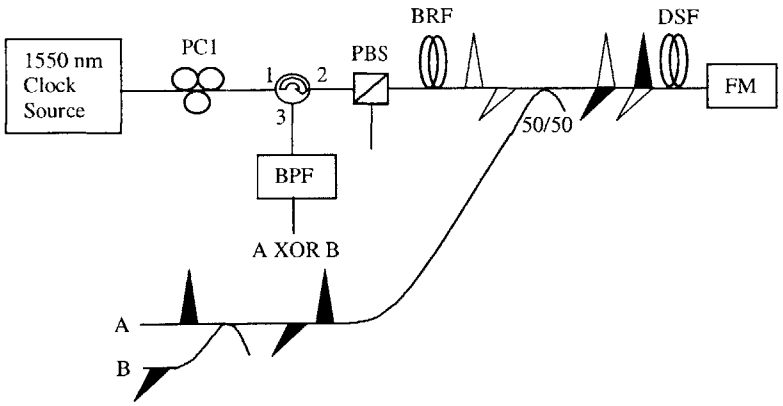

Figure 5-10: The folded UNI as it is applied to regenerative XOR.

signal pulse is not switched out. Thus, the folded UNI operates as an XOR gate.

Figure 5-11 shows the experimental setup used to test the XOR operation of the folded UNI. Two actively mode-locked fiber laser sources supply the 10 GHz optical pulse streams for the signal and control pulses. The pattern generator described in Section 5.2 drives a 2x2 electro-optic switch producing one pattern for the top path, labeled "A," and the inverse pattern for the bottom path, labeled "B." Pulse stream "B" is then delayed by 31 bit periods, producing two pseudorandom bitstreams. These pseudorandom streams pass through a passive multiplexer with multiple-bit delays to produce 10, 20, 40, or 80 Gbit/s pseudorandom pulse streams. The signal pulses also pass through the multiplexer, in the opposite direction, to generate a 10, 20, 40, or 80 Gbit/s signal pulse stream. A high speed 50 GHz photodiode (PD) detects the output of the folded UNI and displays the pulse pattern on the oscilloscope.

The results for 10 and 40 Gbit/s XOR tests are shown in Figures 5-12 and 5-13. In the 10 Gbit/s test, the time averaged signal pulse power into the folded UNI was 5.9 dBm and the time averaged control pulse power was 10 dBm. In the 40 Gbit/s test, because of the higher bit rate, the signal pulse stream power was 12 dBm and the control pulse stream power was 16 dBm. The top plot is pattern "A," the middle plot is pattern "B," and the bottom plot is the XOR of the two patterns. The XOR is successfully executed with good contrast. Much of the noise seen in the 40 Gbit/s data is caused by ringing in the photodiode's impulse response.

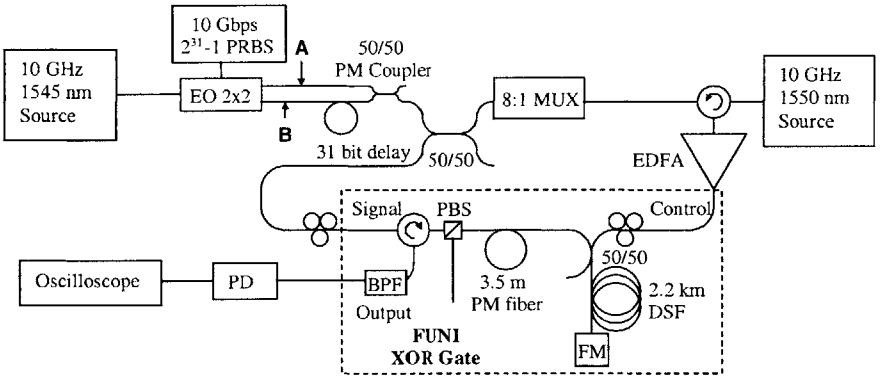

Figure 5-11: Experimental setup used to test the folded UNI XOR.

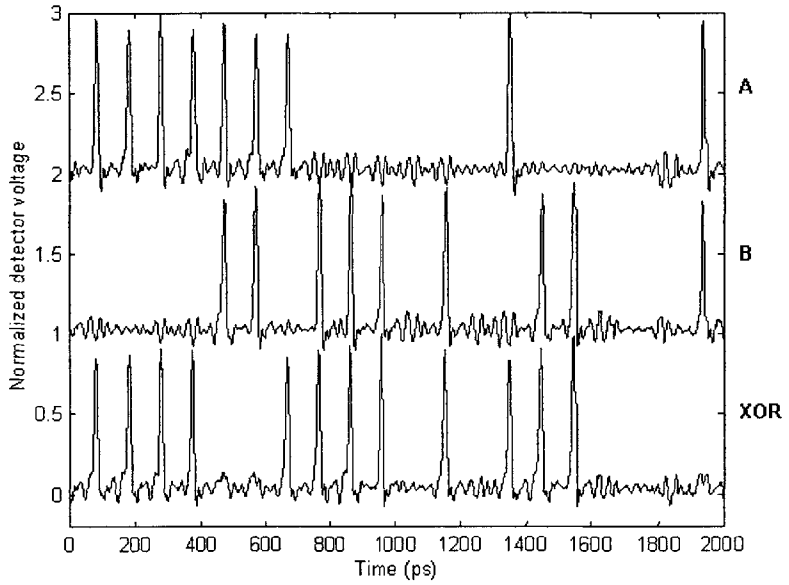

Figure 5-12: The top plot shows the photodiode output of channel A after regeneration in the FUNI. The middle shows the same for channel B. The bottom plot shows the regerated XOR of A and B. All voltages are normalized. A and B are at 10 Gbit/s.

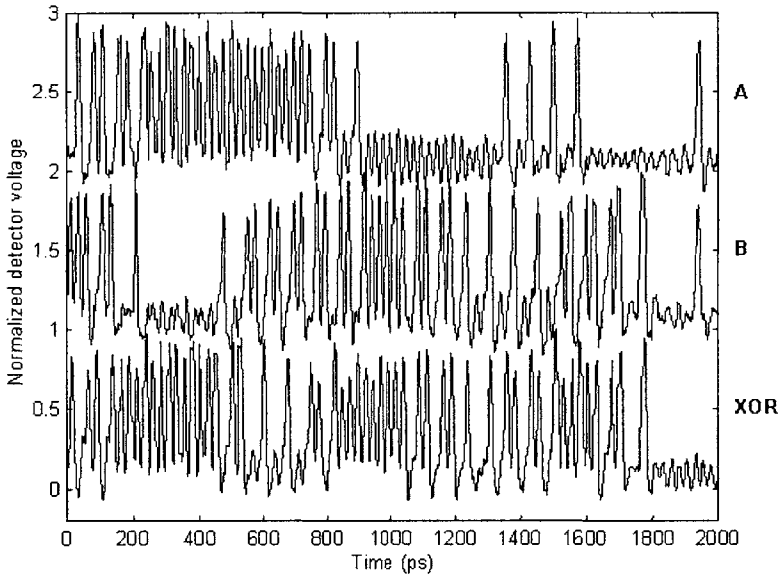

Figure 5-13: Photodiode outputs of regenerated A and B and of the regerated XOR of A and B at 40 Gbit/s. All voltages are normalized.

Chapter 6

Conclusions and Future Work

Optical pulse regeneration will be an essential component to any high data rate time division multiplexed fiber optic network. All-optical pulse regeneration is faster than electronic processing and does not require opto-electronic conversion of data encoded in optical pulses. We showed in this thesis that the folded ultrafast nonlinear interferometer (FUNI) can operate as a regenerator and has many advantages to other regenerator designs.

The Faraday rotating mirror in the folded UNI gives it inherent polarization stability. The close temporal spacing of the orthogonal polarizations of the clock pulses, after passing through the birefringent fiber, ensures that each sees the same fiber in the same conditions. Any changes in fiber properties caused by bending or vibration would have to occur faster than the approximately 5 ps separating the two polarizations for the effect to be noticeable.

Within the folded UNI, therefore, there is no need for polarization control. The polarization of the incoming clock and network data pulses, however, must be controlled. An erbium doped fiber ring laser generates the local clock pulses at a single polarization. Therefore, by using polarization maintaining fiber to deliver these clock pulses to the folded UNI, the folded UNI regenerator design does not need active monitoring of the clock pulses. The polarization of the network data pulses must be controlled before they pass through the polarizing beam splitter. We can adjust the polarization controller on the data pulse stream by simply maximizing power switched

out the "regenerated data" port of the folded UNI.

The folded UNI uses optical fiber as a nonlinear medium. The nearly instantaneous nonlinear response of fiber eliminates amplitude patterning on the regenerated output. Patterning is a serious challenge in designs that use semiconductor optical amplifiers (SOA), which have slow gain recovery times. Moreover, high logical latency is unimportant in regeneration, so the high nonlinear index of refraction of the SOA becomes less of an advantage.

In this thesis, we have discussed and demonstrated a method to directly measure the second order dispersion of optical fiber. We chose dispersion shifted fiber (DSF), which has low second order dispersion, so that dispersion would not be a significant effect in the folded UNI. In the same measurement, we found the relative group delays of pulse propagation in optical fiber. With these data we selected the carrier frequencies to generate the desired walk-off between the data and clock pulses. This walk-off corrects some of the effects of timing jitter in an incoming optical data stream.

We also tested a method of measuring the nonlinear index of refraction. We verified in simulation that the dispersion of the DSF used in the folded UNI was not significant compared to the self-phase modulation. The value of γ measured in Section 4.2.3 was close to the value of γ in similar DSF lengths reported in [42]. γ determines the length of fiber and intensity of data pulses needed in optical pulse regeneration.

The testing of the folded UNI itself included the measurement of the switching window. These data help determine the ability of the folded UNI to correct timing jitter. A wider window, if still smaller than a single bit period, can tolerate more timing jitter than a narrower window. We also tested the bit error rate of the folded UNI, comparing it to a baseline test without the folded UNI. In these tests, we showed a ~5 ps wide switching window and a 1 dB power penalty in bit error rates when compared to a baseline test. The 5 ps switching window is important for the tolerance of timing jitter. The 1 dB power penalty is a consequence of gain ripple in the receiver's erbium doped fiber amplifier.

The folded UNI was also applied to a regenerative XOR. Implementing the XOR

in a device like the UNI is technically difficult because of the patterning effects caused by the SOA. We showed that, even at rates of 40 Gbps, a high speed photodiode could clearly detect the output XOR of two psuedorandom bit streams.

The folded UNI still requires more testing. The folded UNI is sensitive to the network data pulse polarization. This polarization can drift slowly over time because of temperature and other changes in the network outside the folded UNI regenerator. Slow drifts can be controlled by maximizing the power switched out the "regenerated data" port of the folded UNI with simple electronic feedback. There could, however, also be quick changes in the polarization caused by acoustic vibrations somewhere in the network. Moreover, in time division multiplexing, different streams are interleaved in time so that a one data pulse may have a different state of polarization than a subsequent one. These sorts of polarization changes may not be correctible with simple electronic feedback and place another design burden on the rest of the network. Somehow the network will have to suppress noise vibrations and it must be consistent in adding data pulses of only a particular polarization. This dependence of the folded UNI on the data pulse polarization will have to be addressed. Researchers have already suggested polarization independent switch designs [43, 44, 45].

Also, the folded UNI regenerator, as it is now designed, requires different carrier wavelengths for the data pulse stream and the clock pulse stream. The regenerated pulse stream is at the clock pulse carrier wavelength, so that the regenerated output is at a different carrier wavelength than the data input stream. This use of two wavelengths places yet another burden on network design: the design of the network will have to alternate with the alternating carrier frequencies. I would like to consider regenerator designs that rely on a single carrier wavelength for both the data pulse stream and the clock pulse stream. We still would need a way to separate data pulses from clock pulses. One way to discriminate between the network data pulse stream and the clock pulse stream, other than by wavelength, is by using orthogonal polarizations. Using polarization to filter the data pulses from the clock pulses may, however, introduce more polarization sensitivity to the regenerator.

The folded UNI also has high loss, causing the output power to be low. We have

to reduce losses in the design to properly amplify the signal at the receiver. The 50/50 coupler, for example, unnecessarily adds 6 dB of loss, 3 dB for each direction of propagation. We will test a design that replaces the 50/50 coupler in the folded UNI regenerator with a wavelength division multiplexing coupler.

This thesis tested the bit error rate, switching window, and dependence of the bit error rate on the relative delay between the data and clock pulses. Nonetheless, the data pulses were brought directly from their source. In a more realistic test, we would first have the data pulses propagate down a long length of fiber, as would happen in a real network. I would first like to use a fiber loop, through which data pulses would propagate a number of times, and then test the regenerator on the resulting distorted data. Ultimately, I would like to test the folded UNI in a true long haul system.

Appendix A

Split-Step Fourier Code

```
% Solves i*U_z = -.5*i*k_2*U_tt + i*gamma*U*|U|^2 with the FFT.


% Get values for the number of divisions for solving PDE
fprintf('\nEnter the number of time divisions\n');
N = input('(will be rounded to nearest power of 2): ');
% N is rounded to the nearest power of two so FFT will be faster.
N = 2^(ceil(log2(N)));
M = input('Enter the number of space divisions: ');
Len = input('Enter the total length of fiber to calculate over: ');

% N-1 and M-1 are used because N element column vectors, where each
% element is analagous to a fence post, delineate only N-1 intervals.

% timetot is the period of the periodic boundary conditions.
timetot = 1000e-12;
dt = timetot/(N-1);
dz = Len/(M-1);

% k_2 is part of the propagation constant, alpha accounts for loss in
% the fiber.

%k_2 = 0;
k_2 = 1.6e-28;
%k_2 = -20e-27;
k_3 = 0;
alpha = 0;
%gamma = .0019;
```

```
gamma = 3e-3;

% q is number of time steps stored in solution matrices, U and spect.
% The original number of time steps, N, is downsampled to q in the
% funtion file titled dsamcvec.
q = 250;

% Lower case u is a column vector containing the data for all t at z=0.
% u2 holds the data for all t at the current value of z in the calculation.
% Capital U will be contain the u2's at certain evenly spaced values of z.

% The initial conditions are generated in the m-file ''initial,'' given
% below.
u = initial(N, timetot);

% dsamcvec reduces u to a column vector with q rows.
% The code for dsamcvec is given below.
U = dsamcvec(u, q);
u2 = fft(u);
spect = dsamcvec(fftshift(u2), q);

% u2 will be saved in U at equal spacings of z.  The number of u2's saved
% is given by r.
r = 10;
if M>r
index = round(linspace(2,M,r-1));
else
   index = [2:1:M];
end

% w is the radial frequency.
w = [0:(N/2),(1-(N/2)):(-1)]*2*pi/timetot;
eta = transpose((i*.5*k_2*(w.^2) + (i/6)*k_3*(w.^3) - alpha/2));
eta = exp(eta*dz);

% In the next line, we execute one half step of the linear operator.
u2 = u2.*sqrt(eta);
count2 = 1;
for count = 2:M
   u2 = ifft(u2);
   mag = abs(u2);
   % The next line executes one full step of the nonlinear operator.
   u2 = u2.*exp(i*gamma*mag.^2*dz);
   u2 = fft(u2);
   % The next line executes one full step of the linear opeartor.
```

```
   u2 = u2.*eta;
   if count == index(count2)
        count2 = count2 + 1;
        spect = [spect, dsamcvec(fftshift(u2), q)];
        U = [U, dsamcvec(ifft(u2), q)];
        (count/M)*100
    end
end
u2 = ifft(u2);
u2 = u2.*exp(i*gamma*mag.^2*dz);
u2 = fft(u2);
u2 = u2.*sqrt(eta);
u2 = ifft(u2);

tau = linspace(-timetot/2, timetot/2, q);
z = linspace(0, Len, r);
figure
omega = linspace(-(2*pi/timetot)*.5*N, (2*pi/timetot)*.5*N, q);
waterfall(omega, z, transpose(abs(spect)).^2)
colormap([0 0 0]);
figure
waterfall(tau, z, transpose(abs(U)).^2)
colormap([0 0 0]);

****************************************

function y = initial(N, timetot)

T = linspace(-timetot/2, timetot/2, N);
C = 0;
%T_0 = 1.36e-12;
T_0 = 1.80e-12;
P_0 = 3.3;
%P_0 = 4.8175;

% Gaussian
 y = ((P_0)^.5)*(exp(-(T.^2)./(T_0)^2))';

% Chirped Gaussian
% y = P_0*(exp(-((1+C*i)/2)*(T/T_0).^2))';

% Hyperbolic Secant
% y = P_0*(sech(T/.5e-12).*exp(i*C*T.^2/(2*T_0.^2)))';

% Super Gaussian
```

```
% y = (P_0^.5)*(exp(-((1+C*i)/2)*(T/T_0).^6))';

% Square wave
% y = (P_0^.5)*(abs(T)<T_0)';

****************************************

function y = dsamcvec(cvec, q)

% Reduces an nx1 column vector to a qx1 column vector
% unless n<q.

[m n] = size(cvec);

if m>q
y = cvec(round(linspace(1, m, q)), 1);
else
   y = cvec;
end
```

Bibliography

[1] M. N. Islam. *Ultrafast Fiber Switching Devices and Systems.* Cambridge University Press, Cambridge, England, 1992.

[2] R. A. Barry, V. W. S. Chan, K. L. Hall, E. S. Kintzer, J. D. Moores, K. A. Rauschenbach, E. A. Swanson, L. E. Adams, C. R. Doerr, S. G. Finn, H. A. Haus, E. P. Ippen, W. S. Wong, and M. Haner. All-Optical Network Consortium–ultrafast TDM networks. *JLT/JSAC Special Issue on Optical Networks*, 14(5):999, June 1996.

[3] K. J. Blow, N. J. Doran, and B. P. Nelson. Demonstration of the nonlinear fiber loop mirror as an ultrafast all-optical demultiplexer. *Electronics Letters*, 26(14):962–964, July 1990.

[4] M. W. K. Mak, H. K. Tsang, and K. Chan. Widely tunable polarization-independent all-optical wavelength converter using a semiconductor optical amplifier. *IEEE Photonics Technology Letters*, 12(5):525–527, May 2000.

[5] A. H. Chan and M. Medard. Reconfigurable feedback shift regiesters. In *Proceedings of the IEEE International Symposium on Information Theory Symposium on the Theory of Computing*, pages xxvi+542, June 1997.

[6] K. J. Park, T. Mizumoto, A. Matsuura, and Y. Naito. All-optical address extraction for optical routing. *Journal of Lightwave Technology*, 16(7):1575–1577, November 1998.

[7] T. Yamamoto, L. K. Oxenlowe, C. Schmidt, C. Schubert, E. Hilliger, U. Feiste, J. Berger, R. Ludwig, and H. G. Weber. Clock recovery from 160 Gbit/s data signals using phase-locked loop with interferometric optical switch based on semiconductor optical amplifier. *Electronics Letters*, 37(8):509–510, April 2001.

[8] S. Bigo, O. Leclerc, and E. Desurvire. All-optical fiber signal processing and regeneration for soliton communications. *IEEE Journal of Selected Topics in Quantum Electronics*, 3(5):1208–1223, October 1997.

[9] J. K. Lucek and K. Smith. All-optical signal regenerator. *Optics Letters*, 18(15):1226–1228, August 1993.

[10] J. Yu, X. Zheng, F. Liu, A. Buxens, and P. Jeppesen. Simultaneous realization wavelength conversion and signal regeneration using a nonlinear optical loop mirror. *Optics Communications*, 175:173–177, February 2000.

[11] W. A. Pender, P. J. Watkinson, E. J. Greer, and A. D. Ellis. 10 gbit/s all-optical regenerator. *Electronics Letters*, 31(18):1587–1588, July 1995.

[12] M. Jinno and T. Matsumoto. Nonlinear Sagnac interferometer switch and its applications. *IEEE Journal of Quantum Electronics*, 28(4):875–882, April 1992.

[13] K. L. Hall and K. A. Rauschenbach. 100-Gbit/s bitwise logic. *Optics Letters*, 23(16):1271–1273, August 1998.

[14] E. Eiselt, W. Pieper, and H. G. Weber. SLALOM: Semiconductor laser amplifier in a loop mirror. *Journal of Lightwave Technology*, 13(10):2099–2111, October 1995.

[15] Y.-H. Kao, T. J. Xia, M. N. Islam, and G. Raybon. Limitations on ultrafast optical switching in a semiconductor laser amplifier operating at transparency current. *Journal of Applied Physics*, 86(9):4740–4747, November 1999.

[16] S. A. Hamilton, B. S. Robinson, J. D. Moores, F. Hakimi, and P. A. Schulz. Ultrafast synchronous all-optical time division multiplexing system demonstration. In *Proc. of OFC 2001*, page WO3, Anaheim, CA, March 2001. OSA.

[17] D. Marcuse. RMS width of pulses in nonlinear dispersive fibers. *Journal of Lightwave Technology*, 10(1):17, April 1992.

[18] M. Jinno and M. Abe. All-optical regenerator based on nonlinear fibre Sagnac interferometer. *Electronics Letters*, 28(14):1300–1301, July 1992.

[19] Francis B. Hildebrand. *Advanced Calculus for Applications.* Prentice-Hall, Inc., Englewood Cliffs, New Jersey, second edition, 1976.

[20] Robert W. Boyd. *Nonlinear Optics.* Academic Press, Inc., San Diego, California, first edition, 1992.

[21] Govind P. Agrawal. *Nonlinear Fiber Optics.* Optics and Photonics. Academic Press, San Diego, California, second edition, 1995.

[22] K. L. Hall, G. Lenz, A. M. Darwish, and E. P. Ippen. Subpicosecond gain and index nonlinearities in InGaAsP diode lasers. *Optics Communications*, 111(5):589–612, October 1994.

[23] N. S. Patel, K. L. Hall, and K. A. Rauschenbach. Interferometric all-optical switches for ultrafast signal processing. *Applied Optics*, 37(14), May 1998.

[24] K. L. Hall. All-optical switching at 100 gbps. *Optical Fiber Communications Conference Proceedings*, 178:xxvi+542, June 1997.

[25] I. S. Gradshteyn and I. M. Ryzhik. *Table of Integrals, Series, and Products.* Academic Press, Inc., San Diego, California, fourth edition, 1980.

[26] V. E. Zakharov and A. B. Shabat. Exact theory of two-dimensional self-focusing and one-dimensional self-modulation of waves in nonlinear media. *Soviet Physics JETP*, 34(1):62–69, January 1972.

[27] K. W. DeLong and G. I Stegeman. Two-photon absorption as a limitation to all-optical waveguide switching in semiconductors. *Applied Physics Letters*, 57(20):2063, November 1990.

[28] S. Bigo, O. Leclerc, and E. Desurvire. All-optical fiber signal processing and regeneration for soliton communications. *IEEE Journal of Selected Topics in Quantum Electronics*, 3(5):1208–1223, October 1997.

[29] N. J. Doran and D. Wood. Nonlinear-optical loop mirror. *Optics Letters*, 13(1):56–58, January 1988.

[30] K. Uchiyama, H. Takara, S. Kawanishi, T. Morioka, and M. Saruwatari. Ultrafast polarisation-independent all-optical switching using a polarisation diversity scheme in the nonlinear optical loop mirror. *Electronics Letters*, 28(20):1864–1866, September 1992.

[31] M. Nakazawa, E. Yoshida, T. Yamamoto, E. Yamada, and A. Sahara. TDM single channel 640 Gbit/s transmission over 60 km using 400 fs pulse train and walk-off free, dispersion flattened nonlinear optical loop mirror. *Electronics Letters*, 34(9):907–908, April 1998.

[32] Masahiko Jinno. All optical signal regularizing/regeneration using a nonlinear fiber Sagnac interferometer switch with signal-clock walk-off. *Journal of Lightwave Technology*, 12(9):1648–1659, September 1994.

[33] Amnon Yariv. *Optical Electronics in Modern Communications.* Oxford Series in Electrical and Computer Engineering. Oxford University Press, Oxford, fifth edition, April 1997.

[34] B. Olsson, N. Lagerqvist, A. Boyle, and P. Andrekson. Elimination of acoustic sensitivity in nonlinear optical loop mirrors. *Journal of Lightwave Technology*, 17(2):343–346, February 1999.

[35] L. Prigent and J.-P. Hamaide. Measurement of fiber nonlinear Kerr coefficient by four-wave mixing. *IEEE Photonics Technology Letters*, 5(9):1092–1095, September 1993.

[36] K. S. Kim, R. H. Stolen, W. A. Reed, and K. W. Quoi. Measurement of the nonlinear index of silica-core and dispersion-shifted fibers. *Optics Letters*, 19(4):257–259, February 1994.

[37] S. J. Savage, B. S. Robinson, S. A. Hamilton, and E. P. Ippen. All-optical pulse regeneration in an ultrafast nonlinear interferometer with faraday mirror polarization control. In *CLEO 2001 Technical Digest*, pages 316–317, Baltimore, MD, May 2001.

[38] Y. Ueno, S. Nakamura, and K. Tajima. Penalty-free error-free all-optical data pulase regeneration at 84 gbps with symmetric-mach-zehnder-type regenerator. In *Proc. of OFC 2001*, page MG5, Anaheim, CA, March 2001. OSA.

[39] M. Jinno. Effects of group velocity dispersion on self/cross phase modulation in a nonlinear Sagnac interferometer switch. *Journal of Lightwave Technology*, 10(8):1167–1178, August 1992.

[40] T. F. Carruthers and I. N. Duling III. 10-ghz, 1.3-ps erbium fiber laser employing soliton pulse shortening. *Optics Letters*, 21(23):1927, December 1996.

[41] J. D. Moores, K. Bergman, H. A. Haus, and E. P. Ippen. Optical switching using fiber ring reflectors. *Journal of the Optical Society of America B*, 8(3):594–601, March 1991.

[42] R. H. Stolen, W. A. Reed, K. S. Kim, and G. T. Harvey. Measurement of the nonlinear refractive index of long dispersion-shifted fibers by self-phase modulation at 1.55 μm. *Journal of Lightwave Technology*, 16(6):1006–1012, June 1998.

[43] E. A. Kuzin, N. Korneev, J. W. Haus, and B. Ibarra-Escamilla. Polarization independent nonlinear fiber Sagnac interferometer. *Optics Communications*, 183:389–393, April 2000.

[44] D. Sandel. Polarization-independent regenerator with nonlinear optoelectronic phase-locked loop. In *Proc. of OFC'94 Symposium on the Theory of Computing*, pages 310–311, Washington, DC, February 1994. OFC.

[45] N. A. Whitaker, P. M. W. French, M. C. Gabriel, and H. Avramopoulos. Polarization-independent all-optical switching. *IEEE Photonics Technology Letters*, 4(3):260–263, March 1992.